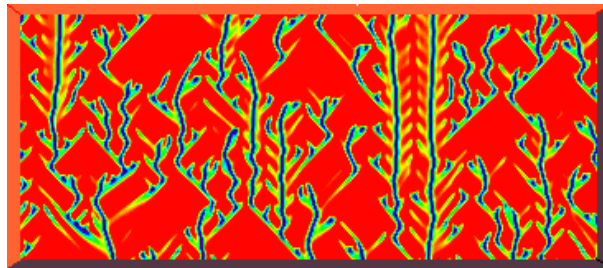DEPARTAMENT DE FISICA

UNIVERSITAT DE LES ILLES BALEARS

DYNAMICS
OF DISORDERED REGIMES IN
SPATIALLY EXTENDED SYSTEMS:

THE
COMPLEX GINZBURG–LANDAU
EQUATION

Memòria presentada per
Raúl Montagne Dugrós *per optar*
al Grau de Doctor en Ciències Físiques
per la Universitat de les Illes Balears.

La present Tesis Doctoral fou dirigida
pels Drs. *M. San Miguel*
i Emilio Hernández-García.

A mis mujeres,
Angélica, Paula y Susana

Contents

Maximino San Miguel Ruibal, catedràtic de Física de la Matèria Condensada del Departament de Física de la Universitat de les Illes Balears i Emilio Hernández–García, professor titular de la mateixa Universitat,

CERTIFIQUEN

Que la present memòria ha estat realitzada per Raúl Montagne Dugrós sota la seva direcció en aquest departament i que constitueix la seva Tesi per optar al títol de Doctor en Ciències Físiques.

I, perquè així consti, firmen la present a Palma de Mallorca a 16 de Octubre de 1996.

Maximino San Miguel   Emilio Hernández–García

Agradecimientos

Una tesis no estaría completa sin los agradecimientos. A lo largo de los cuatro años es mucha la gente que de una u otra manera han colaborado para hacer posible esta tesis. Sólo el esfuerzo combinado de varias personas hizo posible la presentación de esta tesis en los plazos previstos.

Sería injusto no empezar agradeciendo a mi esposa e hijas. Ellas supieron darme la comprensión y ánimos necesarios. En especial, gracias por haber sabido soportarme en estos últimos días.

Luego quiero agradecer, de todo corazón, a mis dos directores de tesis.

Al Profesor Maxi San Miguel por haberme guiado durante estos años. En el aspecto científico, se preocupó que mi formación sirviera tanto para lograr mis objetivos actuales como futuros. Para eso no escatimó jamás, esfuerzos para que asistiera a reuniones científicas y me vinculase con otros físicos, dándome a su vez, la libertad de iniciar colaboraciones independientes. Además durante este tiempo no sólo me dio su apoyo científico, también me dio el calor humano necesario para hacerme sentir a gusto aquí . Mi familia y yo estaremos siempre agradecidos por el apoyo que recibimos de él y su familia. Tuve, además, el privilegio de aprender con él y su familia el *verdarero* significado de la palabra *excursión*.

El Profesor Emilio Hernández–García, con gran humildad y paciencia me explicó los más obscuros vericuetos de la CGLE. Le agradezco las muchas horas que pasó frente a la pantalla del ordenador, a mi lado, enseñándome a *mirar*, puliendo mis rudimentarios conocimientos de programación, cálculo, etc. etc. . Muchos de los cálculos que ahora me parecen fáciles le exigieron a él muchas horas para que yo finalmente los entendiese. Sumadas a todas esas horas de enseñanza le agradezco el apoyo a nivel humano en las buenas y en las malas. Aprendí de forma experimental que siempre podía contar con él.

Al Dr. Pere Colet le agradezco haber pasado interminables horas corrigiendo mis vicios de programación. Aprendí de él todo lo que pude, por mencionar sólo un ejemplo, fue de gran valor para mí su "*rigurrroso*" estudio de estabilidad. Además, su afán perfeccionista me llevó a implementar en dos semanas seis (6) métodos de integración distintos. Aprendí a optimizar los programas de IDL y Fortran hasta límites de eficiencia insospechados por mí . Todo eso sumado a la excepcional calidad humana que esconde bajo su habitual forma de hablar un tanto ..."fuerte". Por último, le agradezco también las magníficas torradas que organizó en estos años.

Al Dr. A. Amengual agradezco haberme ayudado a salir de los atolladeros con el Mathematica. Y un *gran* gracias por haber encontrado no sólo el fallo del programa que intentaba hacer funcionar sin éxito durante meses, sino que también, encontró la cura.

Al Dr. Julyan Cartwright por haberme revelado unos cuantos trucos de Unix, LaTeX

educación posible.

Por último, se supone que alguien pago mi estancia aquí . Pues eso se lo debo a varias instituciones. Agradezco pues, a:

Resumen

Esta tesis está dedicada al estudio de diferentes aspectos de la *dinámica Espacio–temporal compleja*. Las estructuras espacio–temporales están universalmente presentes en la naturaleza. Estas pueden ser formadas vía bifurcaciones, a menudo a partir de un estado de referencia uniforme. Un aspecto interesante de estas estructuras es que tienen un carácter universal y pueden llegar a evolucionar, a través de sucesivas inestabilidades, a Caos Espacio–Temporal (STC) (M. Cross and P. Hohenberg, Science **263**, 1569 (1994), J. Gollub, Nature **367**, 318 (1994)). El carácter universal de este fenómeno permite una descripción en términos de modelos generales. Un modelo paradigmático es la Ecuación de Ginzburg–Landau Compleja (CGLE). La CGLE es una ecuación de amplitud que describe los aspectos universales de la dinámica de sistemas cerca de una bifurcación de Hopf. (M. Cross and P. Hohenberg, Rev. Mod. Phys. **65**, 851 (1993), W. van Saarloos and P. Hohenberg, Physica D **56**, 303 (1992)). La CGLE presenta una rica dinámica compleja espacio–temporal que ha sido recientemente clasificada, tanto para el caso de una dimensión como para el de dos dimensiones, en un diagrama de fases en el espacio de parámetros (B. Shraiman *et al.*, Physica D **57**, 241 (1992), H. Chaté, Nonlinearity **7**, 185 (1994)).

En este contexto general esta tesis contribuye al estudio de la CGLE en una dimensión. Los principales logros alcanzados incluyen la posibilidad de realizar una descripción de los estados de la CGLE en términos de un potencial de no–equilibrio, la caracterización de la transición de fase entre diferentes estados de STC, el control y estabilización de estados ordenados en la fase STC y la sincronización de STC en sistemas extendidos.

Primero, en esta tesis estudiamos numéricamente en el caso unidimensional la validez del funcional calculado por Graham y colaboradores (R. Graham and T. Tel, Phys. Rev. A **42**, 4661 (1990), O. Descalzi and R. Graham, Z. Phys. B **93**, 509 (1994)) como potencial de Lyapunov para la ecuación compleja de Ginzburg–Landau. En la región del espacio de parámetros no–caótica este funcional decae monótonamente en el tiempo a los atractores onda plana, tal como se debería esperar para un funcional de Lyapunov, siempre y cuando no hayan singularidades en la fase. En la región de turbulencia de fase el potencial relaja a un valor característico del atractor turbulento, y la dinámica preserva este valor aproximadamente constante.

Segundo, en ésta tesis se da una caracterización estadística de los estados con número de rotación no nulo en la región de Turbulencia de Fase (PT) de la ecuación de Ginzburg–Landau compleja unidimensional. Encontramos que los estados con número de rotación mas grande que un cierto valor crítico son inestables, es decir, que decaen a estados con número de rotación más pequeño. La transición de Turbulencia de Fase a Turbulencia de Defectos puede ser interpretada como una transición de rompimiento de ergodicidad que

ocurre cuando el rango de número de rotación estables se hace cero. Los estados estables, asintóticos (*wound states*) que no tienen comportamiento espacio–temporal caótico son descritos dentro del régimen de PT de número de rotación no nulo. Además de la completa caracterización numérica de estos estados de número de rotación no nulo también se explican en términos de soluciones de una ecuación de fase.

Hemos considerado también el rol que juega la difusión compleja no–lineal en la estabilidad de las soluciones periódicas en el régimen de STC. Esto es estudiado en el contexto del control de STC. Se demuestra la estabilización de ondas planas inestables en la ecuación de Ginzburg–Landau compleja tanto en los regímenes de turbulencia débil, como la turbulencia de fase o la Intermitencia Espacio–Temporal (STI) como en los regímenes fuertemente caóticos como la turbulencia de defectos.

El comportamiento espacio–temporal caótico fue también considerado para dos ecuaciones de Ginzburg–Landau acopladas (CCGLE). Se muestra que es posible sincronizar STC en sistemas extendidos en el contexto de CCGLE. Se identifica un régimen de intermitencia espacio–temporal (STI) acoplado y se describe en términos de funciones de distribución y medidas de la información. Se describen también propiedades adicionales del sistema descripto por un par de ecuaciones de Ginzburg–Landau complejas acopladas como la desaparición de la STI cuando se pasa de un acoplamiento débil a uno fuerte.

Abstract

This thesis is devoted to study different aspects of *Spatio–temporal complex dynamics*. Spatio–temporal structures are universally present in nature. These structures commonly referred as patterns, can be formed via bifurcations, often from a uniform reference state. An interesting aspect of patterns is that many of them have a universal character and can evolve, under subsequent instabilities, to Spatio–temporal chaos (STC) (M. Cross and P. Hohenberg, Science **263**, 1569 (1994),J. Gollub, Nature **367**, 318 (1994)). The universal character of this phenomenum allows a description through general model equations. A paradigmatic model is the Complex Ginzburg–Landau Equation (CGLE). The CGLE is the amplitude equation describing universal features of the dynamics of extended systems near a Hopf bifurcation (M. Cross and P. Hohenberg, Rev. Mod. Phys. **65**, 851 (1993), W. van Saarloos and P. Hohenberg, Physica D **56**, 303 (1992)). The CGLE displays a rich variety of complex spatio-temporal dynamical regimes that have been recently classified, for the one (and also two) dimensional case, in a phase diagram in the parameter space (B. Shraiman *et al.*, Physica D **57**, 241 (1992), H. Chaté, Nonlinearity **7**, 185 (1994)).

In this general context this thesis contributes to current studies of the $d = 1$ CGLE. The main issues addressed include the feasibility of a description of states of the CGLE in terms of a nonequilibrium potential, the characterization of a phase transition between different states of STC, the control and stabilization of ordered states within a STC phase and the synchronization of STC in extended systems.

First, in this thesis we study numerically in the one-dimensional case the validity of the functional calculated by Graham and coworkers (R. Graham and T. Tel, Phys. Rev. A **42**, 4661 (1990), O. Descalzi and R. Graham, Z. Phys. B **93**, 509 (1994)) as a Lyapunov potential for the Complex Ginzburg-Landau equation. In non-chaotic regions of parameter space the functional decreases monotonically in time towards the plane wave attractors, as expected for a Lyapunov functional, provided that no phase singularities are encountered. In the phase turbulence region the potential relaxes towards a value characteristic of the phase turbulent attractor, and the dynamics there approximately preserves a constant value.

Second, this thesis addresses a statistical characterization of states with nonzero winding number in the Phase Turbulence (PT) regime of the one-dimensional Complex Ginzburg-Landau equation. We find that states with winding number larger than a critical one are unstable, in the sense that they decay to states with smaller winding number. The transition from Phase to Defect Turbulence is interpreted as an ergodicity breaking transition which occurs when the range of stable winding numbers vanishes. Asymptotically stable states (*wound states*) which are not spatio-temporally chaotic are described within the PT regime of nonzero winding number. Besides the complete numerical characterization

of these wound states some analytical insight is brought to such states by explaining them in terms of solutions of a phase equation.

We have also considered the role of nonlinear complex diffusion terms in the stability of periodic solutions in the regime of STC. This is discussed in the context of control of STC. The stabilization of unstable plane waves in the Complex Ginzburg Landau equation in weakly chaotic regimes such as phase turbulence and spatio-temporal intermittency or in strongly chaotic ones like defect turbulence is demonstrated.

STC behaviour has been also considered for two coupled CGLE. It is shown that the synchronization of STC extended systems is possible in the context of Coupled Complex Ginzburg-Landau equations (CCGLE). A regime of coupled spatiotemporal intermittency is identified and described in terms of distribution functions and information measures. Additional properties of coupled CGLE are also described as the disappearance of STI when crossing from weak to strong coupling.

Chapter 1

Introduction

Dream on
We can solve everything in science
   Naturally
Science
   It's a picture of how to get what you want
   out of life
Joni Mitchell, *The Reoccuring Dream*

1.1 Overview

1.1.1 Motivation and Organization of the Thesis

A field of knowledge often named as "Nonlinear and Statistical Physics" has emerged in recent years in the modern interdisciplinary context of research in complex systems. This field incorporates a number of techniques developed in the theory of Dynamical Systems (bifurcation and chaos) and Statistical Mechanics (phase transitions, nonequilibrium systems, correlations). It is probably better defined by its methodology than by study of a specific physical system. In fact a main focus is in the understanding of generic of universal features of nonlinear and nonequilibrium systems. Beyond more mature subjects of research , as low dimensional chaos or stationary pattern formation, present research focuses in the characterization and understanding of the regime of Spatio Temporal Chaos (STC) sometimes also called weak turbulence regime. It is hoped that this regime, at the crossroads of phase transitions and dynamical chaos, can be understood with concepts and methods developed in these fields and, in turn, this can be a significant step towards the understanding of fully developed turbulence. Theoretical studies of this regime are very often based in model equation which describe universal features. A well known prototype example of such models is the Complex Ginzburg–Landau Equation (CGLE) which displays a rich variety of spatiotemporal dynamics.

This thesis is a contribution to the line of research described above which focuses in the analysis of the one dimensional CGLE. In the analysis of this specific model it uses methodology borrowed from other more established fields. On the one hand the idea of a nonequilibrium potential ("Free energy") to describe the complex phases of the CGLE is explored following the general lines of thought of Statistical Mechanics. Also within

the same spirit of Statistical Mechanics a characterization of a phase transition between two different STC phase is addressed. On the other hand the new techniques of control and synchronization of chaos are used here to achieve control and synchronization of STC phases.

Chapter 1 of the thesis is a general review of background material needed for the research which has lead the results presented in chapters 2–5. Each of these chapters is written in a selfcontained way, so that repetition of some definitions and equations is not avoided.

In the remaining of this Chapter 1 an introduction to pattern formation phenomena and STC, mostly from an historic perspective is presented (Sec. 1.1.2). Section 1.1.3 describes different approaches to pattern formation problem to put into context the approach followed here (amplitude equations and numerical analysis). Section 1.2 gives an introduction to the CGLE, its derivation as the amplitude equation for a Hopf bifurcation in extended systems and the description of two specific physical systems that can be described by the CGLE. Section 1.3 contains an introduction to the solutions and phenomenology associated with the CGLE. This sections starts with a description of the plane wave solution of the CGLE an the analysis of their stability. Next we describe the "phase diagram" of this equation and the different spatiotemporal regimes which are known. At the end of this section an introduction to localized solutions of the CGLE is presented.

In chapter 2 we study numerically the validity of the functional calculated by Graham and coworkers as a Lyapunov potential for the Complex Ginzburg-Landau equation. We first discuss in Sect. 2.2 a classification of dynamical flows. In sect. 2.3 we review the essential analytical results for the Lyapunov functional of the CGLE. Next, sections 2.4 and 2.5 contain our numerical analyses. The chapter ends with a summary of the main conclusions on this issue in section 2.6.

In chapter 3 we give a statistical characterization of states with nonzero winding number ν in the Phase Turbulence (PT) regime. Section 3.1 is devoted to an introduction to the Phase Turbulence regime. The characterization of the transition from PT to DT in terms of the range of conserved ν is presented in section 3.2. States with $\nu \neq 0$ found in the PT region of parameters are described in section 3.3 in terms of three elementary *wound* states: Riding turbulence, frozen turbulence and quasiperiodic state. Section 3.4 constitutes an analytical approach that gives insight into the states numerically obtained, in terms of solutions of a phase equation. Also, theoretical predictions are made for such states. The Chapter is closed with some final remarks.

In chapter 4 we study in detail the role of nonlinear complex diffusion terms in the stability of periodic solutions in the regime of spatio temporal chaos. This chapter begins introducing the ideas of control of chaos and giving a concise review of this feature on extended systems. In section 4.2 we introduce the modified CGLE with nonlinear complex diffusion. Section 4.3 is devoted to the linear stability analysis of plane wave solutions for this modified equation. In section 4.4 the analytical prediction of the linear stability analysis is verified through numerical simulations of the equations. This chapter ends with some concluding remarks in section 4.5.

In chapter 5 we address the problem of synchronization of spatiotemporally chaos in extended systems. This study is done considering *two coupled* CGL equations. A regime of coupled spatiotemporal intermittency is identified and described in terms of distribution functions and information measures. Additional properties of coupled CGLE are also

described, namely the disappearance of Spatio–Temporal Intermittency (STI) for strong enough coupling, and the inadequacy of the description in terms of a single equation for that regime.

Chapter 6 of this thesis contains some general conlusions. Appendix A contains details on the numerical integration scheme used thereupon the thesis. Appendix B accounts for localized solutions in two coupled CGLE.

1.1.2   Pattern Formation and Spatiotemporal Chaos

At absolute thermodynamic equilibrium, a given macroscopic system rests in a structure-less and time-independent state. It can be brought out of equilibrium in several ways. A first possibility is to prepare the system in a metastable state and to let the stable phase nucleate. This is, for example, the case of an undercooled liquid that solidifies as soon as a sufficiently large germ is present; at a given temperature the solid phase is more stable than the liquid phase and the fraction of the solid phase spontaneously increases, separated from the remaining liquid by a *solidification front*. A second possibility is to consider *homogeneous* open systems driven far from equilibrium, by imposed gradients of intensive quantities: pressure, temperature, chemical potential. Along the thermody-namic branch, the response of the system in terms of fluxes of extensive quantities will display the same spatio-temporal symmetries as the excitation. However, the system can choose other solutions breaking these symmetries. When a system is removed far from equilibrium by subjecting it to a stress, it will often undergo a transition from a spatially uniform state to a state with spatial variation. This spatially varying state is called *pat-tern*. Besides, this variation can also vary temporally giving rise to oscillatory patterns. The pattern formation phenomena (stationary or oscillatory) is generally associated with nonlinear effects, which lead to qualitatively new phenomena. Among them, *Spatiotem-poral Chaos*[52, 70](STC) is an extreme case of combined complex dynamics and spatial organization.

Patterns in nature have attracted the interest of scientists for a long time. They have been observed in chemistry, fluids, biology, etc. Different efforts from all areas came to quantify these phenomena. On the other hand, such a diversity in the origins of the phenomena prevented for a long time to put all the ideas in a common framework. The history of pattern formation theory can be made up of a number of achievements. The universality of pattern phenomena was put forward in the book[53] "On growth and Form" by D'Arcy Thompson. In this book he showed through a wide variety of photos and analogies how different systems, mostly taken from biology, can look similar, that is, have similar *patterns*.

The list of experiments in fluids is very long, however Rayleigh-Bénard convection evolved into the primary model system for the experimental study of pattern forma-tion. Bénard performed the first systematic investigation of convection in a shallow fluid layer heated from below. The results of his studies, actually the results of his doctoral thesis, were published in two papers[26, 27]. The prime result of Bénard's experiment was the discovery of a stable, steady-state, regular pattern of hexagonal convection cells. Rayleigh[153], in 1916, tried to give an explanation of Bénard's experiments. However, introducing other type of boundary condition in the mathematical problem, he changed Bénard's problem[1], but he succeeded in introducing what we now call the Rayleigh-

Bénard convection. Rayleigh's paper is a pioneering work on the theory of convection caused by heating from below. A first book that summarized this topic was written by Chandrasekhar's[38] in 1961. His book dealt with hydrodynamic and hydromagnetic stability in general. Bénard convection and the Taylor vortex instability were described in all the detail known at that time. Chandrasekhar's book has a nearly complete list of the publications concerned with Bénard convection up to that time.

In the 1960's there was relatively little quantitative experimental work by physicists on patterns. However an exception is the work of Donnelly and coworkers on Taylor-vortex flow[60]. An important theoretical result of that decade, which had a great impact on subsequent experimental activity, should be mentioned. This is the work of Lorenz[117] through which it became widely appreciated that systems describable by coupled nonlinear ordinary differential equations can exhibit non-periodic time dependence. Besides, this work provided the link to the numerous work done in the field of Dynamical Systems by the mathematics community. A list of authors that laid the foundations and developed the tools used nowadays for describing dynamical systems is revised, for example, in [90, 28].

Greatly improved techniques of parameter control and data acquisition and analysis played a vital role in increasing the understanding of the theoretical framework. Among others, the work Libchaber and Maurer[116] is of particular interest since it provided experimental evidence of a chaotic evolution on convection in small aspect ratio.

In the 1970's there was an important push on experiments. Although there is a long history of the study of bifurcations and pattern formation in fluid mechanics by the applied mathematics and engineering community, physicists for the most part had not really appreciated the interesting aspects of this field prior to about 1970. The experimentalist did not feel constrained by the practical needs of the engineer and felt free to concentrate on problems which were just complicated enough to be challenging but still simple enough to be amenable to theoretical analysis and quantitative experimental study. At Bell Laboratories, G. Ahlers started a series of experiments in Rayleigh-Bénard convection[9, 10, 11] and constituted what became one of most important groups dedicated to the study of pattern formation phenomena. Among others, it should also be mentioned the detailed review on Bénard's convection by Busse in 1978[34].

The idea that the global properties are a consequence of self-organization and of cooperative behavior not reducible in a trivial (neither interesting) way to a microscopic point of view took form during this decade. The connection between spatiotemporal pattern formation in macroscopic systems and linear instabilities was first emphasized in 1952 by the outstanding mathematician Turing. But it was not until late in the 1980's that these ideas gained maturity. That stage could only be achieved thanks to the contribution done late on the 1970's. Examples of these relevant contributions are the famous paper of H. Haken in 1975[80] and the book of G. Nicolis and I. Prigogine in 1977[137].

Dynamical systems and the behavior of chaotic nonlinear systems had a big push at the beginning of the 1980's. The next development during this decade was the study of systems of a large number of degrees of freedom with a special emphasis in patterns. This kind of study has been summarized by M.C. Cross and P.C. Hohenberg[51]. The success of this universal approach is due to the cooperation of different fields. Nowadays, there is no single accepted name for pattern formation theory. The main issues can be found under titles such as Synergetics[81], Dissipative Structures[137], Nonequilibrium Statistical Mechanics, Irreversible Thermodynamics, Nonlinear Science, Complex Systems, etc. .

As an example of an experimental set up, the Rayleigh-Bénard Convection Cell, or simply the Rayleigh-Bénard experiment will be explained. A fluid layer is heated from below and kept at a fixed temperature from above (Fig. 1.1). At a small temperature difference (more precisely, gradient) heat is transported by heat conduction and the fluid remains quiescent. When the temperature gradient reaches a critical value, the fluid starts a macroscopic motion. Since heated parts expand, these parts move up by buoyancy, cool and fall back again to the bottom. Amazingly, this motion is well regulated. Either rolls, hexagons are observed as can be seen in Fig. 1.2 . Thus, out of a completely homogeneous state, a dynamic well ordered spatial pattern emerges. When the temperature gradient is further increased, new phenomena occur. The rolls start a wavy motion along their axes. An extended and clear introduction to this topic can be found in the book by Koschmieder[100] .

$$\Delta T > \Delta T_c$$
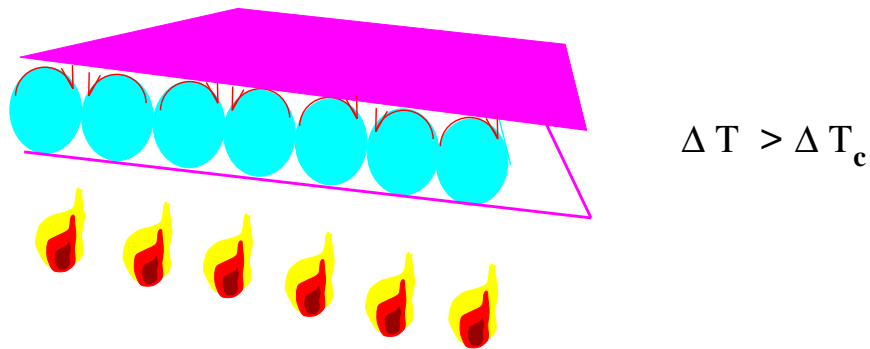
Figure 1.1: The Rayleigh-Bénard convection cell consist of a fluid contained between two parallel horizontal plates. A stationary pattern is obtained heating from below by a heat current.
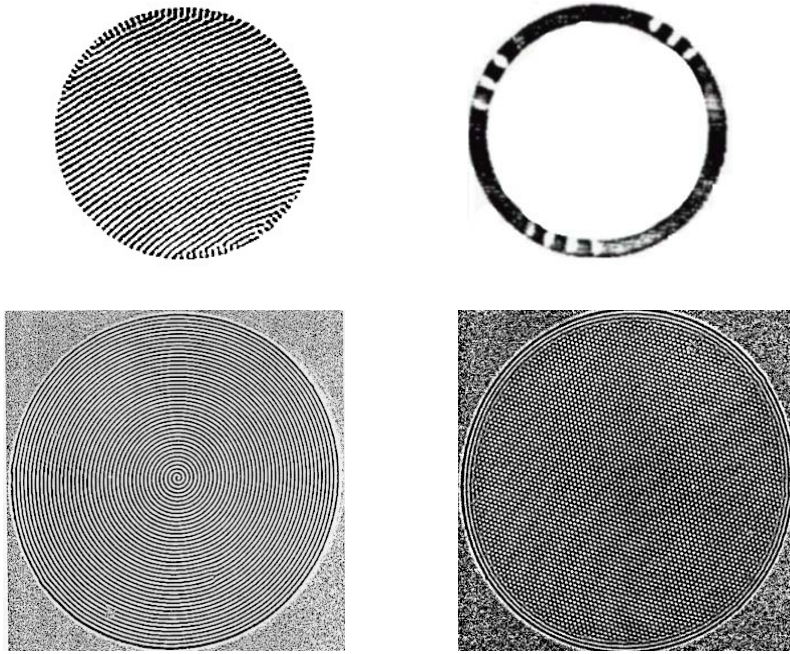
Figure 1.2: Rayleigh Bénard patterns. a) Typical rolls [30]. b) three pulses traveling in an annular cell of a binary mixture[138] c) a one arm spiral[31] d) a defect-free hexagonal lattice of convection cell obtained with a non-Boussinesq sample[31]

A great variety of experimental conditions have been explored since the early days of Bénard's convection. In particular a wide range of fluids have been used beyond. Rolls, hexagons or even spirals can be viewed in non-Boussinesq fluids. Traveling pulses can also be observed in binary mixture with a particular geometry (see Fig. 1.2 b)[138]. Bénard's-Marangoni convection is obtained if the top boundary is left free and standing hexagons are observed (see Fig. 1.3)[145].
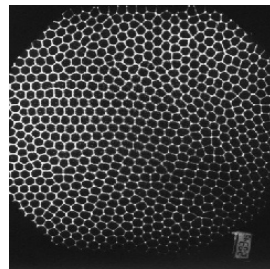
Figure 1.3: Bénard-Marangoni patterns. A spontaneous hexagonal pattern[145]

Convection experiments can also be set up in liquid crystals, including electrohydro-dynamic convection of nematic liquid crystals. This experiment consists in two parallel transparent electrodes with an applied AC voltage separated by a thin layer of nematic liquid crystal[128]. A roll pattern develops as in the R-B case (Fig. 1.4 a). Actually, up to 300 rolls can be seen in this experiment.

Another example of pattern formation, also from the fluid mechanics, is the Taylor Vortex flow. The centerpiece of the Taylor vortex problem is the instability of an infinitely long fluid column between a rotating inner and a resting outer cylinder[172], as was first possed by him in 1923. In fact, he went a step further and studied the instability when both cylinders rotate[170] (Fig. 1.4 b).
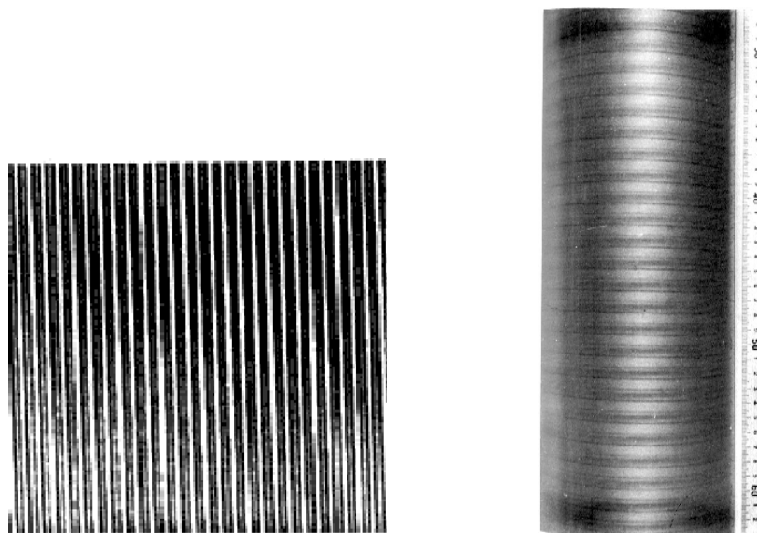
Figure 1.4: a) Typical pattern in electrohydrodynamic convection in nematic liquid crystals[128]. b) Center section of a fluid column with axisymmetric Taylor vortices between a rotating inner and resting outer glass cylinder[100]

Examples from Chemistry can also be found. A nonlinear chemical reaction with sufficiently complex reaction mechanism, maintained far from equilibrium may show the phenomenon of chemical pattern formation. A wide variety of patterns can be observed, concentric circles, spirals, hexagons, etc. (Fig. 1.5).
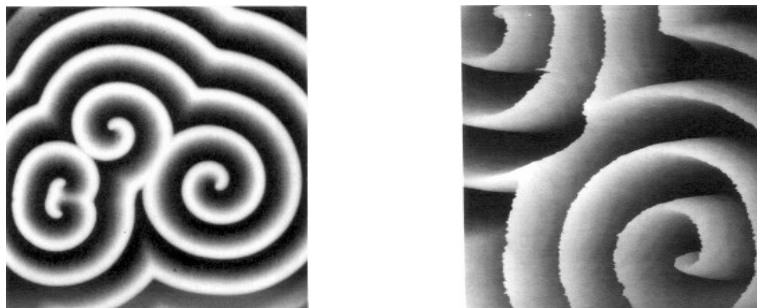
Figure 1.5: a) Spiral waves in the concentration of intermediate species in oscillating chemical reactions[127]. b) Idem as in a) but using a three-dimensional surface image of the collision area between a pair of spiral waves[127].

In Fig. 1.6 some experiments from nonlinear optics are displayed. Laser patterns obtained using counterpropagating laser beams in rubidium vapor are showed. Fig. 1.6a shows the near field pattern and Fig. 1.6b shows the far field[146]. The far field displays the characteristic peaks associated with a hexagonal structure of the near field pattern. Another optical pattern can be observed in Fig. 1.7. The pattern is produced with a nonlinear interferometer with two dimensional feedback .

Figure 1.6: Hexagonal pattern produced by the intensity of two counterpropagating beams that have crossed a rubidium cell [146]
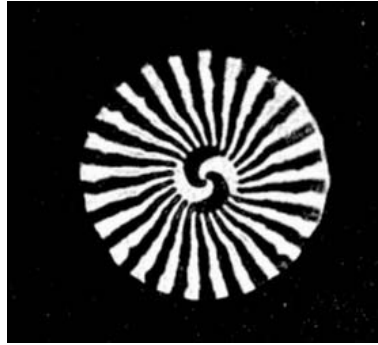
Figure 1.7: Still photograph of a rotatory wave pattern in an liquid crystal valve feedback system with rotated feedback[12].

Underlying universal phenomena can be found in the various experiments coming from different areas presented above. Similar patterns are found no matter which is the actual experiment (chemical reaction, R-B convection, nonlinear optics). The goal of a theory for describing Pattern Formation phenomena is to provide a means of understanding and explaining these patterns from a macroscopic viewpoint that both simplifies and unifies classes of problems which are seemingly unrelated at the microscopic level. Then, the interest is to describe the pattern by quantities like a characteristic wavelength, and to check its stability and possible further bifurcations.

Most of the stationary patterns shown in the experiments described above may undergo a sequence of transitions leading to regimes displaying aperiodic dependence in both space and time. Such disordered regimes will be referred as spatiotemporal chaos (STC). Systems exhibiting chaotic behavior that are not reducible to a model with a small number of degrees of freedom, even at the onset of chaos, are said to display spatiotemporal chaos because their description appears to require a large number of chaotic elements distributed in space. Loosely, the term spatiotemporal chaos is commonly accepted to refer to a deterministic system that has irregular variation and is unpredictable in detail, both in space and in time. The combination of spatial and temporal degrees of freedom has made such states extremely hard to characterize, both experimentally and theoretically. Often the experiments are possible only in regions difficult for theory to address, or theoretical models have no close experimental realizations. However, there are known examples of experimental systems, well characterized and precisely controlled[55, 52] that show such a behavior. Here I will mention a few of them. The Küpper–Lortz unstable state in rotating Rayleigh–Bénard convection is a system that exhibit STC and has been studied profusely experimentally[88], theoretically[130] and numerically[187, 54]. Also in the granddaddy of these experiments Rayleigh–Bénard convection "spiral defect chaos" has been experimentally reported[126, 139]. Figure 1.8 shows two shadowgraphs of the mentioned experiments. In Fig. 1.8a the pattern was obtained for convection in gaseous CO_2 (Prandtl number $= \sigma = 0.96$) in a large aspect ratio system ($\Gamma = radius/height = 78$). The second picture 1.8b shows a pattern for Rayleigh–Bénard convection in a cylindrical container with an aspect ratio $\Gamma = 41$ rotating at rotation rate $\Omega = 16$ (in dimensionless rotation rate) filled with CO_2.
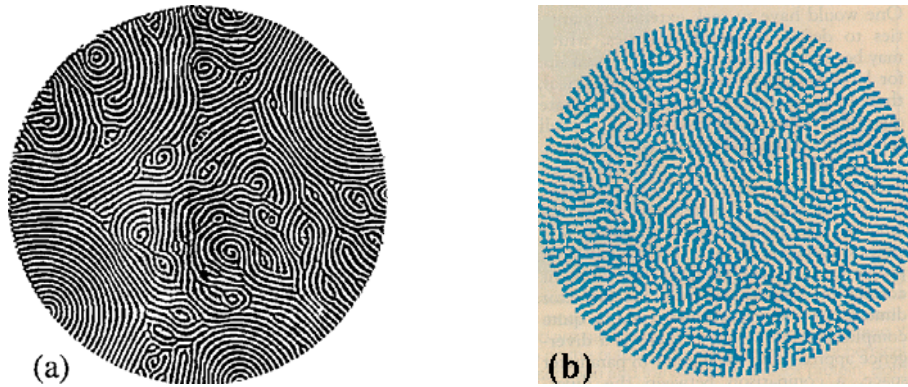
Figure 1.8: Spatio–Temporal Chaos in Rayleigh Bénard convection. a) Spiral defect chaos in large aspect ratio [126]. b) Chaotic patterns in rotating Rayleigh Bénard convection [139].

Another system exhibiting spatiotemporal chaos is electroconvection in nematic liquid crystal[55]. In Figure 1.9 a shadowgraphs of a spatiotemporal chaotic pattern in the weakly nonlinear regime is shown.
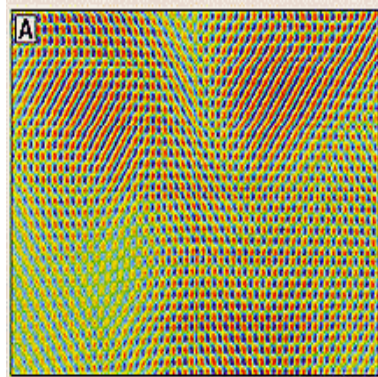
Figure 1.9: Spatio–Temporal Chaos in Electroconvection. An example for a Spatiotemporal chaos in a sample of nematic crystal [55].

An important problem in the study of these complex patterns is finding a suitable method for their analysis. In most cases it is possible to describe STC by weakly nonlinear theories valued in the proximity of threshold. Weak spatiotemporal chaos is an ubiquitous phenomenon in large nonequilibrium systems. Recent experimental and theoretical work has characterized this behavior and yield detailed data on the spatiotemporal evolution. Still there is no yet available a simple unified description of these essential features. Such description seems to be a new challenging task for the theorist and experimentalists in the field of nonequilibrium phenomena where concepts and methods from statistical mechanics and the theory of dynamical systems merge. Success in this field can be an important step

forward in the understanding of fully developed turbulence, which still stands as "the unsolved problem" in classical physics.

1.1.3 Approaches to the Problem

While the concern for unification is central in every attempt of man to explain the natural world, the particular approach followed in the studies of pattern formation phenomena is characterized by a great variety of techniques employed that differentiates from other traditional studies. The study of pattern formation phenomena introduces a new way of thinking based on a subtle interplay between qualitative and quantitative techniques, between topological , geometric and metric considerations, between deterministic and statistical aspects. It uses a large variety of methods from very diverse disciplines. Most important of all, the study of pattern formation phenomena helps to identify the appropriate level of description in which unification and universality can be expected.

The study of pattern formation has benefited from careful and controlled experiments as well as the development of new concepts and new analytic and numerical tools. This leads to different approaches to the problem:

The experimental approach continues giving rich information on the phenomena. A partial list of experiments has been provided in 1.1.2, but the list keeps growing day by day. Other lists can be found in some reviews[51, 179, 136, 33]. The prototypical experiment is that of a large system in d dimensions with control parameter R that can be varied through the first threshold R_c where the uniform state becomes unstable. The bulk of the experiments are focused in hydrodynamic systems. They have significant advantages: basic equations and parameter values are well understood, controlled quantitative experiments can be carried out, and a body of intuition about fluid flow has been built over centuries.

The theoretical approach begins by assuming a set of equations of motion, the microscopic equations, for which we assume that a uniform solution exists, and an instability to a spatially dependent solution arises for certain parameter values. One possible theoretical analysis is perturbation theory. The instability of the uniform state is established by a linear analysis, which reveals the basic physical mechanism leading to pattern formation. Immediately above the linear threshold perturbation theory in the nonlinearity leads to a simplified description in terms of amplitude equations[134, 133], whose forms are universal and whose numerical parameters reflect the details of each physical system. The word "universal" is here borrowed from critical phenomena meaning that: there are classes of phenomena all of which lead to the same equation. An interesting point is that no matter the physical system of departure, and therefore the detailed microscopic model, the analysis mentioned above leads to the **same** amplitude equations, depending only on very general characteristics such as symmetries or kind of instability. Further away from threshold a different type of perturbation is used: weak distortions of regular patterns involving spatial modulations over distance large compared to the basic period can be treated perturbatively leading to "phase equations"[147, 103, 102]. Another general method of analysis uses the qualitative theory of differential equations to find general features of the solutions. This approach is geometrical and topological and can be applied either at the microscopic level of description or the amplitude and phase equations. Apart from perturbation theory and qualitative methods it is sometimes possible to find

restricted classes of nontrivial exact solutions. In addition, statistical tools had proved to be useful in characterizing spatiotemporal chaotic behaviour[139, 69].

Finally there is the numerical approach of the problem. Quantitative data can be obtained through the numerical simulations of nonlinear systems. These "numerical experiments" allow to study systems inaccessible to analytic methods. Rather than simply confirming quantitatively results already anticipated by qualitative analysis, numerical experiments could produce qualitative insight where none has existed before.

Among these different approaches, this thesis focus on the analysis of universal features as described by amplitude equations introduced in the next section, and numerical methods

1.2   The Complex Ginzburg-Landau Equation

1.2.1   Amplitude Equations

The goal of the theory is to understand patterns from a macroscopic point of view that both unifies and simplifies classes of problems that are unrelated at microscopic levels. A significant step in achieving a macroscopic description is the identification of a suitable order parameter (or order parameters) for the system and writing down equations that capture its space–time evolution. These equations have universal properties. Though the coefficients depend on the particular microscopic system under consideration, the shape of the equation is determined by the nature of the symmetries, such as translation and rotation, that the original microscopic system enjoys, and by the type of instability.

The starting point is a reference state. Typically such a choice is associated with the state with the simplest behavior. Usually the choice is the spatially uniform, time–independent solution. From the loss of stability of this state one may determine the dominant shape (or shapes) of the first pattern to emerge.

The basic point of view is that, as the control parameter R is increased, these spatially extended, continuous, dissipative systems, undergo a symmetry–breaking phase transition or bifurcation. The first patterns to arise are periodic, in space and/or time, breaking translational symmetry (spatial and/or temporal). As the control parameter is increased the patterns become more complicated, and eventually exhibit spatiotemporal chaos.

Suppose that at some threshold value $R = R_c$ the system becomes *unstable* to infinitesimal perturbations with wave vector q_0 and frequency Ω_0 (either of which may be zero). For $R > R_c$ we expect a pattern centered around q_0 and Ω_0 to grow and in many cases to saturate to a macroscopic amplitude proportional to some power of $R - R_c$. When $\Omega_0 = 0$ we speak of *stationary* instability and when $\Omega_0 \neq 0$ we have *oscillatory* instablity. It is important to understand that, because of degeneracies, the pattern that finally emerges is not uniquely identified by linear stability investigation of the simple state. The set of states which are equally linearly amplified or remain neutrally stable as $R > R_c$ can contain many modes. Therefore linear theory can not discriminate between competing configurations. Instead, the final outcome is determined by a combination of external biases and the nonlinear coupling between various competing configurations linearly equivalent. The dimension of the system can be drastically reduced by choosing a coordinate system that clearly separates the modes that are dynamically active from those which play a passive role[134]. Near the onset $(R \gtrsim R_c)$ and provided the spectrum of the stability operator

is discrete, such reduction leads to *amplitude equations*[134]. If the spectrum of growth
rates is continuous it is possible (in some cases) to arrive to *envelope equations*[134]. In
what follows I will use the same name of amplitude equation for describing both type of
reduced equations.
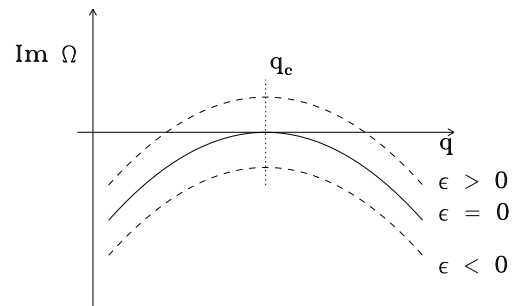
Figure 1.10: Behavior of the growth rate as a function of q
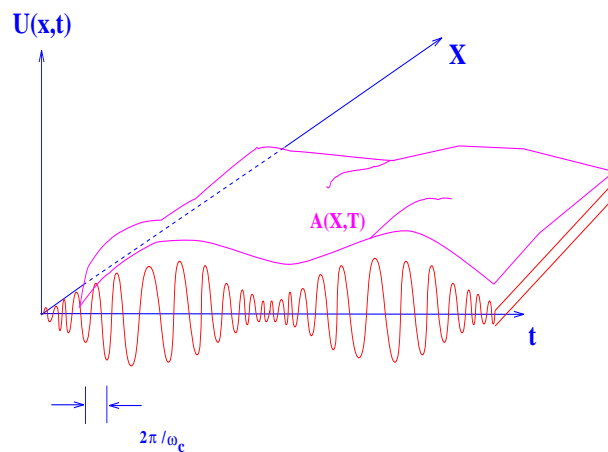
Figure 1.11: Slow modulation of the critical modes. The envelope is represented as a
surface

Amplitude equations describe the slow modulation in space and time of the dominant
modes near the threshold for an instability. I will use as control parameter $\epsilon = R - R_c$ so
that the instability occurs when ϵ becomes positive. In a translationally invariant system
it is then natural to consider the stability of Fourier modes. q_c denotes the wave number of
the mode whose growth rate is zero at $\epsilon = 0$. Then there is a narrow band around q_c where
the growth rate is slightly positive (of order ϵ) for $\epsilon > 0$ (see fig. 1.10). Let us assume that
the bifurcation is such that the pattern slightly above threshold has a small amplitude

(supercritical bifurcation). The pattern is expected to have a wavelength near $2\pi/q_c$. However, due to the fact that the width of the band of unstable modes is nonzero and of order $\epsilon^{1/2}$, there can be slow modulations of the patterns on length scales of order $1/\epsilon^{1/2}$. Close to threshold, a typical field looks like that sketched in fig. 1.11. We will restrict ourselves to the one dimensional case. In the case in which a traveling wave $(Re[\Omega] \neq 0$, that is, the bifurcation is of the Hopf type) mode of the form $\exp[-i\Omega_c t + iq_c x]$ becomes unstable for $\epsilon = 0$, the separation of the dynamics of the patterns close to threshold in terms of a fast component (with length scale set by the critical wave number) and an envelope that varies slowly in space and time can then be formulated by writing the relevant field(s) close to threshold as follows:

$$\text{physical fields} \propto A(x,t)e^{-i\Omega_c t + iq_c x} + A^*(x,t)e^{i\Omega_c t - iq_c x} + \text{higher harmonics} , \qquad (1.1)$$

where $A(x,t)$ is the complex envelope. A complex number is chosen since a phase change corresponds to a spatial translation of the unstable mode. "Higher harmonics" stands for terms proportional to $\exp(2iq_c x)$ and beyond. If the original system has a reflection symmetry $x \to -x$, we have always two such traveling wave modes becoming unstable at the same time, so that 1.1 should read;

$$\text{physical fields} \propto A_1(x,t)e^{i\Omega_c t + iq_c x} + A_2(x,t)e^{i\Omega_c t - iq_c x} + c.c. + \text{higher harmonics} , \quad (1.2)$$

where A_1 and A_2 are right– and left–traveling wave amplitudes, respectively and *c.c.* means complex conjugate. To lowest order in ϵ, A_1 and A_2 obey a set of coupled equations:

$$
\begin{aligned}
\partial_t A_{1,2} \pm v_g \partial_x A_{1,2} &= \mu A_{1,2} + (1 + i\alpha)\partial_x^2 A_{1,2} \\
&\quad -(1 + i\beta)\left(\mid A_{1,2} \mid^2 + \gamma \mid A_{2,1} \mid^2\right) A_{1,2} ,
\end{aligned}
\qquad (1.3)
$$

If the mode suffering the Hopf bifurcation $(Re[\Omega] \neq 0)$ is the one with $q_c = 0$, then 1.2 should be written as

$$\text{physical fields} \propto A(x,t)e^{-i\Omega_c t} + A^*(x,t)e^{i\Omega_c t} + \text{higher harmonics} , \qquad (1.4)$$

and the corresponding equation for A is

$$\tau_0 \frac{\partial A}{\partial t} = \epsilon A + \xi_0^2 \frac{\partial^2 A}{\partial x^2} - g \mid A \mid^2 A . \qquad (1.5)$$

For a given problem, the complex constants τ_0, ξ_0 and g can in principle be calculated from the starting equations. As they only set the scales of time, length, and of the size of the amplitude, they can be properly rescaled giving[1]

$$\frac{\partial A}{\partial t} = \mu A + (1 + ic_1)\frac{\partial^2 A}{\partial x^2} - (1 + ic_2) \mid A \mid^2 A . \qquad (1.6)$$

This equation is commonly referred as the **Complex Ginzburg–Landau Equation**(CGLE)[51, 179, 178, 134]. The coefficients μ, c_1 and c_2 are real. The coefficient μ can be positive or negative above or below the threshold of instability. This coefficient

---

[1] There are many different conventions for these coefficients, I follow those of [125]

can be rescaled to $\mu = 1$. This equation reminds the form of Ginzburg–Landau equation for superconductivity [68]. In fact, it seems that these authors never wrote down an evolution partial differential equation (see historical note on page 403 of [134]). Nevertheless, Landau wrote down amplitude equations (o.d.e.'s) to describe post–bifurcation behaviour of unstable modes. Thus, they introduced the concept of a space dependent order parameter for describing the behaviour of a thermodynamic system close to continuous phase transitions[108] and, as mentioned before, the structures of inhomogenous superconductors.

For the use of 1.6 in systems out of equilibrium pioneering work was made by Newell and Whitehead[135], and Segel[163] studying the post–critical Bénard convection. Later Stewartson and Stuart[167] applied these ideas to a wave system in a plane Poiseuille flow. A few years later, Kuramoto and Tsuzuki derived this equation for a model chemical reaction, the Bruselator[105]. A review of many of those developments has been given by Cross and Hohenberg[51]. For a rather extensive specific review on the CGLE, see Hohenberg and van Saarloos[179]. Now, I will summarize the main features of the CGLE equation.

- Symmetry considerations

    - This equation can be derived from the full equations describing the physical problem under study. Nevertheless, this equation arises naturally near any supercritical Hopf bifurcation if the system is time translationed invariant and reflection symmetric.

    - The reflection symmetry $(x \rightarrow -x)$ dictates that the lowest order spatial derivative term is of second order.

    - If the original pattern has time translational symmetry by an arbitrary time shift $\frac{\phi}{\Omega_c}$ equation (1.6) has to be phase invariant ($A \rightarrow Ae^{i\phi}$).

    - Keeping lowest order nonlinearities satisfying these symmetry requirements leads to the CGLE.

- Special cases

    - For $c_1 = c_2 = 0$ the CGLE reduces to the Real Ginzburg–Landau Equation[135, 163], adequate for describing superconductivity in the absence of a magnetic field. It can be written easily in terms of a "free energy" or Lyapunov functional.

    - In the limit $c_1, c_2 \rightarrow +\infty$ the equation reduces to the defocussing nonlinear Schrödinger equation. And for $c_2 \rightarrow +\infty$ and $c_1 \rightarrow -\infty$ the equation reduces to the focussing nonlinear Schrödinger equation. In both cases the equations are not only Hamiltonian but also integrable[96].

The fact that the CGLE reduces to an equation having a Lyapunov function in one limit and to a Hamiltonian equation in another limit makes it very interesting from a theoretical point of view. Besides, it is commonly stated that the nontrivial dynamical behavior, occurring also in other nonequilibrium systems, originates from the non-potential or non-variational character of the dynamics. Although for $c_1 \neq c_2$ the CGLE has not been derived from a Lyapunov functional the non–existence of such Lyapunov is not proven

and subject of a intense discussion. A detailed discussion of this problem will be the center of Chapter 2.

The CGLE presents, besides the well known plane wave solutions, other interesting solutions such as coherent structures with known analytic expression . It also presents chaotic behavior for certain values of the parameters (see 1.3.2). All these properties are enough for making valuable a study of the CGLE by its own. Besides, the CGLE has been used to explain the results of several experiments as described below.

1.2.2 Concrete Examples

Since the CGLE is the normal form for a Hopf bifurcation, it is possibly suitable for many systems that display such behavior as experiments on chemical reaction–diffusion, binary convection, and nonlinear optics (see 1.1.2). In general, the coefficients of the CGLE arise from the derivation from the microscopic equations. However, there are just a few experiments that allow to determine the values of the CGLE after the experimental data.

Here I will comment only two systems described by the CGLE. A reaction–diffusion chemical model and a fluid experiment. The first particular example is reaction–diffusion model known as the Prigogine–Lefever–Nicolis model (Brusselator model) [109, 110, 181]. This model was derived in an attempt to describe the experimental reaction–diffusion experiment of Belousov–Zhabotinsky.

The reaction scheme for this model is given as:

$$
\begin{aligned}
A &\rightarrow X \,, \\
2X + Y &\rightarrow 3X \,, \\
B + X &\rightarrow Y + D \,, \\
X &\rightarrow E \,,
\end{aligned}
\tag{1.7}
$$
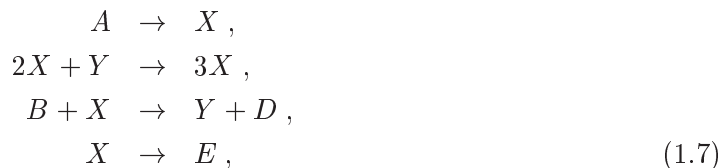
with the concentrations of reactants A and B constant, and the concentrations of species X and Y as the variables of interest. The species D and E leave the system after forming. Additionally all the reaction rates are set equal to one.

The equation of motion for X and Y is given by:

$$
\partial_t \mathbf{X} - \hat{D}\partial_r^2 \mathbf{X} = \mathbf{F}(\mathbf{X}) \,,
\tag{1.8}
$$

where $\mathbf{X}$ is a column vector with components X and Y, $\hat{D}$ is the diagonal diffusion matrix with components D_x and D_y (the diffusion constants), ∂_r^2 is the spatial derivative, and $\mathbf{F}$ is the reaction term obtained from eq. (1.7) by application of the law of mass action:

$$
\mathbf{F} = \left(\begin{array}{c} A - BX - X + X^2Y \\ BX - X^2Y \end{array} \right) \,.
\tag{1.9}
$$

As explained in detail in [9] when $\frac{D_x}{D_y} > \frac{\sqrt{1+A^2}-1}{A}$ the equation for the envelope $u(R,T)$ of the mode that destabilizes for $B > 1 + A^2$ can be written as:

$$
\partial_T u = u + (1 + ic_1)\partial_R^2 u - (1 + ic_2) \mid u \mid^2 u \,,
\tag{1.10}
$$

where T and R are rescaled time and space variables and the coefficients c_1 and c_2 are[106, 181]:

$$
\begin{aligned}
c_1 &= \frac{A(1 - \frac{D_x}{D_y})}{1 + \frac{D_x}{D_y}} \\
c_2 &= \frac{4 - 7A^2 + 4A^4}{3A(2 + A^2)}
\end{aligned}
\tag{1.11}
$$

As a second experiment I will comment here the bluff body flow experiment. In a series of recents papers Provansal and collaborators[115, 114, 113, 15] presented a model for the transition in bluff body wakes. These authors use as a theoretical model for such transition the CGLE. Besides, they calculated the parameters of the CGLE from the experimental data. The wake behind a circular cylinder, placed perpendicular to a uniform stream, is generally considered a reference system for the study of the transition to turbulence in open flows. The first step in this process is the Bérnard–von Kármán instability[23], which is characterized by the appearance of a periodic laminar vortex street in the Reynolds number range $50 < Re < 180$ for circular cylinders ($Re = Ud/\nu$ with U: free stream velocity, d: cylinder diameter, ν: kinematic viscosity). The Bérnard–von Kármán instability for low Reynolds numbers is a supercritical Hopf bifurcation which can be described by a Ginzburg–Landau envelope equation. It had been found that end effects, always present in experiments, are not negligible, even for long cylinders. This led Provansal and collaborators[115, 114, 113, 15] to study the wake of a ring, a bluff body of circular cross section, but without any ends. The ring is held in a plane perpendicular to the flow (see fig. 1.12).
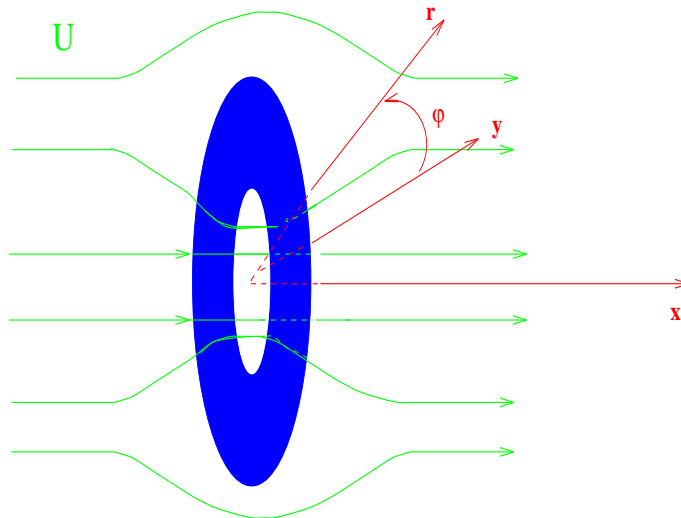
Figure 1.12: The torus is placed in plane perpendicular to the flow U. The cylindrical coordinates are indicated in the figure.

The wake parameters are U, d, ν, and D, the largest diameter of the ring. d^2/ν and d can be used as natural time and lengh units. Cylindrical coordinates (x, r, φ), with the

origin at the center of symmetry of the ring and the x axis pointing in the downstream direction, will be used in the following (see fig. 1.12). In this system, the wake formation region is represented by a one-dimensional array of diffusively coupled nonlinear oscillators distributed along the spanwise direction of the body (φ). The wake pattern is obtained by relating the downstream direction x to the time t. It must be emphasized that the CGLE model is used for modeling diffusive processes along the *spanwise* direction, allowing periodic boundary conditions, and therefore it has no dependence on the x direction. For the ring wake the following CGLE can be written[115, 114]:

$$\frac{\partial A}{\partial t} = \sigma(1 + ic_0)A + \mu(1 + ic_1)\frac{\partial^2 A}{\partial (D\varphi/2)^2} - l(1 + ic_2) \mid A \mid^2 A \ , \qquad (1.12)$$

where $A(\varphi, t)$ is the complex amplitude of the velocity fluctuations, $\sigma = k(\nu/d^2)(Re - Re_0)$, and k, μ, l, c_0, c_1 and c_2 are model parameters [15]. For different aspect ratio (D/d) different Re numbers and different geometries (cylinders or rings) these coefficients were determined (see [15] and references therein). The values of the parameters in the laminar range have been determined from measurements of the amplitude and the frequency of the velocity fluctuations in the wake of the bluff ring. After an appropriate rescaling[15] the equation (1.12) reduces to

$$\frac{\partial A}{\partial t} = (1 + ic_0)A + (1 + ic_1)\frac{\partial^2 A}{\partial z^2} - (1 + ic_2) \mid A \mid^2 A \ , \qquad (1.13)$$

With z the dimensionless spanwise coordinate. A satisfies periodic boundary conditions in z.

Furthermore, these authors found that the model parameters vary with the Reynolds number, suggesting then that secondary instabilities like Benjamin–Feir–Newell (see below 1.3.1) may appear. In fact, based in the experimental determination of the CGLE parameters in the periodic regime they posed the following dependence of these parameters in Re

$$c_0 = \frac{2\pi}{k}\frac{R_o}{Re - Re_c} + c_2 \ , \qquad (1.14)$$

where R_o a dimensionless frequency, the Roshko number, of the parallel vortex shedding is obtained experimentally. Also the parameter k is experimentally determined[15]. They also proposed that these values are valid for the transition range too, and so

$$c_1 = c_2 + 2.7 \ , \qquad (1.15)$$

with

$$c_2 = \begin{cases} -3 & \text{for } Re \leq 100 \\ -4.1 + 0.011Re & \text{for } Re > 100 \ . \end{cases}$$

For $Re < 100$, c_2 is approximately constant. But for $Re > 100$ the wake describes a trajectory in the $[c_1, c_2]$ parameter plane which is a function of the Reynolds number (Re). This allows a description of the different experimental behaviors in terms of the different behavior observed in the CGLE model as one moves through the parameter space (see 1.3.2). Actually the transition regime in this experiment could be explained in terms of

the transition from periodic stable regime to the turbulent regimes in the CGLE reported by Shraiman et al.[165].

In conclusion, in the latter experiment, the authors make several remarkable contributions.

- Once the identification with a supercritical Hopf bifurcation is established, they use the associated normal form, the CGLE, to model the phenomena.

- The coefficients of the CGLE were determined from experimental data and not from a deduction from a microscopic equation.

- They show experimental evidence of the transition from the stable regime to the turbulent regimes of the CGLE that was previously theoretically predicted.

The typical behavior of the CGLE equation through the different regions will be described bellow in 1.3.

As a final remark, very recently M. van Hecke and W. van Saarloos[177, 176] has calculated the coefficients for the CGLE that describes weakly nonlinear convection in large rotating annulus for a range of Prandtl numbers. They showed that the rotation rate can tuned the coefficients of the amplitude equations predicting that this system can be used to study spatio–temporal chaos in a controlled experiment.

1.3 General analysis of the Complex Ginzburg-Landau Equation

1.3.1 Plane Wave Solutions and Eckhaus Instability

The one dimensional Complex Ginzburg–Landau Equation (CGLE) has several known analytical solutions. In what follows I will use the scaled version of the CGLE:

$$\partial_t A = \mu A + (1 + ic_1)\partial_x^2 A - (1 + ic_2) \mid A \mid^2 A \ . \tag{1.16}$$

where ∂_t means partial derivative with respect to time, ∂_x^2 means the second partial derivative with respect to space and $A = A(x, t)$ is a complex function. The parameters c_1, c_2 and μ are real constants with the only restriction that $\mu > 0$, since I will be dealing with the case above threshold.

The simpler solutions known are the traveling waves (TW)

$$A_{tw}(x, t) = A_0 e^{i(kx - \omega t)} \ . \tag{1.17}$$

Both the amplitude($\mid A_0 \mid$) and the frequency (ω) of the traveling wave solutions are related to the wave number k.

$$\mid A_0 \mid = \sqrt{\mu - k^2} \quad \omega = c_2 \mu + (c_1 - c_2)k^2 \tag{1.18}$$

A_0 is undetermined in an arbitrary constant phase.

As can be seen from eq. (1.18) there is a range of existence for the traveling wave solution($-\mu^{1/2} < k < \mu^{1/2}$). There is also a well known band of stability for these solutions that will be reviewed further on. Just like k measures the difference between the

wave number of the physical pattern and the critical wave number, so ω: measures the difference between the frequency of the physical pattern and the frequency of the critical mode. The equation for the frequency (1.18) can be rewritten as $\omega = c_2 \mid A_0 \mid^2 - c_1 k^2$ illustrating that c_1 is the coefficient that measures the strength of the linear dispersion, i.e., the dependence of the frequency of the waves on the wave number, while c_2 is a measure of the nonlinear dispersion. A typical profile of a traveling wave solution is shown in Fig. 1.13. In Fig. 1.13a-c), the phase, the phase gradient, and the modulus as a function of x at a fixed time is shown. The modulus corresponds to the constant $\mid A_0 \mid$ and the gradient of the phase to the wave number (k) while the phase grows linearly with x $(\varphi = kx)$. Finally Fig. 1.13d) represents (for a given time) the complex envelope (A) as a function of x. Note that the plane perpendicular to the x axis is a complex plane. In this last representation the meaning of the winding number or rotation number is clearly be seen, as the number of windings of the traveling wave. Such quantity is defined in terms of the phase φ as

$$\nu \equiv \frac{1}{2\pi} \int_0^L \partial_x \varphi dx \ . \tag{1.19}$$

L is the system size.

The linear stability analysis of the traveling wave solutions 1.17 is quite straightforward, and can be found in various reviews[51, 179, 102, 33, 65].
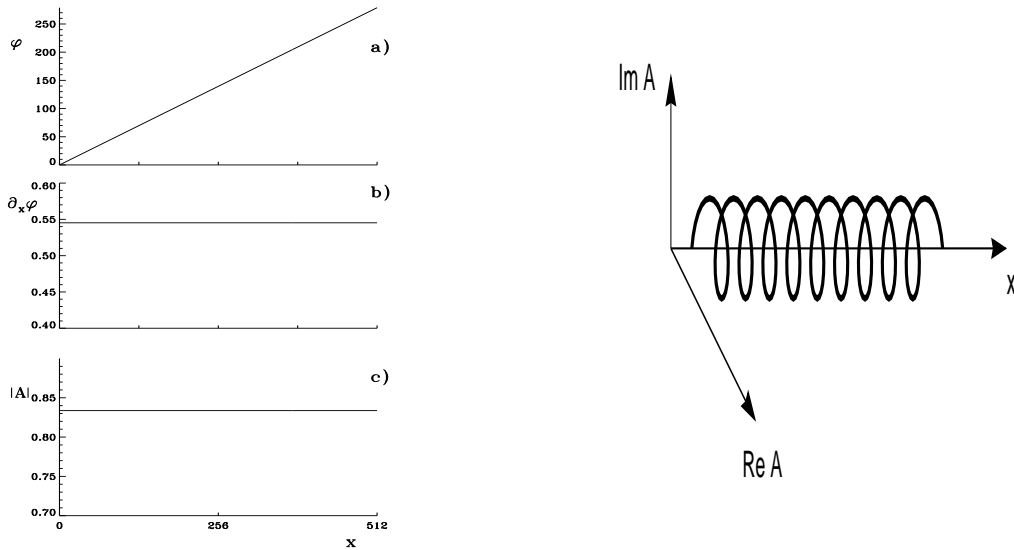
Figure 1.13: Typical profile of a traveling wave solutions at a given time. It corresponds to $c_1 = -1.5$ and $c_2 = -0.9$ and a wave number $k = 0.549$ a) Corresponds to the phase φ as a function of the space x b) the phase gradient $\partial_x \varphi = k$ c) the modulus $\mid A_0 \mid = \sqrt{1 - k^2}$ d) Complex envelope (A) as a function of space.

Consider the time evolution of small perturbations in the amplitude and phase of a

plane wave

$$A(x,t) = (Q + \epsilon r(x,t))e^{i(kx-\omega t+\epsilon\phi(x,t))}\,, \tag{1.20}$$

where $Q = \sqrt{\mu - k^2}$ is the amplitude of the plane wave, $r(x,t)$ and $\phi(x,t)$ are real perturbations in the amplitude and phase respectively and ϵ is a formal parameter to keep track of small numbers.

Substituting (1.20) in (1.16) yields to a polynomial in ϵ up to order ϵ^5. The terms of order ϵ^0 vanish identically. The first order terms yield the linearized equations for the perturbations

$$\partial_t r = 2Q^2 r - 2Qk\partial_x\phi - 2c_1 k\partial_x r - c_1 Q\partial_x^2\phi + \partial_x^2 r \tag{1.21}$$

$$\partial_t \phi = -2c_2 Qr - 2c_1 k\partial_x\phi + 2\frac{k}{Q}\partial_x r + \partial_x^2\phi + \frac{c_1}{Q}\partial_x^2 r \tag{1.22}$$

The linear system (1.21) and (1.22) can be solved using Fourier modes, that is, solutions proportional to $e^{\eta t + iqx}$, where for periodic boundary conditions q is real whereas η is in general a complex quantity. By substituting in (1.21) and (1.22) a dispersion relation can be obtained

$$\begin{vmatrix} \eta + 2Q^2 + q^2 + 2ic_1 kq & 2iQqk - c_1 Qq^2 \\ c_1 q^2 + 2c_2 Q^2 - 2ikq & Q\eta + Qq^2 + 2ic_1 Qqk \end{vmatrix} = 0\,. \tag{1.23}$$

The solutions of (1.23) are

$$\eta = -(Q^2 + q^2 + 2ic_1 qk) \pm \sqrt{u + iv} \tag{1.24}$$

where u and v are polynomials

$$u = Q^4 + 4q^2 k^2 - 2c_1 c_2 Q^2 q^2 - c_1^2 q^4 \tag{1.25}$$

$$v = 4c_1 kq^3 + 4c_2 Q^2 qk \tag{1.26}$$

The real part of η indicates the growth rate.

$$Re(\eta) = -Q^2 - q^2 \pm \sqrt{\frac{u + \sqrt{u^2 + v^2}}{2}} \tag{1.27}$$

There are two different branches. The "amplitude modes" correspond to the negative sign of the square root in (1.27). For any value of c_1, c_2 and q, $Re(\eta)$ as a function of the perturbation wavelength k is always negative and takes the value $Re(\eta) = -2Q^2$ at $q = 0$ as shown in Fig. 1.14.
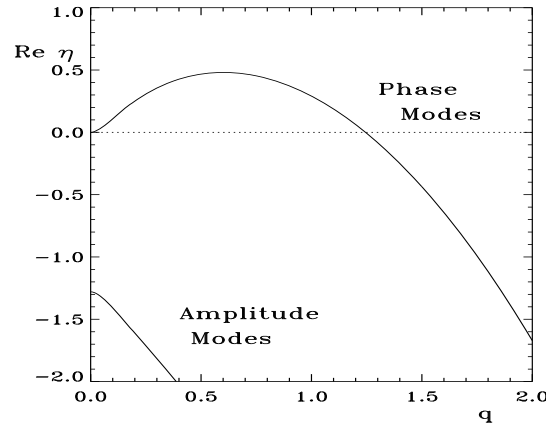
Figure 1.14: The growth rate (1.27) *vs.* the wave number of the modes q of the perturbation. For the set of parameter values $c_1 = -0.2, c_2 = -4.0$ and $k = 0.6$, the "Amplitude modes" are damped, while the "Phase modes" are unstable and identify a mode of fastest growth.

The "phase modes" are associated to the positive sign of the square root in (1.27). This branch vanishes identically at $q = 0$ for any value of the parameters c_1, c_2 or plane wave wavelength k. This indicates that all the plane wave solutions are marginally stable against homogeneous perturbation. The origin of this neutral stability is the phase invariance $A \rightarrow Ae^{i\varphi}$ of the solutions of eq. (1.16). For q very large, this branch is negative and behaves as $-q^2$, so short wavelength perturbations are always damped. However, in general, long wavelength perturbations can be either stable or unstable. To see this we expand (1.27) for small q.

$$Re(\eta) = Dq^2 + O(q^4)\,, \tag{1.28}$$

where

$$D = -(1 + c_1 c_2) + 2(1 + c_2^2)\frac{k^2}{Q^2}\,. \tag{1.29}$$

If this coefficient is positive, there is a range of unstable perturbation wavelengths. The condition $D > 0$ identifies the standard Eckhaus[61] instability. For $1 + c_1 c_2 > 0$ plane wave solutions are linearly stable for wave numbers smaller than a limit value $|k| \leq k_E$. For $|k| > k_E$, plane waves are unstable with respect to long wavelength perturbations (Eckhaus instability [61]). The limit value k_E is given by

$$k_E^2 = \frac{\mu(1 + c_1 c_2)}{3 + c_1 c_2 + 2c_2^2}\,. \tag{1.30}$$

However, this limit is only an upper bound, because it was obtained in an expansion of eq. (1.27). If the full expression (1.27) is considered it may occur that for certain values of k the plane wave is unstable also for $k < k_E$, despite $D < 0$.

The stability and existence ranges of traveling wave solutions is indicated in Fig. 1.15 for given values of c_1 and c_2. The stability range vanishes at $1 + c_1 c_2 = 0$ (the Benjamin–Feir–Newell (BFN) line[173, 131]), and no stable plane wave solution exists for $1 + c_1 c_2 < 0$.
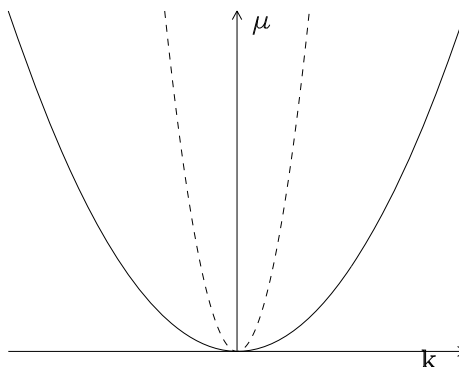
Figure 1.15: Eckhaus instability diagram. The pattern generating primary instability occurs inside the outer parabola (solid line), but the resulting pattern is stable only within the inner parabola(dashed line) corresponding to (1.30).

Intuitively the Eckhaus instability could be understood in the following way. The amplitude A for the homogeneous state ($A = 0$) is unstable. When the wave number k is increased and goes near the limit of existence ($k \to \mu$), the amplitude goes to zero ($A^2 = \mu - k^2$) so for continuity arguments it must be unstable too.

The fact that all traveling wave solutions are unstable for $1 + c_1 c_2 < 0$ leads to various types of chaotic behavior, which are described in the next section.

1.3.2   Regimes in the CGLE

Systematic numerical work for L large [165, 42, 43, 64] has identified regions of the parameter space displaying different kinds of regular and spatio-temporal chaotic behavior, leading to a "phase diagram" for the CGLE. This diagram was obtained with numerical solutions obtained for long time from particular initial conditions and periodic boundary conditions. The initial condition was a steep pulse[43]. Also, in the phase turbulence region, initial conditions with non-zero winding number were explicitly avoided, as will be discussed in chapter 3. Five different regions, each leading to a different asymptotic phase, are shown in Fig. 1.16[2] as a function of the parameters c_1 and c_2 ($\mu = 1$, without loss of generality, L large). In what follows I will describe this regions and I will comment on the transition lines defined by them. The diagram shown in 1.16 is half of the parameter space, the other half is symmetric, due to the symmetry of the equation under simultaneous changes $c_1 \to -c_1, c_2 \to -c_2$.

---

[2]An interactive map of this diagram with the characteristic behaviour of the different zones can be found in http://www.imedea.uib.es/ montagne/cgle/cglem.html
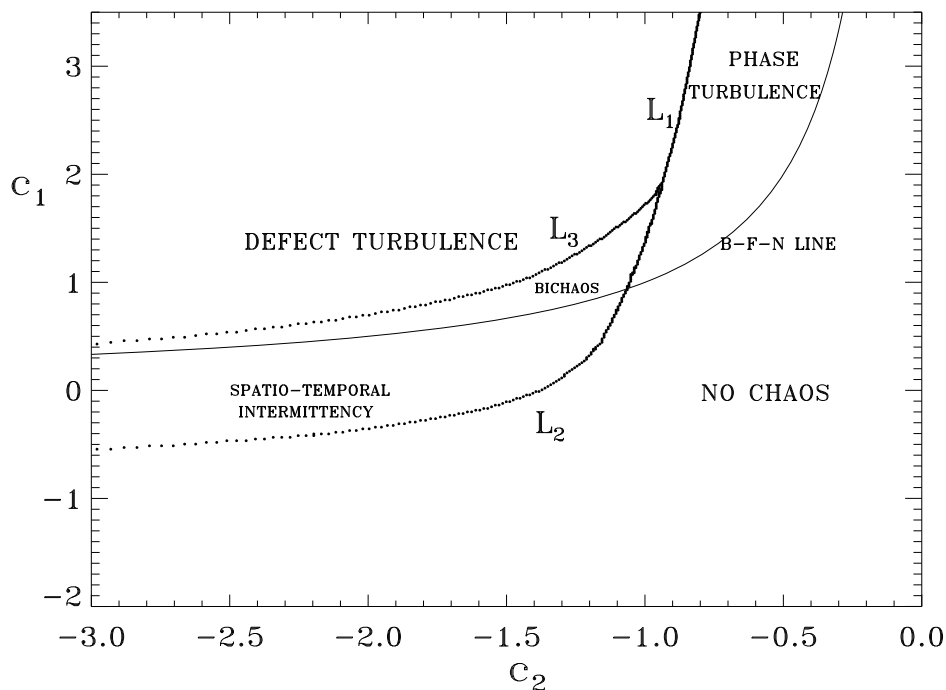
Figure 1.16: Regions of the parameter space $[c_1 - c_2]$ for the $d = 1$ CGLE displaying different kinds of regular and chaotic behavior. The Benjamin-Feir–Newell line (B–F–N line) determined analytically is shown as a solid line.

Two of these regions are in the BFN stable zone and the other three in the BFN unstable one. One of the main distinctions between the different asymptotic phases is in the behavior of the modulus of A at long times. In some regions it never vanishes, whereas in others it vanishes from time to time at different points. A detailed description of the asymptotic behavior in the different regions is as follows:

1. Non-Chaotic region. The evolution here ends in one of the Eckhaus-stable TW solutions for almost all initial conditions. The attractors in this region are stable TW solutions.

2. Spatio-Temporal Intermittency region. Despite the fact that there exist stable TWs, the evolution from random initial conditions is not attracted by them. Instead, a chaotic attractor is reached in which typical configurations of the field A consist of regions of TW interrupted by turbulent bursts. The modulus of A in such bursts typically touches zero quite often. In Fig. 1.17 we show typical spatiotemporal evolution for Spatio–Temporal Intermittency (STI). In 1.17a) I show the $\mid A \mid^2$ with time running upwards and x in the horizontal direction. The lighter red corresponds to the maximum value of $\mid A \mid^2$ and darker to the minimum. The triangular zones correspond to regions of constant modulus, that is, regions of TW. These regions are limited by localized structures, that evolve in a complicated way. Sometimes

these localized structures burst in other "hole–like" objects that resemble the Bekki–Nozaki holes, that will explained in next section. Figure 1.17b) shows the phase $\varphi(x, t)$. It can be observed that, corresponding to the regions of constant modulus (i.e. TW zones) the lines of constant phase remain continuous whereas they are interrupted at the edge of the triangle by a phase discontinuity due in general to a zero of the modulus. In Fig. 1.17c–e) a snapshot for the phase, the phase gradient and the modulus at a given time are shown, respectively.

3. Defect Turbulence (DT). This is a strongly disordered region in which the modulus of A has a finite density of space-time zeros (defects). In addition, the temporal correlation functions have a quasi-exponential decay [165, 42]. Finally, the winding number ν, defined in (1.19), presents strong fluctuations. In this region there are not only defects, but also other localized structures displaying a rich dynamics. In Figure 1.18 a typical configuration is shown. It can be seen in 1.18a) how the defects evolve, colliding with each other, disappearing and creating new ones. It can be seen in 1.18b) how at each (space–) time that the modulus goes to zero the phase is not defined and thus, a discontinuity appears. As before, in 1.18c–e) snapshots show the turbulent aspect for the three variables.

4. Phase Turbulence (PT). This is a weakly disordered phase in which $|A(x, t)|$ remains away from zero, meaning that the density of spatiotemporal defects is zero. The temporal correlations decay slower than exponentially [165, 42]. The behavior of the phase in this region strongly resembles the turbulent behavior of the the Kuramoto–Sivashinsky equation (KSE)[101, 102, 166]. Besides, within certain limits (that will discussed in Chapter 3) the phase of states of the CGLE can be approximated by a KS-like equation. On the other hand, while it was said that the winding number remain constant[165, 42, 43], it was recently demonstrated that this is so[125, 123] only if it lies in a given range (see Chapter 3). A typical configuration is shown in Fig. 1.19 as in previous figures. The modulus shows (Fig. 1.19a) the evolution of tiny pulses and wave shocks wiggling around. The lines of constant phase (1.19b) are continuous due to the absence of defects. In the snapshots 1.19c–e) it can be seen how the modulus keeps far apart from zero (notice the scale), and the pulse and shocks are very small. The phase gradient presents a strong turbulent aspect.

5. Bi-Chaos region. Depending on the particular initial condition, the system ends up on attractors similar to the ones in regions 3, 4, or in a new attractor in which the configurations of A consists of regions of phase and defect turbulence. In Figure 1.20 a typical configuration of this last a attractor is shown. It can be observed how regions of Phase Turbulence (triangular patches) alternate with localized structures being themselves very often defects, corresponding to a Defect Turbulence behavior.

These regions are limited by several lines. The BFN line is the only one obtained analyticaly in the diagram 1.16. It corresponds to the Benjamin–Feir–Newell line, explained in 1.3.1. The other three lines were obtained numerically. The line L_2 corresponds to the limit of Spatio–Temporal Intermittency (2) and the No–Chaos region (1). Although this line was obtained from numerical observation, there is a great coincidence with the analytically obtained line AI for the stability of the holes solution of the diagram in Fig. 1.24. The lines L_1 and L_3 were first obtained

through numerical observations in combination with some statistical analysis. L_3 separates the Bichaos from the Phase Turbulence region.

Recently, the transition line L_1 from DT (region 3) to PT (region 4) has received much attention. Several questions about this line have been posed and the answer to them is an effervescent theme of research[119, 63, 32, 64, 62, 125, 123, 174, 175]. The main question is if the PT–DT transition is a true phase transition in the sense that it remains well defined in the infinite system size limit. Such question, together with the analysis of proper diagnostic tools to characterize the transition will be addressed in Chapter 3.
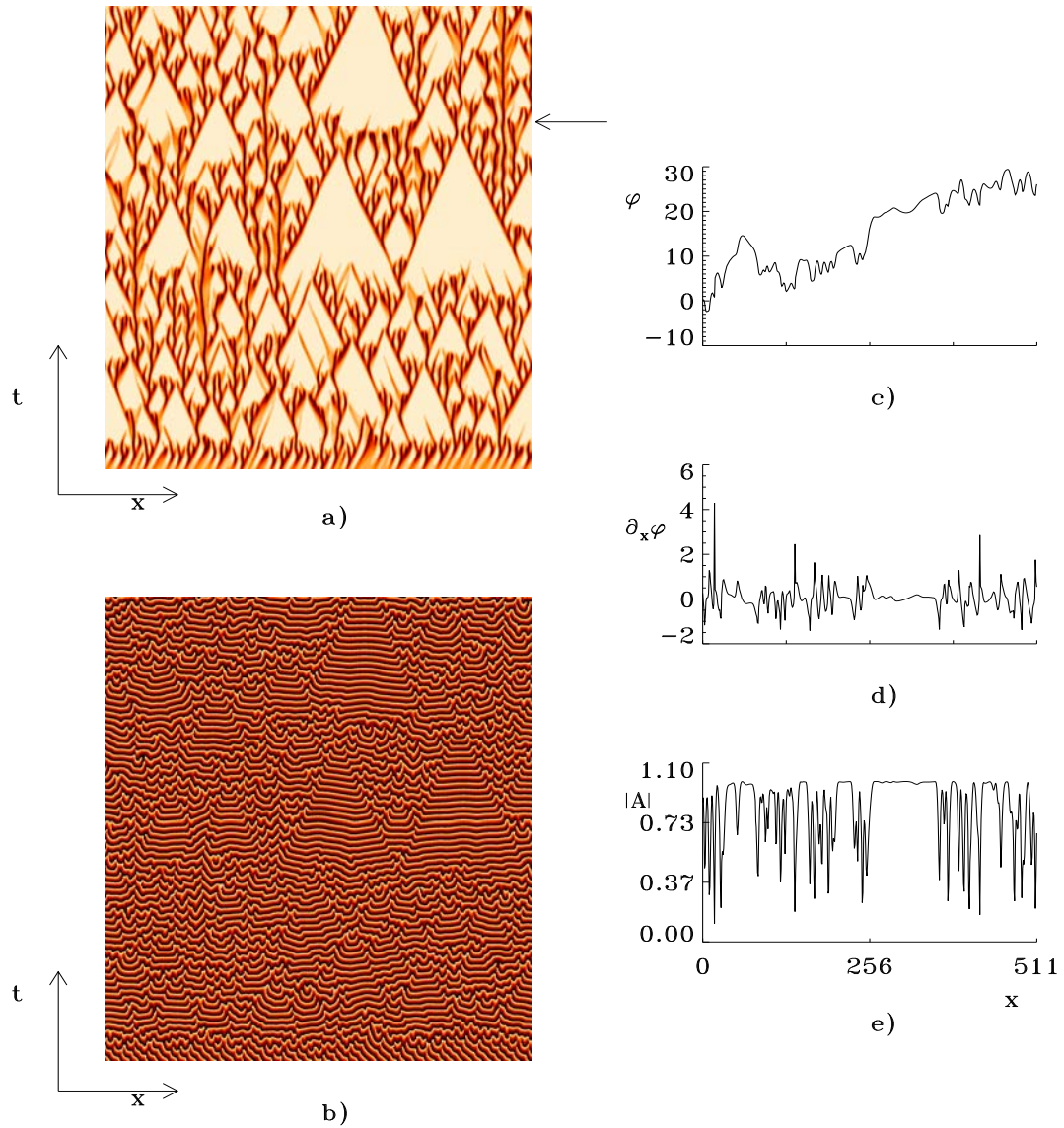
Figure 1.17: a) Spatiotemporal evolution of $| A(x, t) |$. Typical configuration starting from random initial condition for 250 time units in the STI region. The lighter color corresponds to the maximum value of $| A(x, t) |$ and darker to the minimum. $c_1 = 0.0$, and $c_2 = -2.1$. b) Idem as (a) but for $\varphi(x, t)$ c) A snapshot of the phase $\varphi(x, t)$ as a function of x for $t = 210$ which is indicated by an arrow in a). d) Idem as c) but for $\partial_x \varphi(x, t)$. e) Idem as c) but for $| A(x, t) |$.
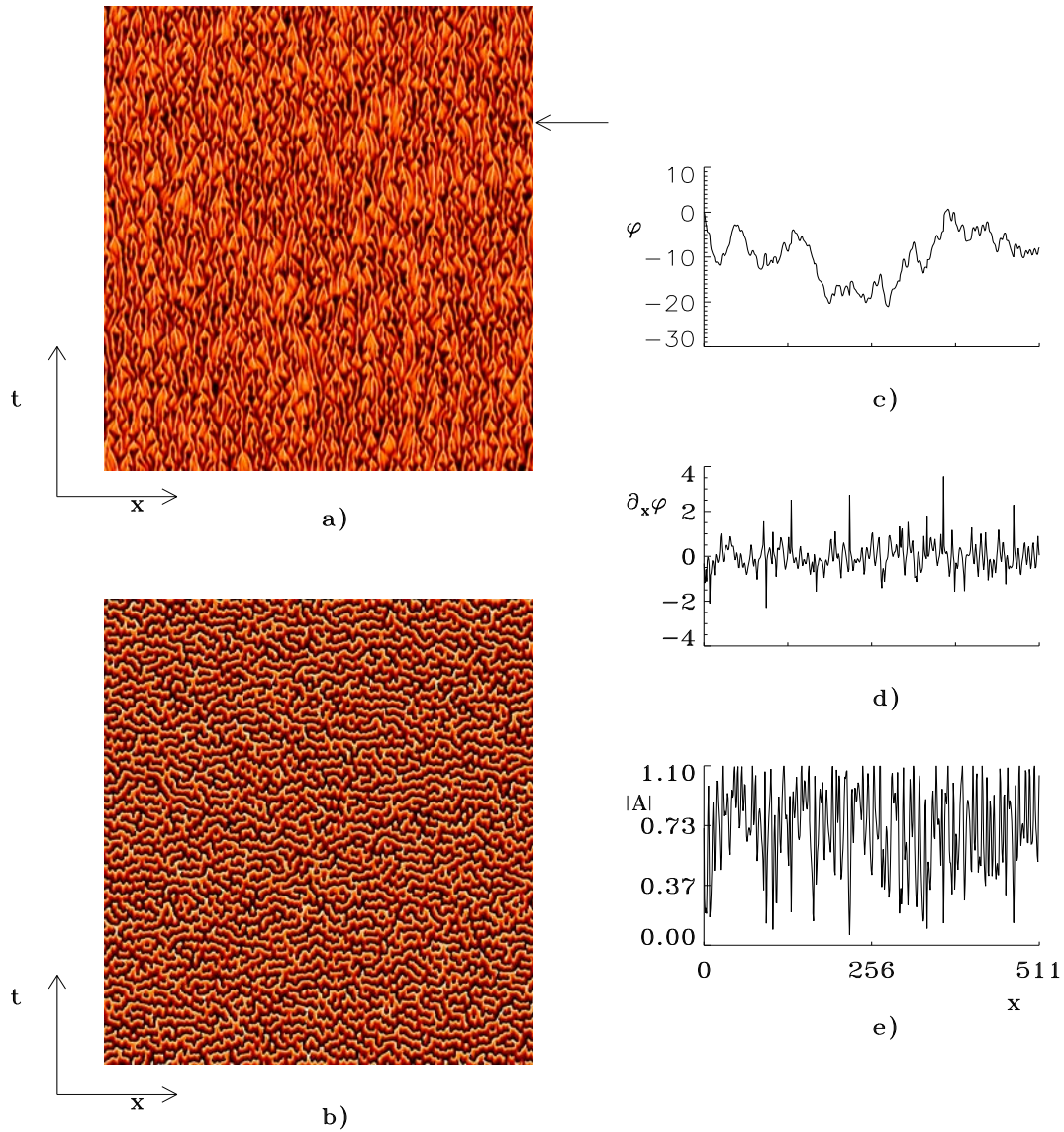
Figure 1.18: a) Spatiotemporal evolution of $\mid A(x,t)\mid$. Typical configuration starting from random initial condition for 250 time units in the DT region. The lighter color corresponds to the maximum value of $\mid A(x,t)\mid$ and darker to the minimum. $c_1 = 1.5$, and $c_2 = -2.1$. b) Idem as (a) but for $\varphi(x,t)$ c) A snapshot of the $\varphi(x,t)$ as a function of x for $t = 220$ which is indicated by an arrow in a). d) Idem as c) but for $\partial_x\varphi(x,t)$. e) Idem as c) but for $\mid A(x,t)\mid$.
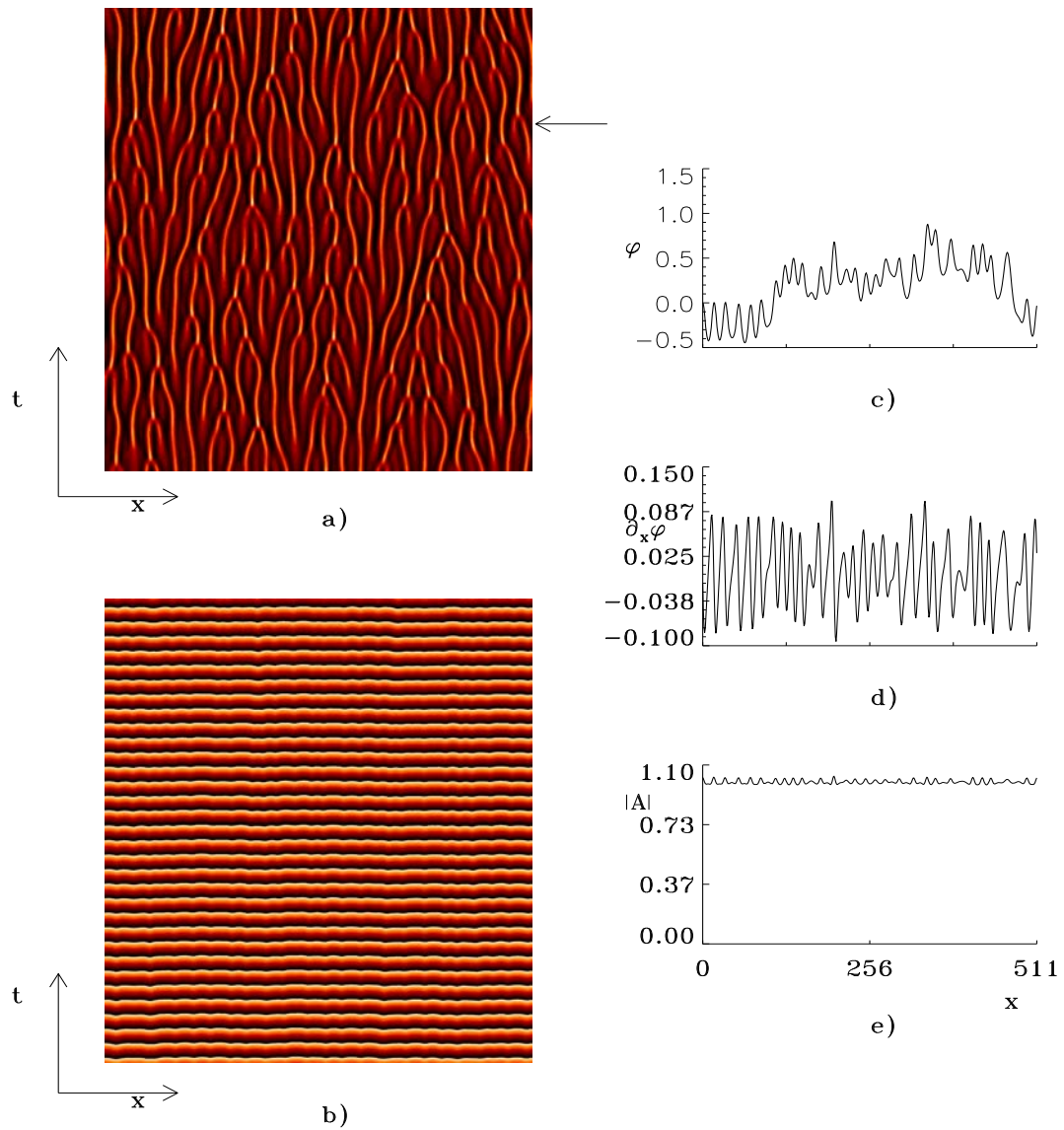
Figure 1.19: a) Spatiotemporal evolution of $\mid A(x,t)\mid$. Typical configuration starting from random initial condition for 250 time units in the PT region. The lighter color corresponds to the maximum value of $\mid A(x,t)\mid$ and darker to the minimum. $c_1 = 1.5$, and $c_2 = -0.9$. b) Idem as (a) but for $\varphi(x,t)$ c) A snapshot of the $\varphi(x,t)$ as a function of x for $t = 220$ which is indicated by an arrow in a). d) Idem as c) but for $\partial_x \varphi(x,t)$. e) Idem as c) but for $\mid A(x,t)\mid$.
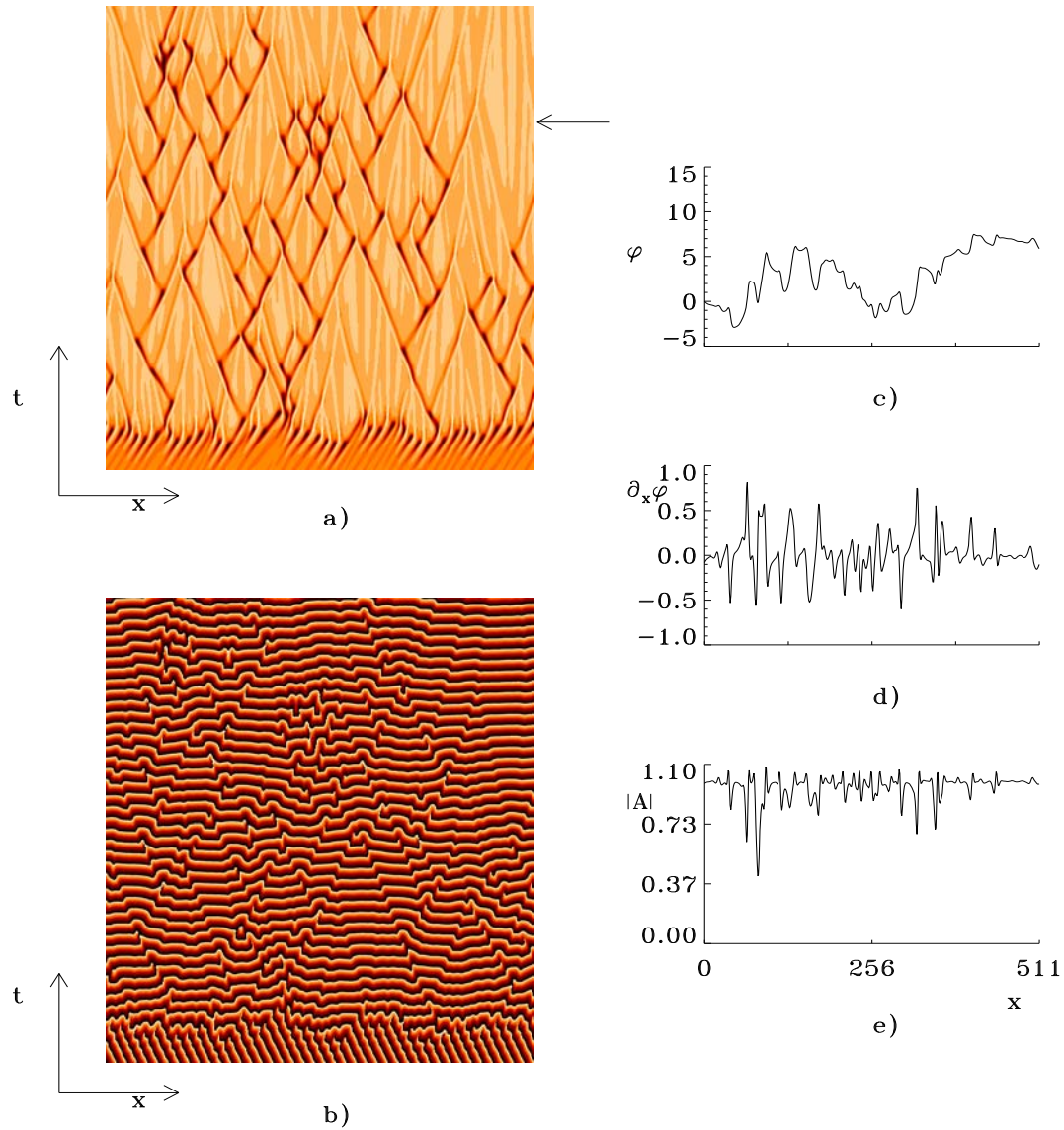
Figure 1.20: a) Spatiotemporal evolution of $| A(x,t) |$. Typical configuration starting from random initial condition for 250 time units in the Bichaos region. The lighter color corresponds to the maximum value of $| A(x,t) |$ and darker to the minimum. $c_1 = 1.1$, and $c_2 = -1.2$. b) Idem as (a) but for $\varphi(x,t)$ c) A snapshot of the $\varphi(x,t)$ as a function of x for $t = 210$ which is indicated by an arrow in a). d) Idem as c) but for $\partial_x \varphi(x,t)$. e) Idem as c) but for $| A(x,t) |$.

1.3.3   Localized Solutions

In addition to the traveling wave solutions there are other solutions of the CGLE that can be obtained in a closed analytic form. In what follows I will give a brief overview of the other known analytic solutions of the CGLE. I will consider solutions generically called *coherent structures*[179]. These are solutions that are either localized or that consist of domains of regular traveling waves connected by localized defects or interfaces. Names such as front, pulse or hole are given to them according to the shape of its modulus. When they emit or absorb perturbations from the surroundings they are also called source or sink, respectively.
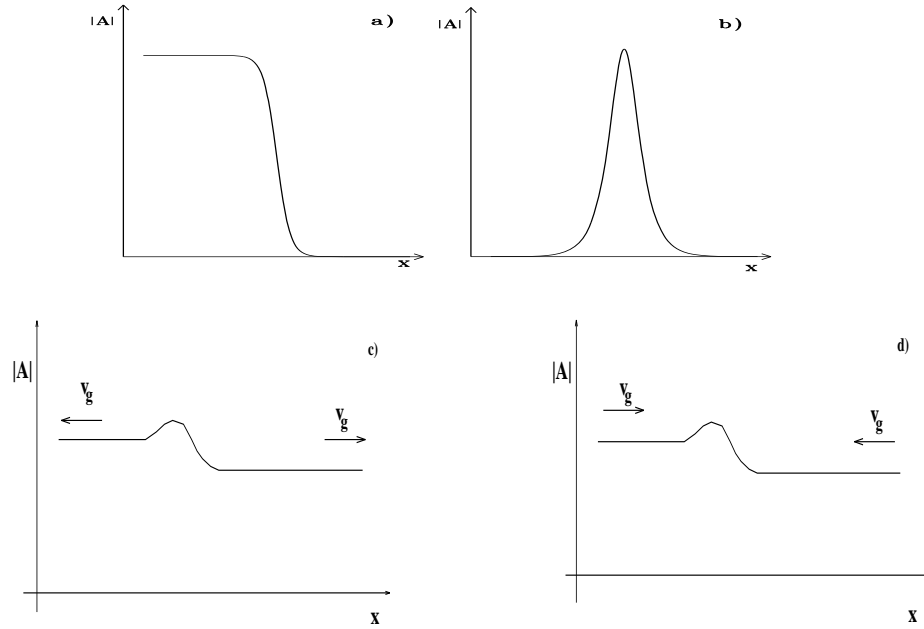
Figure 1.21: Possible coherent structures solutions. a) Front. b) Pulse. c) A shock acting as a source (v_g is a group velocity in the frame moving with the structure) d) Sink.

In particular, I address uniformly moving solutions of the CGLE. This analysis can be simplified if the partial differential equation (PDE) (1.16) is reduced to a set of ordinary differential equations (ODE). This can be easily achieved through the change of variables $\xi = x - vt$ where v is the velocity of the uniformly translating solutions. Specifically, by using the ansatz

$$A(x,t) = e^{-i\omega t}\hat{A}(x - vt), \quad \hat{A}(x - vt) = \hat{A}(\xi) = a(\xi)e^{i\Phi(\xi)} , \qquad (1.31)$$

where ω and v are real parameters. Substituting (1.31) into the PDE (1.16), this is reduced to a set of ODE's for the amplitude and the phase of $\hat{A}$. Actually, this set of ODE's can be put as a set of first order ODE's setting

$$q(\xi) = \partial_\xi \Phi , \quad \kappa(\xi) = a^{-1}\partial_\xi a . \qquad (1.32)$$

Inserting (1.32) in (1.16), one obtains (for details see [179])

$$
\begin{aligned}
\partial_\xi a &= \kappa a \\
\partial_\xi q &= -\omega + c_1 v\kappa - vq - 2\kappa q + \left[c_1 \mu - (c_1 - c_2)a^2 \right] \\
\partial_\xi \kappa &= -c_1 \omega - v\kappa - c_1 vq - \kappa^2 + q^2 - \left[\mu - (1 + c_1 c_2)a^2 \right] \ ,
\end{aligned}
\tag{1.33}
$$

The study of the dynamical system (1.33) was performed by W. van Saarloos and P. C. Hohenberg[179]. They found fixed points, and studied their stability. From their analysis they identified several possible coherent structures illustrated in Fig. 1.21 . Also guided by heuristic stability arguments they make an ansatz for the solution of this set of ODE's. Introducing such ansatz in eqs. (1.33) leads to a set of overdetermined nonlinear algebraic system of equations. The compatibility of such system is a set of equations that couple the parameters introduced in the ansatz with the free parameters ω and v introduced in (1.31) (see [179]). The solution so obtained is a front solution. This front solution connects a traveling wave solution of wavenumber k with the state $A(x,t) = 0$. Other known solutions can be obtained with other ansatz.

This moving front solution can be obtained in a simpler way: introducing the ansatz (1.31) in the CGLE (1.16) and assuming $\Phi(\xi) = k\xi$ leads to the following expression for the front

$$
A(x,t) = a(x - vt)e^{i[kx - \omega t]} \ ,
\tag{1.34}
$$

where

$$
\begin{aligned}
a(x - vt) &= \sqrt{\frac{h_1}{h_2 + h_1 e^{-2h_1(x-vt)}}} \\
\omega &= \omega_{tw} - 2c_1 k^2 \\
\omega_{tw} &= c_2 \mu + (c_2 - c_1)k^2 \\
v &= 2c_1 k \\
h_1 &= \frac{-\omega + c_1 + 2c_1 k^2}{2k} \\
h_2 &= \frac{c_1 - c_2}{2k} \ ,
\end{aligned}
\tag{1.35}
$$

K. Nozaki and N. Bekki[25] obtained additional exact solutions of the CGLE. The well known Nonlinear Schrödinger equation (NLSE) (an integrable equation) has coherent exact solutions known as bright and dark solitons. These solutions can be obtained with different methods (see for example [132]): inverse scattering, symmetry reduction or the Hirota's bilinear method. K. Nozaki and N. Bekki applied the Hirota's bilinear method[84] to the CGLE in order to obtain exact solutions. The main idea is that after a suitable transformation of the amplitude $A(x,t)$ of the CGLE (1.16), the equation thus obtained can be solved exactly. The transformation is the following

$$
A(x,t) = \frac{Ge^{i(Kx - \Omega t)}}{F^{1 + i\alpha}} \ ,
\tag{1.36}
$$

where K, Ω and α are real parameters to be determined. The functions $F(x,t)$ and $G(x,t)$, with the restriction that $F(x,t)$ is real, are obtained solving a bilinear differential equation

in terms of a modified bilinear operator function[140, 25]. After a tedious algebra three exact solutions can be obtained (for a detailed calculation see W. van Saarloos and P. C. Hohenberg[179] pags. 337-338). These solutions are known as the *Bekki–Nozaki solutions* (B–N). For these solutions the parameters α, β and A_0 are fixed and given by

$$
\begin{aligned}
\alpha &= -\beta \pm \sqrt{2 + \beta^2} \ , \beta = \frac{3}{2} \frac{1 + c_1 c_2}{c_2 - c_1} \\
A_0 &= \frac{1 + c_1 c_2}{(1 + c_1^2)(\alpha^2 - 2)} \ .
\end{aligned}
\tag{1.37}
$$

Setting $K = \Omega = 0$ a standing solitary wave or pulse solution is obtained

$$
A(x, t) = \frac{g e^\theta}{(1 + e^{\theta + \theta^*})^{1 + i\alpha}} \ , \ \theta = kx - \omega t \ ,
\tag{1.38}
$$

where k, g and θ are complex (* means complex conjugate) and

$$
\begin{aligned}
(Re\,k)^2 = k_r^2 = \frac{3\mu A_0}{2 - A_0(1 + \alpha^2)} \ , && Im\,k = k_i = k_r \alpha \ , \\
\mid g \mid^2 = 4k_r^2/A_0 \ , Im\,\omega = k_r^2 \left[c_1(\alpha^2 - 1) - 2\alpha \right] \ , && Re\,\omega = 0 \ ,
\end{aligned}
$$

When $K, \Omega \neq 0$ one obtains either a standing hole solution

$$
A(x, t) = g e^{i(Kx - \Omega t)} \frac{1 - e^{2\kappa x}}{(1 + e^{2\kappa x})^{1 + i\alpha}} \ ,
\tag{1.39}
$$

$$
\begin{aligned}
\kappa^2 &= \frac{-A_0 \mu}{1 - \alpha^2 A_0} \ , \\
\mid g \mid^2 &= \frac{\kappa^2}{A_0} = \mu - K^2 \ , \\
K &= \alpha \kappa \ , \ \Omega = c_1 K^2 + c_2 \mid g \mid^2 \ ,
\end{aligned}
\tag{1.40}
$$

or a moving shock

$$
A(x, t) = g \frac{e^{i(Kx - \Omega t)} e^{-\kappa(x - ct)}}{\left[1 + e^{-\kappa(x - ct)} \right]^{1 + i\alpha}} \ ,
\tag{1.41}
$$

$$
\begin{aligned}
\kappa^2 &= A_0 \mu \left[1 - A_0 (\alpha + \frac{3}{2} c_1)^2 \right] \ , \\
\mid g \mid^2 &= -\frac{\kappa^2}{A_0} = \mu - (K + \alpha \kappa)^2 \ , \\
K &= \frac{3 \kappa c_1}{2} \ , \ c = 3(1 + c_1^2)\kappa \ , \\
\Omega &= c_1 (K + \alpha \kappa)^2 + c_2 \mid g \mid^2 -c\alpha \kappa \ .
\end{aligned}
\tag{1.42}
$$

W. van Saarloos and P. C. Hohenberg[179] showed that a hole solution is a wave source. On the other hand, shock solutions are sinks. It should be noted that in these solutions only the modulus of g is defined since the CGLE is invariant under a change in the phase.

I followed here the notation used by Nozaki and Bekki in their first paper ([140]). The shock solution presented above was first obtained by these authors. On the other hand, the solitary wave solution was previously obtained by Pereira and Stenflo[144]. The above expression for the hole solution appeared in ([140]) and has zero velocity. A year later Nozaki and Bekki in ([25]) reported the moving hole solution with velocity $c \neq 0$. The B–N hole solution for $c \neq 0$ can be expressed, similarly as in (1.36)

$$A(x,t) = \frac{Ge^{i(q_+(\chi/2)-\omega t)}}{F^{1+i\alpha}} \, , \, \chi = x - ct \, , \tag{1.43}$$

with

$$G = a_2\left(e^{\kappa_0\chi} + ze^{-\kappa_0\chi}\right) \, , \, F = e^{\kappa_0\chi} + e^{-\kappa_0\chi} \, , \tag{1.44}$$

where $a_2, \kappa_0, q_+, \omega, c, \alpha$ are real constants and z is complex. They depend on the coefficients of the equation and on a free parameter which can be chosen to be either the velocity c or a wavenumber q_1 (see below).

$$
\begin{aligned}
a_2^2 &= \mu + q_2^2 \\
\kappa_0 &= \frac{q_1 - q_2}{2\alpha} \\
q_+ &= q_2 + q_1 \\
\omega &= \mu c_2 - c\frac{q_1 q_2}{q_1 + q_2} \\
c &= (c_1 - c_2)(q_1 + q_2) \\
\alpha &= -\beta \pm \sqrt{2 + \beta^2} \\
\beta &= \frac{3}{2}\frac{1 + c_1 c_2}{c_2 - c_1} \\
z &= \frac{q_1 + q_2 - \eta(q_1 - q_2)}{q_1 + q_2 + \eta(q_1 - q_2)} \\
\eta &= \frac{(1 + ic_1)(1 - i\alpha^{-1})}{1 + ic_2}
\end{aligned} \tag{1.45}
$$

Where q_1, q_2 and c are related by the following expression

$$\frac{c^2}{d_0^2} + \frac{(q_1 - q_2)^2}{d_1^2} = 1 \, , \tag{1.46}$$

with

$$d_0^2 = \frac{4\eta_r}{(c_1 - c_2)^2(1 + \eta_r)} \, , \, d_1^2 = \frac{4\eta_r}{\mid \eta \mid^2 + \eta_r} \tag{1.47}$$

being $\eta = \eta_r + i\eta_i$ the parameter η in (1.45).

It is commonly accepted that, on the basis of the analysis of the ODE (1.33) one expects the existance of a source with $c = 0$ as well as a *discrete* set of sources with $c \neq 0$ [179]. However, Bekki–Nozaki[140, 25] found a *continuous one–parameter family* of exact source solutions of the CGLE, the hole family.

The Bekki–Nozaki solutions were reobtained by R. Conte and M. Musette[49] using the Painlevé method. These authors show how all the known solutions can be described in

the unified scheme of the Painlevé method. Since all the exact solutions necessarily obey the singularity structure of the equation[49], a prerequisite is to determine such structure. For doing so these authors use the Painlevé analysis extended to PDE's by the the WTC (Weiss–Tabor–Carnevale) method[184, 188]. Then, using a truncated expansion, in an adequate representation, the same exact solutions found by Bekki–Nozaki are obtained. Here I will write these solutions in the Conte–Musette notation, since several properties of these solutions become much more clear.

I recall that the B–N hole–family of solutions is a one–parameter family and I use as the free parameter the velocity of the solutions c. The following constants are the same for the three solutions:

$$A_0^2 = \frac{9}{2}\frac{1+c_1^2}{D_i^2}\left(D_r \pm \Delta\right) \ , \quad \Delta = \sqrt{D_r^2 + \frac{8}{9}D_i^2} \ ,$$
$$D_r = -(1 + c_1 c_2) \ , \qquad D_i = c_1 - c_2 \ ,$$
$$\alpha = \frac{D_i}{3(1+c_1^2)}A_0^2 \ ,$$

$$(1.48)$$

The hole solution can be written

$$A(x,t) = A_0\left(\frac{k}{2}\tanh\left(\frac{k}{2}\xi\right) - \nu c\right)e^{i\left[\alpha \ln \cosh\left(\frac{k}{2}\xi\right)+\frac{c\xi}{2D_i}-\Omega t\right]} \ , \quad \xi = x - ct \ ,$$

$$(1.49)$$

with ν a complex constant,

$$\nu = \frac{D_i + \alpha D_r - i(D_r - \alpha D_i)}{2(1 + \alpha^2)(1 + c_1^2)D_i} \ ,$$

$$(1.50)$$

and Ω, k and c must satisfy the following relationships

$$\Omega - (2c_1 - 3\alpha)\frac{k^2}{4} + \frac{2D_i^2 c_1 + 2D_i + 3c_2(\pm\Delta - D_r)}{8(1 + c_1^2)D_i^2}c^2 = 0 \ ,$$

$$(3\alpha c_1 + 2)\frac{k^2}{4} - \frac{c_1 D_i \mp 3\Delta - 3(1 + c_1^2)}{8(1 + c_1^2)D_i^2}c^2 - \mu = 0 \ .$$

$$(1.51)$$

The shock solution is

$$A(x,t) = A_0\frac{k}{2}\left(\tanh\left(\frac{k}{2}\xi\right) + \epsilon\right)e^{i\left[\alpha \ln\left(\cosh\left(\frac{k}{2}\xi\right)\right)+\nu_1 c\xi+\nu_2 c^2 t\right]}$$

$$(1.52)$$

where

$$\epsilon^2 = 1 \ ,$$
$$\nu_1 = \frac{3c_1 - \alpha}{6(1+c_1^2)} \ , \quad \nu_2 = \frac{1 + 9(1+c_1^2)}{36(1+c_1^2)^2} \ ,$$

and k and c are fixed by the following relationships

$$\frac{k}{2} = \epsilon\frac{-c}{6(1+c_1^2)} \ , \quad \frac{1 - 9(1+c_1^2)}{36(1+c_1^2)^2}c^2 + \mu = 0 \ .$$

Finally, the solitary wave or pulse solution is

$$A(x,t) = -iA_0 k \operatorname{sech}\ (kx)\ e^{i\left[\alpha \ln \cosh(kx)+\left((1-\alpha^2)c_1-2\alpha\right)t\right]} \ ,$$

$$(1.53)$$

where k is given by

$$\left(2\alpha c_1 + (1 - \alpha^2)\right) k^2 + \mu = 0 \ . \tag{1.54}$$

It can be shown, after some algebra, that the expressions reported above are equivalent to the ones given by Bekki–Nozaki (for example, it can be shown that the constant α defined in (1.48) is just $-\alpha$ given in (1.45)). I now summarize the most relevant properties of these exact solutions. Note first that the holes and the shock have a propagating velocity c associated with them. The pulse however has a stationary modulus. Also, the expression given above in Conte–Mussete's notation makes easier the comparison with the exact solutions of the NLSE. For instance, for the hole solution (1.49) the expression resembles very much the one of the dark soliton for the NLSE (see for example [96] and references therein). Also the profile is very similar (Fig. 1.22a). For the pulse solution (1.53) the appropriate comparison is with the bright soliton of the NLSE (see also [96]). The profile of the pulse solution for the CGLE is similar to the bright soliton of the NLSE (see Fig. 1.21b). A sketch of the shock solution is given in Fig. 1.21d .
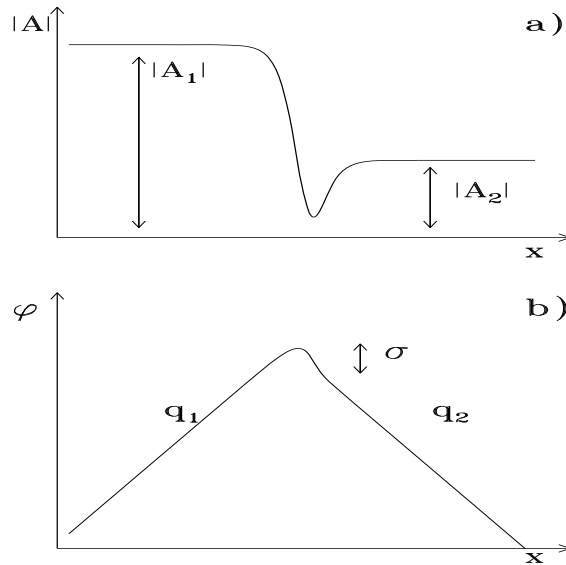
Figure 1.22: Typical profile for a traveling hole for $c_1 = -0.35$ $c_2 = 2.0$ and velocity $c = -0.2$. a) The amplitude of the hole is shown, and $\mid A_1 \mid$ and $\mid A_2 \mid$ are the amplitude of the asymptotic traveling waves. b) The phase for the hole of a) is shown. Notice the phase jump σ corresponding to the dip shown in a). The two slopes indicated in the figure correspond to the two wavenumbers of the asymptotic plane waves.

Substantial effort has been devoted to the description of these exact solutions since their discovery. However, the largest part of this effort was directed to the holes solutions. Some of the main features of the hole solutions known up to now are decribed below.

The Bekki–Nozaki hole solution (B–N hole) is characterized by a *sharp phase jump* (σ) and a *dip* of amplitude ($\mid A \mid = a_{min}$) where this phase jump is located (see Fig. 1.22a) and 1.22b)). The B–N hole is an heteroclinic orbit connecting two fixed points of the dynamical

system (1.33), where the fixed points correspond to traveling wave solutions[179]. As a consequence the B–N hole approaches asymptotically ($\xi \to \pm\infty$) traveling wave (TW) solutions. The asymptotic TW solutions have wave numbers q_1 and q_2 and amplitudes $A_{1,2} = \sqrt{1 - q_{1,2}^2}$ respectively. The wavenumbers can be written

$$q_{1,2} = \frac{c}{D_i} \pm \alpha k \;, \tag{1.55}$$

The phase jump σ can be expressed

$$\tan\sigma = \frac{2k\nu_i c}{4(\nu_r c)^2 - k^2 + (\nu_i c)^2} \tag{1.56}$$

where $\nu = \nu_r + i\nu_i$ being ν the expression given by (1.50).

This phase jump σ is zero in the following cases:

1. $c = 0$.

2. $c_2 - c_1 = \frac{1 + c_1 c_2}{\alpha}$.

3. $q_1 = \pm q_2$.

The sharp change σ becomes true discontinuity of size π in the phase for the standing hole $(c = 0)$, since the modulus $| \, A \, |$ vanishes at $\xi = x = 0$. The free parameter of the B–N hole solution can be chosen as the speed c or one of the wavenumbers of the asymptotic TW since they are related by the following expressions. From (1.55)

$$c = D_i(q_2 + q_1) \;, \tag{1.57}$$

together with

$$\frac{k^2}{a_1^2} + \frac{c^2}{a_2^2} = 1 \tag{1.58}$$

Notice that (1.58) is the equation[3] of an ellipse where a_1 and a_2 are known functions of c_1 and c_2 (see [179, 112, 25]) and k is related to $q_{1,2}$ through (1.55). When (1.58) is written in terms of the variables q_1 and c the ellipse gives, for each c, two values in the vertical axis , namely, q_1 and q_2. These values correspond to the two wavenumbers of the asymptotic traveling waves (see Fig.1.23).

---

[3]with the appropriate change of notation the equation (1.58) is the same as (1.46)
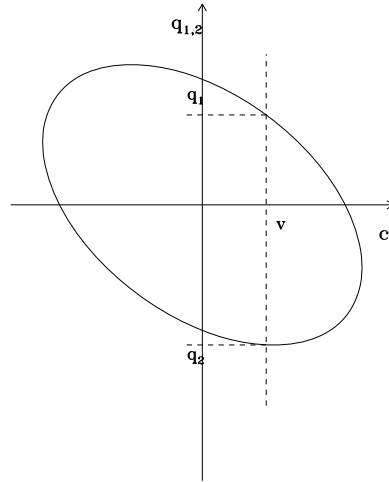
Figure 1.23: The relation (1.58) represents an ellipse. The horizontal axis represent the velocity of the moving holes and in the vertical axis the wavenumbers of the asymptotic traveling waves.

While the study of the B–N hole solutions has been very intensive their stability analysis is not an easy task. Several attempts ended up with some analytical–numerical results. H. Chaté and Manneville[44] obtained some conclusions on phase and core instabilities for the hole solution for velocity $c = 0$ and $c = 0.2$. The phase instability being associated with the stability of the asymptotic TW, while the core instability is associated with the instability of the "dip" itself. Further studies on the stability of the hole solutions were done by L. Kramer and collaborators[149, 148, 169, 168] and others[161]. Kramer and collaborators had been able to draw a stability region for the standing hole ($c = 0$) as a function of the coefficients of the CGLE. This graphic is reproduced in Fig. 1.24. The hole solutions were found to be stable in a narrow region of the c_1–c_2 plane. The region is bounded from above by the border of (absolute) instability of the emitted plane waves (solid curve AI in Fig. 1.24). From the other sides the stable range is bounded by the instability of the core with respect to localized eigenmodes corresponding to a discrete spectrum of the linearized problem (solid curve CI in Fig. 1.24). This line was determined analytically by Kramer et al.[168].
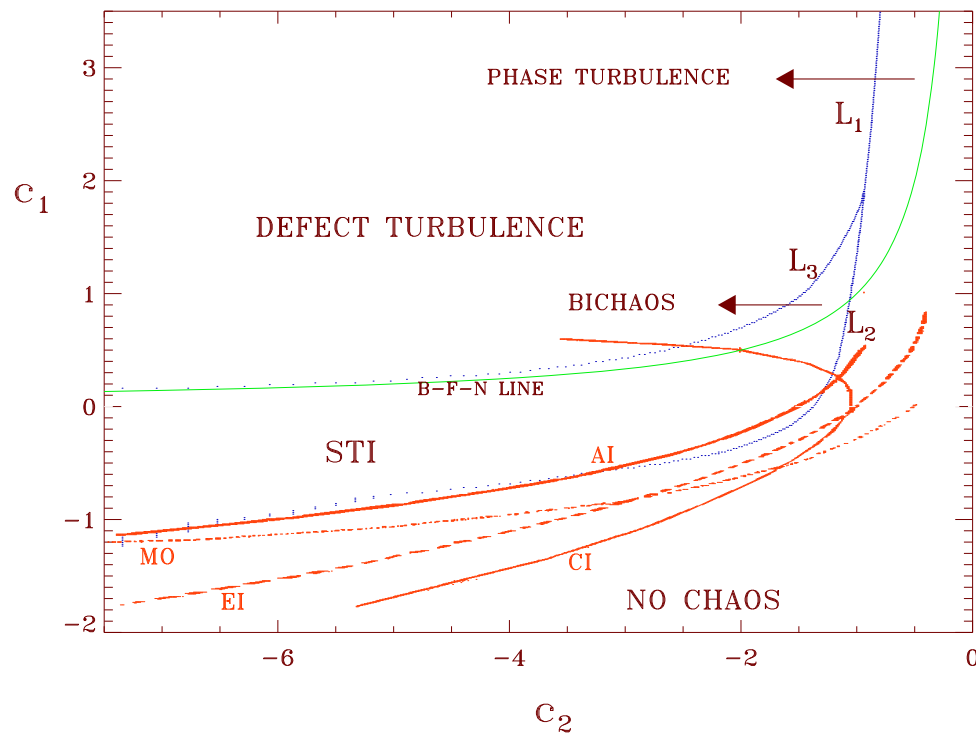
Figure 1.24: Stability diagram for the standing hole solutions[168](red lines). The different regions that were explained in 1.3.2 are also displayed (blue lines). Waves emitted by the standing hole become convectively unstable above the dashed curve EI (Eckhaus Instability)and absolutely unstable above the solid curve AI (Absolute Instablity). Outside the region bounded by the solid curve CI (Core Instability) the core of the standing hole becomes unstable. Stable standing holes can be found below AI and inside CI. The dotted line MO (Monotonic–Oscillatory) gives the boundary between monotonic (below) and oscillatory (above) interaction between standing holes.

Transient hole type solutions were observed experimentally by Lega et al.[112] in the secondary oscillatory instability in Rayleigh–Bénard convection in an annular geometry. In that work careful measurement of the different parameters of the hole were contrasted against numerical and analytical results successfully.

As to the other solutions of the B–N family few results are yet known. The pulse solution has received some attention by Kishiba et al. [95] who found them numerically in a very small region of the parameter space. New solutions reported in [13, 14] are in fact a particular case of the general form found by Conte and Musette.

Chapter 2

Numerical Study of a Lyapunov functional for the Complex Ginzburg-Landau Equation

> Isn't it true– isn't it true?
>   Good question – I know – who cares?
> Look here, they tell you
> If you had this
> If you had that
>   Latest styles and colors
> If you had that for us, mmmmm
> Wouldn't it be fabulous ? . . .
>
> Joni Mitchell, *The reoccuring dream*

2.1   Introduction

The Complex Ginzburg–Landau Equation (CGLE) is the amplitude equation describing universal features of the dynamics of extended systems near a Hopf bifurcation [51, 179].

$$\partial_t A = aA + (D_r + iD_i)\nabla^2 A - (b_r + ib_i) \mid A \mid^2 A \ . \tag{2.1}$$

Examples of this situation include binary fluid convection [98], transversally extended lasers [50] and chemical turbulence[104]. We will considered here only the one-dimensional case, $A = A(x,t)$, with $x \in [0, L]$. Suitable scaling of the complex amplitude A, space, and time shows that for fixed sign of a there are only three independent parameters in (2.1) (with D_r and $b_r > 0$ that we assume henceforth). They can be chosen to be L, $c_1 \equiv D_i/D_r$, and $c_2 \equiv b_i/b_r$.

The CGLE for $a > 0$ displays a rich variety of complex spatio-temporal dynamical regimes that have been recently classified in a phase diagram in the parameter space $\{c_1, c_2\}$ [165, 42, 43]. It is commonly stated that such nontrivial dynamical behavior,

---

[1]This Chapter corresponds to *Numerical Study of a Lyapunov functional for the Complex Ginzburg-Landau Equation*, by R. Montagne, E. Hernández-García and M. San Miguel, Physica D, **96**, 47 (1996).

occurring also in other nonequilibrium systems, originates from the non-potential or non-variational character of the dynamics [8]. This general statement needs to be qualified because it involves some confusion in the terminology. For example the term "non-variational" is often used meaning that there is no Lyapunov functional for the dynamics. But Graham and co-workers, in a series of papers [74, 75, 76, 57, 58], have shown that a Lyapunov functional does exist for the CGLE, and they have constructed it approximately in a small-gradient approximation. The correct statement for the CGLE is that it is not a gradient flow. This means that there is no real functional of A from which the right hand side of (2.1) could be obtained by functional derivation.

Part of the confusion associated with the qualification of "nonvariational" dynamics comes from the idea that the dynamics of systems having non-trivial attractors, such as limit cycles or strange chaotic attractors, can not be deduced from the minimization of a potential which plays the role of the free energy of equilibrium systems. However, such idea does not preclude the existence of a Lyapunov functional for the dynamics. The Lyapunov functional can have local minima which identify the attractors. Once the system has reached an attractor which is not a fixed point, dynamics can proceed on the attractor due to "nonvariational" contributions to the dynamical flow which do not change the value of the Lyapunov functional. This just means that the dynamical flow is not entirely determined once the Lyapunov functional is known. This situation is very common and well known in the study of dynamical properties within the framework of conventional statistical mechanics: The equilibrium free energy of the system is a Lyapunov functional for the dynamics, but equilibrium critical dynamics [86] usually involves contributions, such as mode-mode coupling terms, which are not determined just by the free energy. The fact that the dynamical evolution is not simply given by the minimization of the free energy is also true when studying the nonequilibrium dynamics of a phase transition in which the system evolves between an initial and a final equilibrium state after, for example, a jump in temperature across the critical point [78].

A Lyapunov functional plays the role of a potential which is useful in characterizing global properties of the dynamics, such as attractors, relative or nonlinear stability of these attractors, etc. In fact, finding such potentials is one of the long-sought goals of nonequilibrium physics [72, 73], the hope being that they should be instrumental in the characterization of nonequilibrium phenomena through phase transitions analogies. The use of powerful and very general methods based on these analogies has been advocated by a number of authors [35, 36, 165, 42, 43]. In this context, it is a little surprising that the finding of a Lyapunov functional for the CGLE [76, 57, 58] has not received much attention in the literature. A possible reason for this is that the construction of nonequilibrium potentials has been historically associated with the study of stochastic processes, in particular in the search of stationary probability distributions for systems driven by random noise [72, 73, 79]. We want to make clear that the finding of the Lyapunov functional for the CGLE [76, 57, 58], as well as the whole approach and discussion the present work is completely within a purely deterministic framework and it does not rely on any noise considerations. A second possible reason for the relative little attention paid to the Lyapunov functional for the CGLE is the lack of any numerical check of the uncontrolled approximations made on its derivation. The main purpose of this Chapter is precisely to report such numerical check of the results of Graham and collaborators, thus delimiting the range of validity of the approximations involved. We also provide a characterization

of the time evolution of the Lyapunov functional in different regions of the phase diagram of the CGLE [165, 42, 43], which illustrates the use of such potential.

Our main findings are that the expressions by Graham and coworkers behave to a good approximation as a proper Lyapunov potential when phase singularities (vanishing of the modulus of A) are not present. This includes non-chaotic regimes as well as states of phase turbulence. In this last case some small but systematic discrepancies with the predictions are found. In the presence of phase singularities the potential is ill-defined and then it is not a correct Lyapunov functional.

The Chapter is organized as follows. For pedagogical purposes, we first discuss in Sect. 2.2 a classification of dynamical flows in which notions like relaxational or potential flows are considered. The idea of a potential for the CGLE is clearer in this context. In Sect. 2.3 we review basic phenomenology of the CGLE and the main analytical results for the Lyapunov functional of the CGLE. Sections 2.4 and 2.5 contain our numerical analyses. Section 2.4 is devoted to the Benjamin-Feir stable regime of the CGLE and Sect. 2.5 to the Phase Turbulent regime. Our main conclusions are summarized in Sect. 2.6.

2.2 A classification of dynamical flows

In the following we review a classification of dynamical systems that, although rather well established in other contexts [72, 73], it is often overlooked in general discussions of deterministic spatio-temporal dynamics. Non-potential dynamical systems are often defined as those for which there is no Lyapunov potential. Unfortunately, this definition is also applied to cases in which there is no *known* Lyapunov potential. To be more precise, let us consider dynamical systems of the general form

$$\partial_t A_i = V_i[A] \tag{2.2}$$

where A_i represents a set of, generally complex, dynamical variables which are spatially dependent fields: $A_i = A_i(\mathbf{x}, t)$. $V_i[A]$ is a functional of them. The notation A_i^* represents the complex conjugate of A_i and for simplicity we will keep the index i implicit. Let us now split V into two contributions:

$$V[A] = G[A] + N[A] , \tag{2.3}$$

where G, the *relaxational* part, will have the form

$$G[A] = -\frac{\Gamma}{2} \frac{\delta F[A]}{\delta A^*} , \tag{2.4}$$

with F a real and scalar functional of A. Γ is an arbitrary hermitic and positive-definite operator (possibly depending on A). In the particular case of real variables there is no need of taking the complex conjugate, and hermitic operators reduce to symmetric ones. The functional $N[A]$ in (2.3) is the remaining part of $V[A]$. The important point is that, if the splitting (2.3) can be done in such a way that the following orthogonality condition is satisfied (c.c. denotes the complex conjugate expression):

$$\int d\mathbf{x} \left(\frac{\delta F[A]}{\delta A(\mathbf{x})} N[A(\mathbf{x})] + \text{c.c.} \right) = 0 , \tag{2.5}$$

then the terms in N neither increase nor decrease the value of F, which due to the terms in G becomes a decreasing function of time:

$$\frac{dF[A(\mathbf{x},t)]}{dt} \leq 0 \ . \tag{2.6}$$

If F is bounded from below then it is a Lyapunov potential for the dynamics (2.2). Equation (2.5) with $N = V - G$, that is

$$\int d\mathbf{x} \left(\frac{\delta F[A]}{\delta A(\mathbf{x})} \left(V[A(\mathbf{x})] + \frac{\Gamma}{2} \frac{\delta F[A]}{\delta A^*(\mathbf{x})} \right) + \text{c.c.} \right) = 0 \ , \tag{2.7}$$

can be interpreted as an equation for the Lyapunov potential F associated to a given dynamical system (2.2). It has a Hamilton-Jacobi structure. When dealing with systems perturbed by random noise, Γ is fixed by statistical requirements, but in deterministic contexts such as the present work, it can be arbitrarily chosen in order to simplify (2.7).

Solving (2.7) is in general a difficult task, but a number of non-trivial examples of the splitting (2.3)-(2.6) exist in the literature. Some of these examples correspond to solutions of (2.7) found in the search of potentials for dynamical systems [76, 74, 75]. Other examples just correspond to a natural splitting of dissipative and non-dissipative contributions in the dynamics of systems with well established equilibrium thermodynamics, as for example models of critical dynamics [86] or the equations of nematodynamics in liquid crystals [160].

Once the notation above has been set-up, we can call relaxational systems those for which there is a solution F of (2.7) such that $N = 0$, that is all the terms in V contribute to decrease F. Potential systems can be defined as those for which there is a nontrivial (i.e. a non-constant) solution F to (2.7). In relaxational systems there is no long-time dynamics, since there is no time evolution of A once a minimum of F is reached. On the contrary, for potential systems for which $N \neq 0$, the minima of F define the attractors of the dynamical flow, but once one of these attractors is reached, nontrivial sustained dynamics might exist on the attractor. Such dynamics is determined by N and maintains a constant value for the functional F.

A possible more detailed classification of the dynamical flows is the following:

1.- Relaxational gradient flows: Those dynamical systems for which $N = 0$ with Γ proportional to the identity operator. In this case the time evolution of the system follows the lines of steepest descent of F. A well known example is the so called Fisher-Kolmogorov equation, also known as model A of critical dynamics [86], or (real) Ginzburg-Landau equation for a real field $A(\mathbf{x},t)$:

$$\dot{A} = \alpha A + \gamma \nabla^2 A - \beta \mid A \mid^2 A \ , \tag{2.8}$$

where α, γ and β are real coefficients. This equation is of the form of Eqs. (2.2)-(2.4) with $N = 0$, $\Gamma = 1$, and $F = F_{GL}[A]$, the Ginzburg-Landau free energy:

$$F_{GL}[A] = \int d\mathbf{x} \left(-\alpha \mid A \mid^2 + \gamma \mid \nabla A \mid^2 + \frac{\beta}{2} \mid A \mid^4 \right) \tag{2.9}$$

2.- Relaxational non-gradient flows: Still $N = 0$ but with Γ not proportional to the identity, so that the relaxation to the minimum of F does not follow the lines of steepest descent of F. The matrix operator Γ might depend on A or involve spatial derivatives. A well known example of this type is the Cahn-Hilliard equation of spinodal decomposition, or model B of critical dynamics for a real variable A. [86]:

$$\dot{A} = (-\frac{1}{2}\nabla^2)\left(-\frac{\delta F_{GL}[A]}{\delta A}\right) \ , \tag{2.10}$$

The symmetric and positive-definite operator $(-\nabla^2)$ has its origin in a conservation law for A.

3.- Non-relaxational potential flows: N does not vanish, but the potential F, solution of (2.7) exists and is non-trivial. Most models used in equilibrium critical dynamics [86] include non-relaxational contributions, and therefore belong to this category. A particularly simple example is

$$\dot{A} = -(1+i)\frac{\delta F_{GL}[A]}{\delta A^*} \ , \tag{2.11}$$

where now A is a complex field. Notice that we can not interpret this equation as being of type 1, because $(1 + i)$ is not a hermitic operator, but still F_{GL} is a Lyapunov functional for the dynamics. Equation (2.11) is a special case of the Complex Ginzburg-Landau Equation (CGLE), in which $V[A]$ is the sum of a relaxational gradient flow and a nonlinear-Schrödinger-type term $N[A] = -i\frac{\delta F_{GL}[A]}{\delta A^*}$.

The general CGLE[179] is of the form (2.8) but A is complex and α, γ and β are arbitrary complex numbers. For the special case in which $\frac{Re[\gamma]}{Im[\gamma]} = \frac{Re[\beta]}{Im[\beta]}$, as for example in (2.11), the Lyapunov functional for the CGLE is known exactly [171]. Such choice of parameters has important dynamical consequences[154]. Beyond such special cases, the calculations by Graham and coworkers indicate [57, 58] that the CGLE, a paradigm of complex spatio-temporal dynamics, might be classified within this class of non-relaxational potential flows because a solution of (2.7) is found. The difficulty is that the explicit form of the potential is, so far, only known as a uncontrolled small-gradient expansion.

4.- Non-potential flows: Those for which the only solutions F of (2.7) are the trivial ones (that is F = constant). Hamiltonian systems as for example the nonlinear Schrödinger equation are of this type.

2.3   A Lyapunov Functional for the CGLE

It is well known that for $a < 0$ the one dimensional CGLE (2.1) has $A = 0$ as a stable solution, whereas for $a > 0$ there are Traveling Wave (TW) solutions of the form

$$A_k = A_0 e^{i(kx+\omega t)+\varphi_0} \tag{2.12}$$

with $A_0 = \sqrt{(a - D_r k^2)/b_r}$, $|k| < \sqrt{a/b_r}$, and $\omega = (b_i a + D_- k^2)/b_r$. We have introduced

$$D_- \equiv D_r b_i - D_i b_r \ . \tag{2.13}$$

φ_0 is any arbitrary constant phase.

The linear stability of the homegeneus solution ((2.12) with $k = 0$) with respect to long wavelength fluctuations divides the parameter space $\{c_1, c_2\}$ in two regions: the Benjamin-Feir (BF) stable and the BF unstable zone. This line is given by [173, 131]

$$D_+ \equiv D_r b_r + D_i b_i = 0, \tag{2.14}$$

In the BF unstable region ($D_+ < 0$) there are no stable TW solutions, while in the BF stable region ($D_+ > 0$) TW's with a wavenumber $k < k_E$ are linearly stable. For $k > k_E$, TW's become unstable through the long wavelength instability known as the Eckhaus instability [61, 91]. The Eckhaus wavenumber k_E is given by

$$k_E^2 = \frac{a b_r D_+}{D_r(3D_+ b_r + 2D_- b_i)} \tag{2.15}$$

Recent numerical work for $a > 0$ and L large [165, 42, 43, 64] has identified regions of the parameter space displaying different kinds of regular and spatio-temporal chaotic behavior (obtained at long times from random initial conditions and periodic boundary conditions), leading to a "phase diagram" for the CGLE. The five different regions, each leading to a different asymptotic phase, are shown in Fig. 2.1 as a function of the parameters c_1 and c_2 ($a > 0$, L large). Two of these regions are in the BF stable zone and the other three in the BF unstable one. One of the main distinctions between the different asymptotic phases is in the behavior of the modulus of A at long times. In some regions it never vanishes, whereas in others it vanishes from time to time at different points. A more detailed description of the asymptotic behavior in the different regions is as follows:

1. Non-Chaotic region. The evolution here ends in one of the Eckhaus-stable TW solutions for almost all the initial conditions.

2. Spatio-Temporal Intermittency region. Despite the fact that there exist stable TW, the evolution from random initial conditions is not attracted by them but by a chaotic attractor in which typical configurations of the field A consist of patches of TW interrupted by turbulent bursts. The modulus of A in such bursts typically touches zero quite often.

3. Defect Turbulence. This is a strongly disordered phase in which the modulus of A has a finite density of space-time zeros. In addition the space and time correlation functions have a quasi-exponential decay [165, 42].

4. Phase Turbulence. This is a weakly disordered phase in which $|A(x, t)|$ remains away from zero. The temporal correlations decay slower than exponentially [165, 42].

5. Bi-Chaos region. Depending on the particular initial condition, the system ends on attractors similar to the ones in regions 3, 4, or in a new attractor in which the configurations of A consists of patches of phase and defect turbulence.
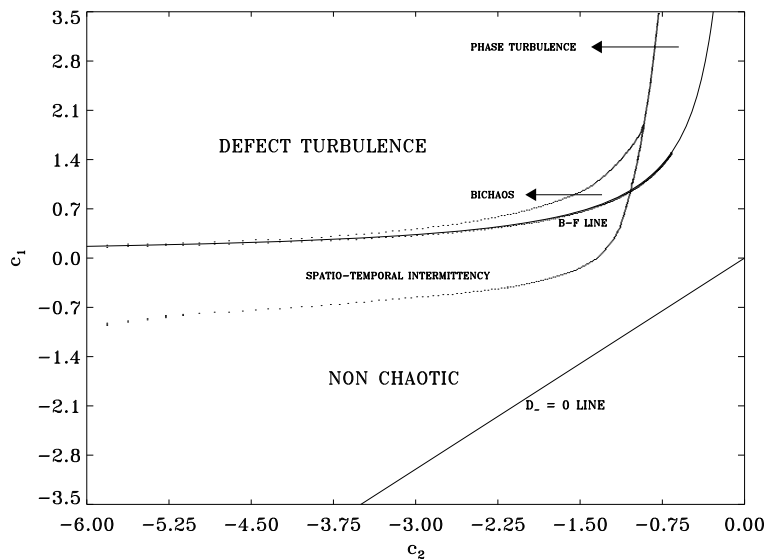
Figure 2.1: Regions of the parameter $[c_1 - c_2]$-space ($a = 1$) for the $d = 1$ CGLE display-ing different kinds of regular and chaotic behavior. Two analytically obtained lines,the Benjamin-Feir line (B-F line) and the D_- line, are also shown.

An approximate Lyapunov functional for the CGLE was calculated by Graham and collaborators [57, 58, 56]. Earlier attempts to find a Lyapunov functional were based on polynomial expansions[171, 71, 182, 183], while more recent and successful approaches focussed in solving the Hamilton-Jacobi equation (2.7) with $\Gamma = 1$ in different ways. This was done first by a minimization procedure involving an action integral[74, 75, 76], and more recently by a more direct expansion method [57, 58, 56]. This last method provides also expressions in higher dimensions, but we will restrict here to the one-dimensional case. In any case, the solution involves an uncontrolled gradient expansion around space-independent solutions of the CGLE. Such expansion obviously limits the validity of the result to regions in the phase diagram in which there are not strong gradients. This excludes the regions in which zeros in the modulus of A are typical, since the phase of A becomes singular there. In particular Spatio-temporal intermittency regimes, Bi-chaos and Defect Turbulence are out of the range of validity of Graham's expansion. The meaningfulness of the potential in the other regions of parameter space remains still an open question because of the uncontrolled small gradient approximations used to calculate it, and calls for some numerical check.

In their solution of the Hamilton Jacobi equation, Graham and collaborators find different branches of the Lyapunov functional with expressions valid for different values of the parameters. In particular they identify the BF line (2.14) as separating two branches of the solution to (2.7).

The explicit expressions (obtained with $\Gamma = 1$) are given in polar coordinates:

$$A(x,t) = r(x,t)e^{i\varphi(x,t)} \tag{2.16}$$

In terms of the amplitude r, the phase φ, and their spatial derivates (denoted as r_x, φ_x, φ_{xx}, etc.) the Lyapunov functional per unit of length $\Phi \equiv F/L$ was found[57, 58], for $a < 0$:

$$\Phi = \int \left\{ b_r r^4 - 2ar^2 + 2 \left[D_r + \frac{D_- b_i r^4}{3(a - b_r r^2)^2} \right] r_x^2 - \frac{2D_- r^3}{3(a - b_r r^2)} r_x \varphi_x + 2D_r r^2 \varphi_x^2 \right\} dx \tag{2.17}$$

We note that even in this relatively simple case $a < 0$, the result for Φ is only approximate and its structure reveals a highly non-trivial dynamics.

For $a > 0$, in the BF stable region ($D_+ > 0$) the expression for Φ results:

$$
\begin{aligned}
\Phi =\ & \int \Bigg\{ b_r r^4 - 2ar^2 \\
& + \left[(A_1 r + B_1/r^2)r_x^2 + (A_2 r + B_2/r)r_x \varphi_x + 2(D_r r^2 - D_- b_i a/\mid b \mid^2 b_r)\varphi_x^2 \right] \\
& + \left[\frac{D_- D_r b_i}{3b_r \mid b \mid^2} \varphi_x^4 + \left(-\frac{D_-^2 a}{2b_r^4 r^2} - \frac{D_-}{b_r^2}(D_-/b_r + 2D_i)\ln r + C_1 \right) \varphi_{xx}^2 + \frac{2D_- D_r}{3b_r^2 \mid b \mid^2}(b_i^2 - b_r^2)\frac{\varphi_x^3 r_x}{r} \right. \\
& \left. + \frac{2D_- D_r b_i}{3b_r^3 \mid b \mid^2}(b_i^2 - 2b_r^2)\frac{\varphi_x^2 r_x^2}{r^2} - \frac{4D_r b_i D_-}{3b_r^3 r}\left(1 + \frac{\ln(b_r r^2/a)}{1 - b_r r^2/a} \right)r_x \varphi_x \varphi_{xx} \right] \Bigg\} dx
\end{aligned}
\tag{2.18}
$$

where

$$
\begin{aligned}
A_1 &= 2(D_r + b_i D_-/3b_r^2), \\
A_2 &= 2D_-/b_r, \\
B_1 &= \frac{2D_- b_i a}{3b_r^3 \mid b \mid^2}(2b_r^2 - b_i^2), \\
B_2 &= \frac{2D_- a}{b_r^2 \mid b \mid^2}(b_r^2 - b_i^2),
\end{aligned}
\tag{2.19}
$$

Clearly, Φ is ill-defined when $r = 0$.

By writing-out the Euler-Lagrange equations associated to the minimization of Φ the TW solutions (2.12) are identified as local extrema of Φ. Since they occur in families parametrized by the arbitrary phase φ_0, the minima associated to the TW of a given k are not isolated points but lay on a one-dimensional closed manifold. The non-variational part of the dynamics (N in (2.3)) can be explicitly written-down by substracting $G = -\frac{1}{2}\frac{\delta F}{\delta A^*}$ with $F = L\Phi$ to the right-hand-side of (2.1). It is seen to produce, when evaluated on the manifold of minima of Φ with a given k, constant motion along it. This produces the periodic time dependence in (2.12) and identify the TW attractors as limit cycles.

The value of k for which the corresponding extrema change character from local minima to saddle points is precisely the Eckhaus wavenumber k_E. It is remarkable that, although expression (2.18) was obtained in a gradient expansion around the homogeneous TW, their minima identify exactly all the TW's of equation (2.1), and their frequencies and points of

instability are also exactly reproduced. This gives confidence on the validity of Graham's approximations. It should be stressed however that they are not exact and can lead to unphysical consequences. For instance, the value of the potential Φ evaluated on a TW of wavenumber k ($|k| < \sqrt{a/b_r}$) is [76]

$$\Phi_k \equiv \Phi[A_k] = \frac{2D_+ a}{|b|^2} k^2 \left(1 - \frac{k^2}{6k_E^2}\right) + \Phi_{k=0} \tag{2.20}$$

where $\Phi_{k=0} = -a^2/b_r$. For a range of parameter values this expression gives mathematical sense to the intuitive fact that the closer to zero is k the more stable is the associated TW (because its potential is lower). But for some parameter values the minimal potential corresponds to large wavenumbers close to $\pm\sqrt{a/b_r}$. This is counterintuitive and calls for some numerical test. The test will be described below and it will be shown that the wavenumbers close to $\pm\sqrt{a/b_r}$ are out of the range of validity of the small gradient approximations leading to (2.18).

We already mentioned in the previous section that the Lyapunov functional for the CGLE is exactly known for special values of the parameters [76, 57, 154]. This happens for $D_- \equiv D_r b_i - D_i b_r = 0$, which lies in the BF-stable region as indicated in Fig. 2.1. In this case it is clear that (2.1) can be written as

$$\dot{A} = -\frac{1}{2}\frac{\delta F_{GL}[A]}{\delta A^*} + ib_i \left(-|A|^2 + \frac{D_r}{b_r}\nabla^2\right) A , \tag{2.21}$$

where $F_{GL}[A]$ is (2.9) for complex A and with $\alpha = 2a$, $\beta = 2b_r$, and $\gamma = 2D_r$. It is readily shown that the term proportional to b_i is orthogonal to the gradient part, so that F_{GL} is an exact solution of (2.7) for these values of the parameters, and (2.21) is a relaxational non-gradient flow (see classification in section 2.2). It is seen that the approximate expressions (2.17) and (2.18) greatly simplify when $D_- = 0$ leading both to the same expression:

$$L\Phi = \int \left\{-2ar^2 + b_r r^4 + 2D_r r r_x^2 + 2D_r r^2 \varphi_x^2\right\} dx \tag{2.22}$$

When expressed in terms of A and A^* it reproduces F_{GL} in (2.21). Thus the gradient expansion turns out to be exact on the line $D_- = 0$.

In the Benjamin-Feir unstable region ($a > 0, D_+ < 0$) the gradient expansion for Φ becomes[58, 56]:

$$\begin{aligned}
\Phi &= \int \left\{ b_r r^4 - 2ar^2 + \left[(A_1 r + \tilde{B}_1/r^2)r_x^2 + (A_2 r + \tilde{B}_2/r)r_x\varphi_x + 2D_r(r^2 - \frac{a}{b_r})\varphi_x^2\right] \right. \\
&+ \left[\frac{D_r^2}{b_r}\varphi_x^4 + \left(\frac{b_r}{2a^2 r^2}\left(\frac{\tilde{B}_2^2}{4} + \frac{4D_r^2 a^2}{b_r^2}\right)(r^2 - \frac{a}{b_r}) - \frac{A_2}{2b_r}(\frac{A_2}{4} + D_i)\ln(\frac{r^2 b_r}{a}) + \frac{D_i^2}{b_r}\right)\varphi_{xx}^2 \right. \\
&- \frac{4D_r b_i D_-}{b_r^3 r}\left(1 + \frac{D_r |b|^2 + 2b_r D_+}{b_i D_-(1 - \frac{b_r r^2}{a})}\ln(\frac{r^2 b_r}{a})\right)\varphi_x r_x \varphi_{xx} \\
&+ \left. \frac{2D_r}{3b_r^2 r}(5b_i D_r + D_i b_r)\varphi_x^3 r_x + \frac{2b_i D_r}{3b_r^3 r^2}(7b_i D_r + D_i b_r)\varphi_x^2 r_x^2\right] \right\} dx \tag{2.23}
\end{aligned}$$

where, in addition to the previous definitions

$$\tilde{B}_1 = -\frac{2ab_i}{3b_r^3}(D_r b_i + 2D_i b_r),$$

$$\tilde{B}_2 \quad = \quad -\frac{2a}{b_r^2}(D_r b_i + D_i b_r),$$

$$(2.24)$$

It was noted before that this expression can be adequate, at most, for the Phase Turbulent regime, since in the other BF unstable regimes $|A|$ vanishes at some points and instants, so that (2.23) is ill-defined.

The long time dynamics occurs in the attractor defined by the minima of Φ. The Euler-Lagrange equations associated to the minimization of (2.23) lead to a relationship between amplitude and phase of A which implies the well known adiabatic following of the amplitude to the phase dynamics commonly used to describe the phase turbulence regime by a nonlinear phase equation. The explicit form of this relationship is

$$
\begin{aligned}
r^2 \quad = \quad & \frac{a}{br} - \frac{D_r}{b_r}(\nabla\varphi)^2 - \frac{D_i}{b_r}\nabla^2\varphi + \frac{b_i D_i^2}{2ab_r^2}\nabla^4\varphi + 2\frac{D_r D_i b_i}{ab_r^2}\nabla\varphi\nabla^3\varphi \\
+ \quad & 2\frac{b_i D_r^2}{ab_r^2}\nabla\varphi\nabla\nabla^2\varphi + \left[\frac{D_r D_i b_i}{ab_r^2} - \frac{\mid D \mid^2}{ab_r}\right](\nabla^2\varphi)^2
\end{aligned}
$$

$$(2.25)$$

It defines the attractor characterizing the phase turbulent regime. Dynamics in this attractor follows from the nonrelaxational part N in (2.3). When (2.25) is imposed in such nonrelaxational part of the dynamics the generalized Kuramoto-Shivashinsky equation containing terms up to fourth order in the gradients [157] is obtained [58, 56].

We finally note that in the phase turbulent regime the Lyapunov functional Φ gives the same value [58, 56] when evaluated for any configuration satisfying (2.25), at least within the small gradient approximation. This corresponds to the evolution on a chaotic attractor (associated to the Kuramoto-Sivashinsky dynamics coming from N) which is itself embedded in a region of constant Φ (the potential plateau [73]). This plateau consists of the functional minima of Φ (2.25). All the (unstable) TW are also contained in the same plateau, since they satisfy (2.25).

2.4   Numerical studies of the Lyapunov functional in the Benjamin-Feir stable regime

We numerically investigate the validity of $\Phi[A]$ in (2.17), (2.18), and (2.23) as an approximate Lyapunov functional for the CGLE. When evaluated on solutions $A(x,t)$ of (2.1) it should behave as a monotonously decreasing function of time, until $A(x,t)$ reaches the asymptotic attractor. After then, Φ should maintain in time a constant value characteristic of the particular attractor.

All the results reported here were obtained using a pseudo-spectral code with periodic boundary conditions and second-order accuracy in time. Spatial resolution was typically 512 modes, with runs of up to 4096 modes to confirm the results. Time step was typically $\Delta t = .1$ except when differently stated in the figure captions. Since very small effects have been explored, care has been taken of confirming the invariance of the results with decreasing time step and increasing number of modes. System size was always taken as $L = 512$, and always $D_r = 1$ and $b_i = -1$, so that $c_1 = D_i$ and $c_2 = -1/b_r$. When a random noise of amplitude ϵ is said to be used as or added to an initial condition it means

that a set of uncorrelated Gaussian numbers of zero mean and variance ϵ^2 was generated, one for each collocation point in the numerical lattice.

2.4.1 Negative a

The uniform state $A = 0$ is stable for $a < 0$. We start our numerical simulation with a plane wave $A = A_0 e^{ikx}$ of arbitrary wavenumber $k = 0.295$ and arbitrary amplitude $A_0 = 1$ (note that the TW's (2.12) do not exist for $a < 0$), and calculate Φ for the evolving configurations. In order to have relevant nonlinear effects during the relaxation towards $A = 0$ we have chosen a small value for the coefficient of the linear term ($a = -0.01$). The remaining parameters were $D_i = 1$ and $b_r = 1.25$ ($c_1 = 1$, $c_2 = -0.8$). Despite the presence of non-relaxational terms in (2.1), Φ decreases monotonously (see Fig. 2.2) to the final value $\Phi(t = \infty) = \Phi[A = 0] = 0$ confirming its adequacy as a Lyapunov potential.
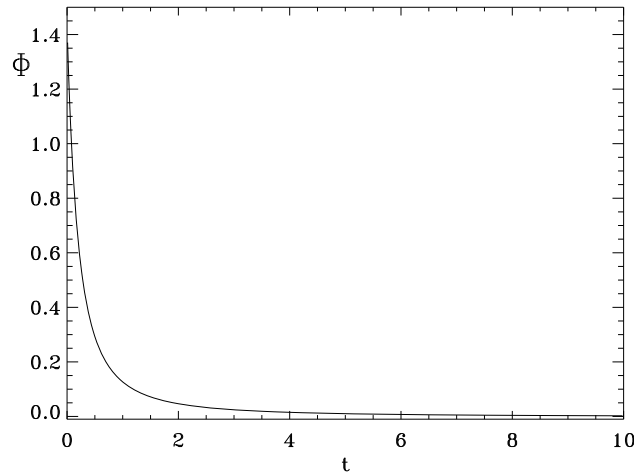
Figure 2.2: Relaxation to the simple attractor for $a < 0$. The parameter values are $a = -0.01, c_1 = 1$ and $c_2 = -0.8$. The initial condition is a TW of arbitrary wavenumber $k = 0.295$ and arbitrary amplitude $A_0 = 1.0$.

2.4.2 Positive a. Benjamin-Feir stable regime

We take in this section always $a = 1$. Non-chaotic (TW) states and Spatio-Temporal Intermittency are the two phases found below the BF line in Fig. 2.1. We first perform several numerical experiments in the non-chaotic region:

A first important case is the one on the line $D_- = 0$, for which (2.22) is an exact Lyapunov functional F_{GL}. We take $D_i = -1$ and $b_r = 1$ ($c_1 = c_2 = -1$), on the $D_- = 0$ line, and compute the evolution of $\Phi = \frac{F_{GL}}{L}$ along a solution of (2.1), taking as initial condition for A a Gaussian noise of amplitude $\epsilon = 0.01$. Despite of the strong phase gradients present specially in the initial stages of the evolution, and of the presence of non-relaxational terms, Φ decays monotonously in time (Fig. 2.3). The system evolved towards a TW attractor of wavenumber $k = 0.0245$. The value of Φ in such state is, from

Eq. (2.20), $\Phi_{k=0.0245} = -0.998796$. It is important to notice that our numerical solution for A and numerical evaluation of the derivatives in Φ reproduce this value within a 0.3% in the last time showed in Fig. 2.3, and continues to approach the theoretical value for the asymptotic attractor at longer times[1].

We continue testing the Lyapunov functional for $D_i = 1$, $b_r = 1.25$ ($c_1 = 1$,$c_2 = -0.8$. This is still in the non-chaotic region but, since $D_- \neq 0$, Φ is not expected to be exact, but only a small gradient approximation. We check now the relaxation back to an stable state after a small perturbation. As initial condition we slightly perturb a TW of Eckhaus-stable wavenumber ($k = 0.13 < k_E$) by adding random noise of amplitude $\epsilon = 0.09$. Φ decays monotonously (Fig. 2.4) from its perturbed value to the value $\Phi_{k=0.13} = -0.796632$ as the perturbation is being washed out, as expected for a good Lyapunov functional.

A more demanding situation was investigated for $D_i = -1$ and $b_r = 0.5$ (again in the non-chaotic region, $c_1 = -1$ and $c_2 = -2$, and $D_- \neq 0$). Two TW of different wavenumbers ($k_1 = 0.4$, $k_2 = 0.08$, both Eckhaus-stable) were joined (at two points because of the periodic boundary conditions) and the resulting state (see inset in Fig. 2.5) was used as initial condition. The interfaces between the two TW's contain initially discontinuities in the gradient of the phase which are washed out in a few integration steps. The two interfaces move at constant velocity but one of them remains sharp, whereas the other widens in time, progressively replacing the two initial waves. An important observation is that during the whole process the modulus of $A(x,t)$ never vanishes and then the winding number, defined as

$$\nu \equiv \frac{1}{2\pi} \int_0^L \nabla\varphi \, dx \qquad (2.26)$$

remains constant ($\nu = 20$) (with periodic boundary conditions ν is constant except at the instants in which the phase becomes singular, that is when $r = 0$).

The state (limit cycle) finally reached is a TW of $k = 2\pi\nu/L = 0.245$. Despite of the complicated and non-relaxational processes occurring Φ behaves as a good Lyapunov functional monotonously decreasing from the value $\Phi(t = 0) = -1.825$ corresponding to the two-wave configuration to the value $\Phi = -1.863$ of the final attractor (Fig. 2.5). The dynamics of the moving fronts is more complicated than in some relaxational models [37]. For this particular set of parameters and initial wavenumbers, the center of the diffuse front moves invading the region of longest wavenumber, while the sharp one moves towards the small wavenumber region.

The good behavior of Φ will be obviously lost if the field $A(x,t)$ vanishes somewhere during the evolution. As the next numerical experiment (for $D_i = 1$ and $b_r = 1.25$, that is $c_1 = 1$, $c_2 = -0.8$) we used as initial condition a small ($\epsilon = 0.01$) random Gaussian noise. The system was left to evolve towards its asymptotic state (a TW). Fig. 2.6 shows that after a transient Φ monotonously decreases. During the initial transient it widely fluctuates, increasing and decreasing and loosing then its validity as a Lyapunov functional. This incorrect behavior occurs because during the initial stages $A(x,t)$ is small and often vanishes, changing ν. When A (and then r) vanishes the phase and (2.18) are ill-defined and out of the range of validity of a small gradient approximation. Note the contrast with the case $D_- = 0$ in which the potential is exact and well behaved even

---

[1] If a smaller time step is used greater accuracy is obtained. For example, if the time step is reduced to 0.05 the value of Φ is reproduced within 10^{-7}%. But this takes quite a long computing time.
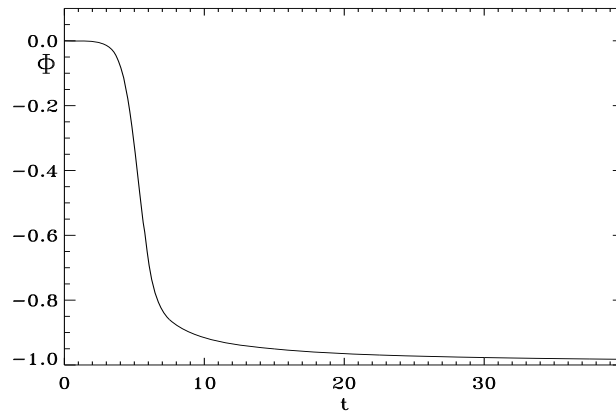
Figure 2.3: Time evolution of Φ on the D_- line. The parameter values are $a = 1, c_1 = -1$ and $c_2 = -1$. The initial condition is a a Gaussian noise of amplitude $\epsilon = 0.01$. The system evolved towards a TW attractor of wavenumber $k = 0.0245$.
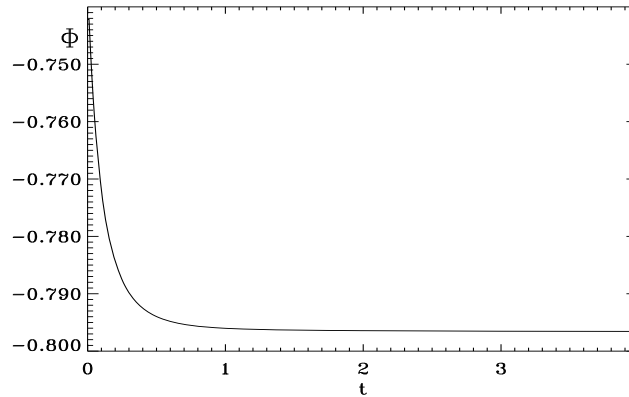
Figure 2.4: Time evolution of Φ in the non-chaotic region for $c_1 = -1$ and $c_2 = -0.8$. The initial condition is an Eckhaus stable TW of wavenumber $k = 0.13$ perturbed by random noise of small amplitude $\epsilon = 0.09$.
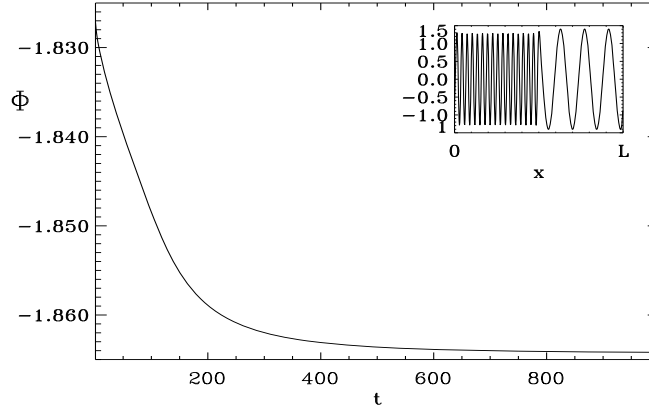
Figure 2.5: Same as Fig. 2.4 but for $c_1 = -1$ and $c_2 = -2$. The initial condition for A consists of two Eckhaus stable TW of different wavenumbers ($k_1 = 0.4, k_2 = 0.08$) joined together. The inset shows the real part of this initial configuration.

when ν is strongly changing. The particular values of the maxima and minima during the transient in which ν is changing depend on the spatial and temporal discretization, since it is clear from (2.18) that Φ is ill-defined or divergent when r vanishes. Note that this incorrect behavior of Φ for $D_- \neq 0$ is not a problem for the existence of a Lyapunov functional, but comes rather from the limited validity of the hypothesis used for its approximate construction. Nevertheless, as soon as the strong gradients disappear Φ relaxes monotonously to the value $\Phi = -0.79997$, corresponding to the final state, a TW of wavenumber $k = -0.0123$.
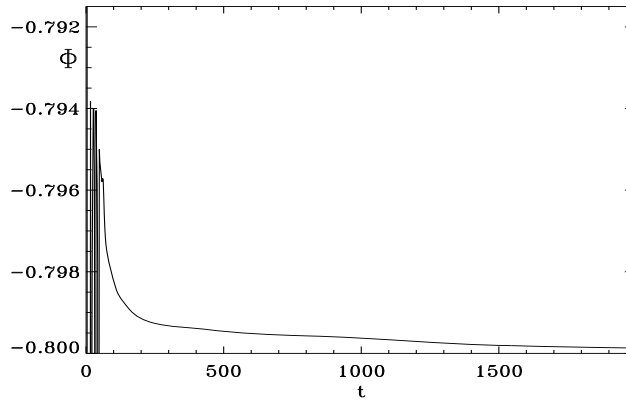
Figure 2.6: Same as Fig. 2.4 but for $c_1 = 1$ and $c_2 = -0.8$. The initial condition is a random noise of amplitude $\epsilon = 0.01$.

As another test in the non-chaotic region, for $D_i = -1$ and $b_r = 0.5$ ($c_1 = -1$,

$c_2 = -2$) we use as initial condition an Eckhaus-unstable TW ($k = 0.54 > k_E = 0.48$) slightly perturbed by noise. The system evolves to an Eckhaus-stable TW ($k = 0.31$) by decreasing its winding number (initially $\nu = 44$ and finally $\nu = 26$). Fig. 2.7 shows the evolution of Φ from its initial value $\Phi(0) = -1.485$ the final one $\Phi = -1.77$. Although there is a monotonously decreasing baseline, sharp peaks are observed corresponding to the vanishing of r associated with the changes in ν. When ν finally stops changing, so that A is close enough to the final TW, Φ relaxes monotonously as in Fig. 2.4.

It was explained in Sect. 2.3 that there are parameter ranges in which Φ is smaller near the boundaries for existence of TW, that is near $k = \pm\sqrt{a/b_r}$, than for the homogeneous TW: $k = 0$. This happens for example for $D_i = 1$, $b_r = 1.25$ ($c_1 = 1$, $c_2 = -0.8$). The corresponding function Φ_k is shown in Fig. 2.8.

If this prediction is true, and if Φ is a correct Lyapunov functional, evolution starting with one of these extreme and Eckhaus-unstable TW would not lead to any final TW, since this would increase the value of the Lyapunov functional. This would imply the existence for this value of the parameters of an attractor different from the TW's perhaps related to the Spatio-Temporal Intermittency phenomenon. We use as initial condition at the parameter values of Fig. 2.8 an unstable TW of wavenumber $k = 0.64$ ($\Phi \approx -0.81$), slightly perturbed by noise. From Fig. 2.8, the system should evolve to a state with a value of Φ value even lower than that. What really happens can be seen in Fig. 2.9. The system changes its winding number from the initial value $\nu = 52$, a process during which Φ widely fluctuates and is not a correct Lyapunov functional, and ends-up in a state of $\nu = 5$, with a value of Φ larger than the initial one. After this the system relaxes to the associated stable TW of $k = 2\pi\nu/L = 0.061 < k_E = 0.23$. As clearly stated by Graham and coworkers, the expressions for the potential are only valid for small gradients. Since k is a phase gradient, results such as Fig. 2.8 can only be trusted for k small enough.

Finally, we show the behavior of Φ in the Spatio-Temporal Intermittency regime. Since ν is constantly changing in this regime it is clear that (2.18) will not be a good Lyapunov functional and this simulation is included only for completeness. We take $D_i = 0$ and $b_r = 0.5$ ($c_1 = 0$, $c_2 = -2$) and choose as initial condition a TW with $k = 0.44 > k_E = 0.30$ ($\Phi = -1.89814$), with a small amount of noise added. The TW decreases its winding number and the system reaches soon the disordered regime called Spatio-Temporal Intermittency.

Fig. 2.10 shows that the time evolution of Φ is plagued with divergences, reflecting the fact that ν is constantly changing (see inset). It is interesting to observe however that during the initial escape from the unstable TW Φ shows a decreasing tendency, and that its average value in the chaotic regime, excluding the divergences, seems smaller than the initial one.

2.5 Numerical studies of the Lyapunov functional in the Phase Turbulence regime

The Phase Turbulence regime is characterized by the absence of phase singularities (thus ν is constant). This distinguishes it as the only chaotic regime for which Φ would be well-defined. Graham and co-workers[58, 56] derived especially for this region an expression proposed as Lyapunov functional in the small gradient approximation (2.23).
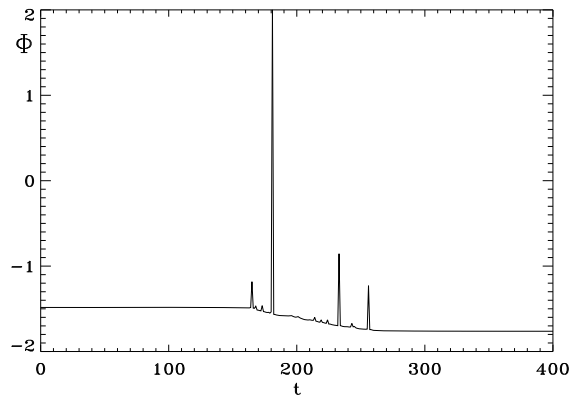
Figure 2.7: Same as Fig. 2.4 but for $c_1 = -1$ and $c_2 = -2$. The initial condition is an Eckhaus-unstable TW ($k = 0.54 > k_E = 0.48$) slightly perturbed by noise.
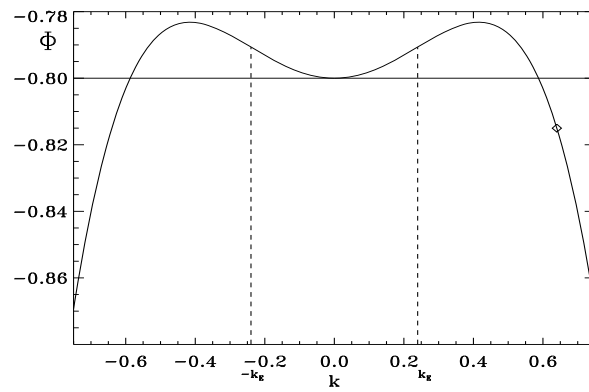
Figure 2.8: The function $\Phi_k \equiv \Phi[A_k]$ as a function of k. The parameter values are $a = 1, c_1 = 1$ and $c_2 = -0.8$. The values of k_E are indicated by dashed lines. The diamond indicates the point $\Phi_{k=0.64}$ taken as initial condition for the simulation in Fig. 2.9.
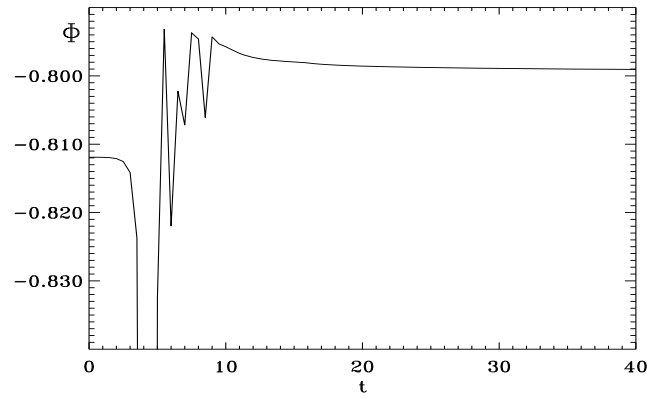
Figure 2.9: Time evolution of Φ for $c_1 = 1$ and $c_2 = -0.8$. The initial condition is an Eckhaus-unstable TW ($k = 0.64 > k_E = 0.23$) slightly perturbed by noise.
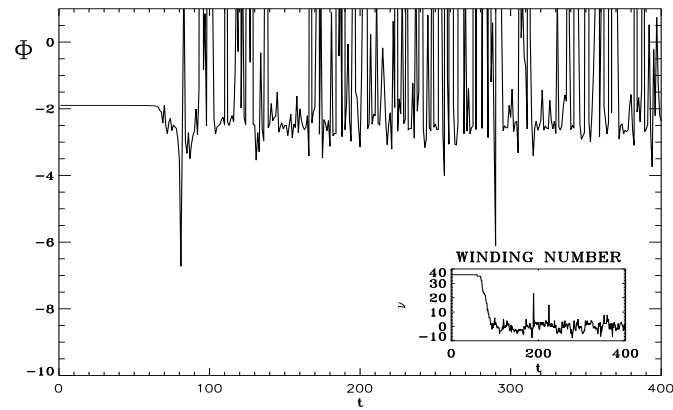
Figure 2.10: Time evolution of Φ in the STI region ($c_1 = 0.0$ and $c_2 = -2$). The initial condition is an Eckhaus-unstable TW ($k = 0.45 > k_E = 0.30$) slightly perturbed by noise. The winding number evolution is plotted in the inset.

We recall that the calculations in [58, 56] predict that the phase turbulent attractor lies on a potential plateau, consisting of all the complex functions satisfying (2.25), in which all the unstable TW cycles are also embedded. The value of the potential on such plateau can be easily calculated by substituting in (2.23) an arbitrary TW, and the result is

$$\Phi_{pl} = -\frac{a^2}{b_r} \ . \tag{2.27}$$

We note that this value does not depend on D_i nor D_r and then it is independent of c_1, the vertical position in the diagram of Fig. 2.1, within the phase turbulence region.

In this section we take also $a = 1$. We perform different simulations for $D_i = 1.75$ and $b_r = 1.25$ ($c_1 = 1.75$, $c_2 = -0.8$). In the first one, we start the evolution with the homogeneous oscillation solution (TW of $k = 0$). This solution is linearly unstable, but since no perturbation is added, the system does not escape from it. The potential value predicted by (2.27) is $\Phi_{pl} = -0.8$. This value is reproduced by the numerical simulation up to the sixth significant figure for all times (Fig. 2.11, solid line). This agreement, and the fact that the unstable TW is maintained, gives confidence in our numerical procedure.

In a second simulation, a smooth perturbation (of the form μe^{iqx} with $q = 0.049$ and $\mu = 0.09$) is added to the unstable TW and the result used as initial condition. This choice of perturbation was taken to remain as much as possible within the range of validity of the small gradient hypothesis. After a transient the perturbation grows and the TW is replaced by the phase turbulence state (the winding number remains fixed to 0). The corresponding evolution of Φ is shown in Fig. 2.11 (long-dashed line). The value of the potential increases from Φ_{pl} to a higher value, and then irregularly oscillates around it. Both the departure and the fluctuation are very small, of the order of 10^{-4} times the value of Φ. Simulations with higher precisions confirm that these small discrepancies from the theoretical predictions are not an artifact of our numerics, but should be attributed to the terms with higher gradients which are not included in (2.23). As a conclusion, the prediction that the phase turbulence dynamics, driven by non-relaxational terms, maintains constant Φ in a value equal to the one for TW is confirmed within a great accuracy.

It is interesting however to study how systematic are the small deviations from the theory. To this end we repeat the launching of the TW with a small perturbation for several values of $D_i = c_1$, for the same value of b_r as before. The prediction is that Φ should be independent of c_1. The inset in Fig. 2.11 shows that the theoretical value $\Phi_{pl} = -0.8$ is attained near the BF line, and that as c_1 is increased away from the BF line there are very small but systematic discrepancies. The values shown for the potential are time averages of its instantaneous values, and the error bars denote the standard deviation of the fluctuations around the average.

Again for $c_1 = 1.75$, $c_2 = -0.8$, we perform another simulation (Fig. 2.11, dotted line) consisting in starting the system in a random Gaussian noise configuration, of amplitude 0.01, and letting it to evolve towards the phase turbulence attractor. As in other cases, there is a transient in which Φ is ill-defined since the winding number is constantly changing. After this Φ decreases. This decreasing is not monotonous but presents small fluctuations around a decreasing trend. The decreasing finally stops and Φ remains oscillating around approximately the same value as obtained from the perturbed TW initial condition. The final state has $\nu = -1$, so that in fact the attractor reached is different
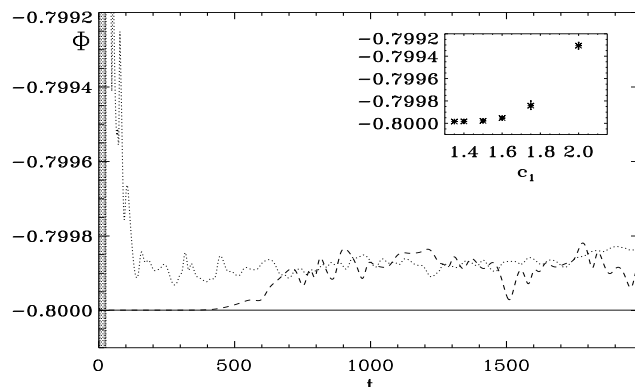
Figure 2.11: Time evolution of Φ in the Phase Turbulence region ($c_1 = 1.75$ and $c_2 = -0.8$). Solid line: evolution of a unperturbed unstable traveling wave. Dotted line: evolution from noise. Dashed line: evolution from a slightly perturbed traveling wave. The inset shows final average values of Φ as a function of the c_1 parameter ($c_2 = -0.8$). The symbol syze is approximately equal to the error bars indicate the standard deviation of the fluctuations around the average value.

from the one in the previous runs ($\nu = 0$) but the difference is the smallest possible and the difference in value of the associated potentials can not be distinguished within the fluctuations of Fig. 2.11. These observations confirm the idea of a potential which decreases as the system advances towards an attractor, and remains constant there, but at variance with the cases in the non-chaotic region here the decreasing is not perfectly monotonous, and the final value is only approximately constant.

Since the small discrepancies with the theory increase far from the BF line, and since it is known that condition (2.25) can be obtained from an adiabatic-following of the modulus to the phase that losses accuracy far from the BF line, one is lead to consider the role of adiabatic following on the validity of Φ as a potential. To this end we evaluated Φ along trajectories $A(x, t)$ constructed with the phase obtained from solutions of (2.1), but with modulus replaced by (2.25), so enforcing the adiabatic following of the modulus to the phase. No significant improvement was obtained with respect to the cases in which the adiabatic following was not enforced since that, in fact, adiabatic following was quite well accomplished by the solution of (2.1). Then it is not the fact that the solutions of (2.1) do not fulfill (2.25) exactly, but the absence of higher gradient terms in both (2.25) and (2.23) the responsible for the small failures in the behavior of Φ.

Finally, it is interesting to show that the Lyapunov potential Φ can be used as a diagnostic tool for detecting changes in behavior that would be difficult to monitor by observing the complete state of the system. For example the time at which the phase turbulence attractor is reached can be readily identified from the time-behavior of Φ in Fig. 2.11. More interestingly it can be used to detect the escape from metastable states. For example, Fig. 2.12 shows Φ for evolution from a Gaussian noise initial condition ($\epsilon = 0.01$). $D_i = 2$ and $b_r = 1.25$ ($c_1 = 2$, $c_2 = -0.8$). The system reaches first a long

lived state with $\nu = 2$ not too different from the usual phase turbulent state of $\nu = 2$. After a long time however the system leaves this metastable state and approaches a more ordered state that can be described [125, 123] as phase turbulent fluctuations around quasiperiodic configurations related to those of [91]. More details about this state will be described elsewhere [125, 123]. What is of interest here is that from Fig. 2.12 one can easily identify the changes between the different dynamical regimes. In particular the decrease in the fluctuations of Φ near $t \approx 1000$ identifies the jump from the first to the second turbulence regimes.
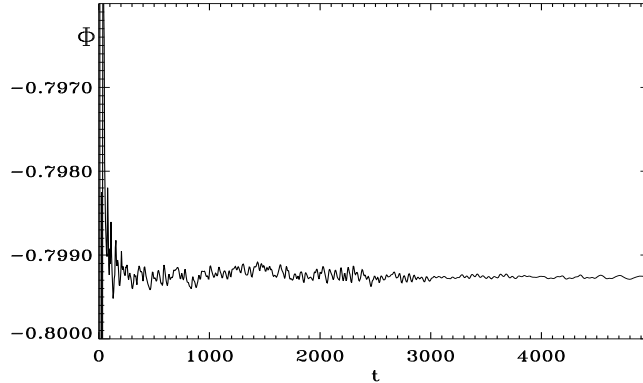
Figure 2.12: Same as Fig. 2.11 but for $c_1 = 2$ and $c_2 = -0.8$. The initial condition was random noise with an amplitude $\epsilon = 0.01$, time step 0.005. In this case 2048 Fourier modes were taken into account. Note the transition occurring around $t \approx 1000$ to a less fluctuating state.

2.6   Conclusions and outlook

The validity of the expressions for the Lyapunov functional of the CGLE found by Graham and coworkers has been numerically tested. The most important limitation is that they were explicitly constructed in a approximation limited to small gradients of modulus and phase. This precludes its use for evolution on attractors such that zeros of r and thus phase singularities appear (defect turbulence, bi-chaos, spatio-temporal intermittency). The same problem applies to transient states of evolution towards more regular attractors, if phase singularities appear in this transient (for instance decay of an Eckhaus unstable TW, evolution from random states close to $A = 0$, etc.). It would be interesting to have the expansion of the Lyapunov potential for small gradients of the real and imaginary components of A, instead of using polar coordinates. This would eliminate the problem of the ill-definition of the phase, and clarify further the stability of the gradient expansion.

Apart from this, if changes in winding number are avoided, expressions (2.17), (2.18), and (2.23) display the correct properties of a Lyapunov functional: minima on stable attractors, where non-relaxational dynamics maintains it in a constant value, and decreasing value during approach to the attractor. These properties are completely satisfied in the

non-chaotic region of parameter space, even in complex situations such as TW competition, as long as large gradients do not appear. It is remarkable that, although the potential is constructed trough an expansion around the $k = 0$ TW, its minima identify exactly the remaining TW, its stability, and the non-relaxational terms calculated by substracting the potential terms to (2.1) give exactly their frequencies. In the phase turbulence regime, however, there are small discrepancies with respect to the theoretical predictions: lack of monotonicity in the approach to the attractor, small fluctuations around the asymptotic value, and small discrepancy between the values of the potential of TW's and of turbulent configurations, that were predicted to be equal. All these deviations are very small but systematic, and grow as we go deeper in the phase turbulence regime. They can be fixed in principle by calculating more terms in the gradient expansion.

In addition in order to clarify the conceptual status of non-relaxational and non-potential dynamical systems one can ask about the utility of having approximate expressions for the Lyapunov functional of the CGLE. Several applications have been already developed for the case in which (2.1) is perturbed with random noise. In particular the stationary probability distribution is directly related to Φ, and in addition barriers and escape times from metastable TW have been calculated [76, 56]. In the absence of random noise, Φ should be still useful in stating the nonlinear stability of the different attractors. In practice however there will be limitations in the validity of the predictions, since Φ has been constructed in an expansion which is safe only near one particular attractor (the homogeneous TW).

Once known Φ, powerful statistical mechanics techniques (mean field, renormalization group, etc.) can in principle be applied to it to obtain information on the static properties of the CGLE (the dynamical properties, as time-correlation functions, would depend also on the non-relaxational terms N, as in critical dynamics [86]). Zero-temperature Monte Carlo methods can also be applied to sample the phase turbulent attractors, as an alternative to following the dynamical evolution on it. All those promising developments will have to face first with the complexity of Eqs. (2.17), (2.18), and (2.23). Another use of Lyapunov potentials (the one most used in equilibrium thermodynamics) is the identification of attractors by minimization instead of by solving the dynamical equations. In the case of the TW attractors, solving the Euler-Lagrange equations for the minimization of Φ is in fact more complex than solving directly the CGLE with a TW ansatz. But the limit cycle character of the attractors, and their specific form, is derived, not guessed as when substituting the TW ansatz. For the case of chaotic attractors (as in the phase turbulence regime) minimization of potentials can provide a step towards the construction of inertial manifolds. In this respect it should be useful considering the relationships between the Lyapunov potential of Graham and coworkers and other objects based on functional norms used also to characterize chaotic attractors [59, 22].

Chapter 3

Wound-up phase turbulence

> Turning and turning
> Within the widening gyre
> The falcon cannot hear the falconer
> Things fall apart
> The center cannot hold
> And a blood dimmed tide
> Is loosed upon the world ...
>
> Joni Mitchell, *Slouching toward Bethlehem*

3.1 Introduction

3.1.1 The complex Ginzburg-Landau equation and its phase diagram

Spatio-temporal complex dynamics [51, 52, 55] is one of the present focus of research in nonlinear phenomena. This subject lies at the intersection of two important lines of thought: on the one hand the generalization of the ideas of dynamical systems theory to high dimensional situations[32, 33, 63], and on the other the application of some concepts and tools developed in the field of statistical mechanics, specially in the study of phase transitions, to the analysis of complex nonequilibrium systems [165, 87].

Much effort has been devoted to the characterization of different dynamical states and transitions among them for model equations such as the Complex Ginzburg-Landau Equation (CGLE) [51, 63, 165, 125, 42, 43, 91, 179, 45, 64, 124]. The CGLE is an equation for a complex field $A(\mathbf{x}, t)$:

$$\partial_t A = A + (1 + ic_1)\nabla^2 A - (1 + ic_2) \mid A \mid^2 A . \tag{3.1}$$

$A(\mathbf{x}, t)$ represents the slowly varying, in space and time, complex amplitude of the Fourier mode of zero wavenumber when it has become unstable through a Hopf bifurcation (the

---

[2]First results of this Chapter appear in *Winding number instability in the phase–turbulence regime of the Complex Ginzburg-Landau equation.* by R. Montagne, E. Hernández-García, and M. San Miguel, *Phys. Rev. Lett.* **77** (1996), 267. The Chapter corresponds to *Wound–up phase turbulence in the Complex Ginzburg-Landau equation* by R. Montagne, E. Hernández-García, A. Amengual, and M. San Miguel, submitted for publication (1996).

signs used in (3.1) assume it to be supercritical). The CGLE is obtained universally when analyzing the dynamics sufficiently close to the bifurcation point. In one dimensional geometries, (3.1) or a coupled set of them with additional group velocity terms describe also the evolution of the amplitudes of Hopf-bifurcated traveling waves [51, 179, 17]. Binary fluid convection [99], transversally extended lasers [50, 159], chemical turbulence[105, 104], bluff body wakes [114], the motion of bars in the bed of rivers [162], and many other systems have been described by the CGLE in the appropriate parameter range. We will restrict ourselves in this Chapter to the one-dimensional case, that is $A = A(x,t)$, with $x \in [0, L]$.

The one-dimensional Eq(3.1) has traveling wave (TW) solutions

$$A_k = \sqrt{1 - k^2}e^{i(kx - \omega_k t)}, \ \omega_k = c_2 + (c_1 - c_2)k^2 \qquad (3.2)$$

with $k \in [-1, 1]$. When $1 + c_1 c_2 > 0$ there is a range of wavenumbers $[-k_E, k_E]$ such that TW solutions with wavenumber in this range are linearly stable. Waves with k outside this range display a sideband instability (the Eckhaus instability [91]). The limit of this range, k_E, vanishes as the quantity $1 + c_1 c_2$ approaches zero, so that the range of stable traveling waves vanishes by decreasing $1 + c_1 c_2$. The line $1 + c_1 c_2 = 0$, is the Benjamin–Feir–Newell line[173, 131], labeled BFN in Fig.3.1. Above that line, where $1 + c_1 c_2 < 0$, no traveling wave is stable and different turbulent states exist. A major step towards the analysis of phases and phase transitions in (3.1) was the numerical construction in [165, 42, 43] of a phase diagram that shows which type of regular or chaotic behavior occurs in different regions of the parameter space $[c_1, c_2]$. Fig. 3.1 has been constructed from the data in [165, 42, 43]. Above the BFN line, three types of turbulent behavior are found, namely *phase turbulence* (PT), *defect* or *amplitude turbulence* (DT), and *bichaos* (BC).

Figure 3.1: Regions of the parameter space $[c_1, c_2]$ for the CGLE displaying different kinds of regular and chaotic behavior. Lines L_1, L_3 were determined in[165, 42, 43]. See the text for the explanation of the different points.

Phase turbulence is a state in which $A(x,t) = |A|e^{i\varphi}$ evolves irregularly but with its modulus always far from $|A| = 0$. Since the modulus never vanishes, periodic boundary

conditions enforce the *winding number* defined as

$$\nu \equiv \frac{1}{2\pi} \int_0^L \partial_x \varphi dx \qquad (3.3)$$

to be a constant of motion, fixed by the initial condition. ν is always an integer because of periodic boundary conditions . The quantity $\bar{k} \equiv 2\pi\nu/L$ can be thought of as an *average* or *global wavenumber*. To the left of line L_1 (region DT), in contrast, the modulus of A becomes zero at some instants and places (called *defects* or *phase slips*). In such places the phase φ becomes undefined, so allowing ν to change its value during evolution. BC is a region in which either PT, DT, or spatial coexistence of both can be observed depending on initial conditions. It should be noted that chaotic states exist also below the BFN line: To the left of the line L_2, a chaotic attractor called *Spatio Temporal Intermittency* (STI) coexists with the stable traveling waves [42]. A diagram qualitatively similar to Fig. 3.1 has also been found for the two-dimensional CGLE [46, 119]. Despite the relevance of ν in the dynamics of the CGLE, most studies of the PT regime have only considered in detail the case of $\nu = 0$. In fact the phase diagram in Fig. 3.1 was constructed [165, 42, 43] using initial conditions that enforce $\nu = 0$. Apart from some limited observations[43, 91, 119], systematic consideration of the $\nu \neq 0$ (*wound*) disordered phases has been started only recently [125, 174, 175]. This is the subject of the present Chapter.

3.1.2 The PT-DT transition

Among the regimes described above, the transition between PT and DT has received special attention [165, 64, 157, 125, 174]. The PT regime is robustly observed for the large but finite sizes and for the long but finite observation times allowed by computer simulation, with the transition to DT appearing at a quite well defined line (L_1 in Fig. 3.1) [45, 119], but it is unknown if the PT state would persist in the thermodynamic limit $L \to \infty$. One possible scenario is that in a system long enough, and after waiting enough time, a defect would appear somewhere, making thus the conservation of ν only an approximate rule. In this scenario, PT state is a long lived unstable state. In the alternative scenario, the one in which PT and the transition to DT persist even in the thermodynamic limit, this transition would be a kind of ergodicity breaking transition [141, 125] in which the system restricts its dynamics to the small portion of configuration space characterized by a particular ν. DT would correspond to a "disordered" phase and different "ordered" phases in the PT region would be classified by its value of ν. The idea of using a quantity related to ν as an order parameter [125] has also been independently proposed in [174].

The question of which of the scenarios above is the appropriate one is not yet settled. Recent investigations seem to slightly favor the first possibility [43, 45, 64, 119]. The most powerful method in equilibrium statistical mechanics to distinguish true phase transitions from sharp crossovers is the careful analysis of finite-size effects [21]. Such type of analysis has been carried out in [45, 119] , giving some evidence (although not definitive) that the PT state will not properly exist in an infinite system or, equivalently, that the L_1 line in Fig. 3.1 approaches the BFN line as $L \to \infty$. Here we present another finite-size scaling analysis, preliminarily commented in [125], based in the quantity ν as an order parameter. Our result is inconclusive, perhaps slightly favoring the vanishing of PT at large system

sizes. In any case, the PT regime is clearly observed in the largest systems considered and its characterization is of relevance for experimental systems, that are always finite. In this Chapter we characterize this PT regime as we now outline.

3.1.3   Outline of the Chapter

We show that in the PT regime there is an instability such that a conservation law for the winding number occurs only for ν within a finite range that depends on the point in parameter space. PT states with too large $|\nu|$ are only transients and decay to states within a band of allowed winding numbers. Our results, presented in Section 3.2, allow a characterization of the transition from PT to DT in terms of the range of conserved ν: as one moves in parameter space, within the PT regime and towards the DT regime, this range becomes smaller. The transition is identified with the line in parameter space at which such stable range vanishes. Analogies with known aspects of the Eckhaus and the Benjamin-Feir instabilities are stressed. States with $\nu \neq 0$ found in the PT region of parameters at late times are of several types, and Section 3.3 describes them in terms of three [125] elementary *wound* states. Section 3.4 gives some insight into the states numerically obtained by explaining them in terms of solutions of a phase equation. In addition, theoretical predictions are made for such states. The Chapter is closed with some final remarks.

3.2   The winding number instability

The dynamics of states with non-zero winding number and periodic boundary conditions has been studied numerically in the PT region of parameters. In order to do so we have performed numerical integrations of Eq. (3.1) in a number of points, shown in Fig. 3.1. Points marked as $\diamond$ correspond to parameter values where intensive statistics was performed. The points overmarked with $\times$ correspond to places where finite-size scaling was analyzed. Finally the symbol $+$ correspond to runs made in order to determine accurately the PT-DT transition line (L_1) position. Our pseudospectral integration method is described in the Appendix A. Unless otherwise stated, system size is $L = 512$ and the spatial resolution is typically 512 modes, with some runs performed with up to 4096 modes to confirm the results. The initial condition is a traveling wave, with a desired winding number ν_i, slightly perturbed by a white Gaussian random field. Only results for $\nu_i > 0$ are shown here. The behavior for $\nu_i < 0$ is completely symmetrical.

The initial evolution of the state is well described by the linear stability analysis around the traveling wave [179, 111, 91]. Typically, as seen from the evolution of the power spectrum, the unstable sidebands initially grow. This growth stops when an intense competition among modes close to the initial wave and to the broad sidebands is established. Configurations during this early nonlinear regime are similar to the ones that would be called *riding turbulence* and described in Section 3.3. At long times the system approaches one of several possible dynamical states. In general, they can be understood in terms of three of them, which are called basic states. In the next section these final states are discussed. When the initial winding number is above a critical value ν_c, which depends on c_1 and c_2, there is a transient period between the early competition and the final state during which the winding number changes.

In Fig. 3.2b the winding number has been plotted as a function of time. The winding number changes from the initial value $\nu = 20$ to the final value $\nu = 14$. The discrete jumps in ν are due to the integer nature of this quantity, and they are smeared out when averages over several realizations are performed. The resemblance with the dynamics of the Eckhaus instability of regular waves is striking. In fact, since the changes in ν occur on top of a chaotic wave, the analogy is stronger with the Eckhaus instability in the presence of stochastic fluctuations [83, 82].

Figure 3.2: a) Spatiotemporal evolution of the phase $\varphi(x,t)$ coded in grey levels with time running upwards and x in the horizontal direction. The lighter grey correspond $\varphi(x,t) = -\pi$ and darker to $\varphi(x,t) = \pi$. The time interval shown in the picture goes from $t = 500$ to 1000 time units of a total run of 10^4. $c_1 = 2.1$, $c_2 = -0.60$, and the initial condition was a TW with $\nu_i = 20$ that decayed to $\nu_f = 14$. The arrow indicates the time at which ν begins to change. b) The complete time evolution of the winding number for this initial condition.

In the latter case a local wavenumber independent of position cannot be defined because of noise, while for phase turbulent waves the disorder is generated by the system dynamics. Nevertheless configurations in both cases can be characterized by a global wavenumber such as ν or $\bar{k}$. The analogy is also instructive since it can be shown [180, 82] that for the one–dimensional relaxational dynamics considered in [83, 82, 180] (which is related to Eq.(3.1) with $c_1 = c_2 = 0$) there is no long range order in the system, so that there is no proper phase transition in the thermodynamic $L \to \infty$ limit. Despite this, for large but finite sizes and long but finite times, sharp transitions are observed and critical exponents and scaling functions can be consistently introduced [83]. This example should make clear that even in the case that the PT-DT transition would not exist in the thermodynamic limit, its characterization in large finite systems is justified. The development of phase slips from PT waves of high enough ν can be viewed as a kind of Eckhaus-like instability

for turbulent waves, whereas the usual Eckhaus instability [91] appears for regular waves. This similarity was one of the main motivations for the kind of analysis that follows. For each point in parameter space and initial winding number considered, we averaged over 50 independent random realizations of the white Gaussian perturbation added to the initial wave. Figs. 3.3a and 3.3b show the temporal evolution of this average $\bar{\nu}(t)$ and its variance σ for $c_1 = 2.1$ and $c_2 = -0.6$. Four values of the initial winding number ($\nu_i = 10, 15, 20, 25$) are shown. Typically, the curve $\bar{\nu}(t)$ decays from ν_i to a final winding number ν_f.

Figure 3.3: a) Temporal evolution of $\bar{\nu}(t)$ for four different initial winding numbers $\nu_i = 25$ (solid), 20(dotted), 15 (dashed) 10 (dashed-dotted). $c_1 = 2.1, c_2 = -0.83$ (PT regime). b) Winding number standard deviation σ.

The variance displays the behavior typical of a decay from a unstable state [19], namely a pronounced maximum at the time of fastest variation of $\bar{\nu}(t)$. The final value of σ gives the dispersion in the final values of the winding numbers. Although the behavior shown in Fig. 3.3 is very similar to the observed in [83] for a stochastic relaxational case, the scaling laws found there do not apply here. The main qualitative difference is that in a range of ν_i the sign of the average final $\bar{\nu}$ is here opposite to the initial one. In addition for some of the initial winding numbers (i.e. $\nu_i = 20$ in Fig. 3.3) $\bar{\nu}(t)$ is not monotonously decaying, showing a small recovery after the fast decrease in $\bar{\nu}$. These features are also observed for other values of $[c_1, c_2]$. Figure 3.3 is typical for $[c_1, c_2]$ in the PT region of Fig. 3.1. For comparison we show $\bar{\nu}(t)$ and its variance in Fig. 3.4 for the point $c_1 = 1.6$ and $c_2 = -1.0$, in the "bichaos" region. The main difference is in the fluctuations presented by the curves. They are related to the characteristic dynamic of the bichaos regime: The final configuration depends on the initial conditions and it can correspond to PT, DT or even coexistence of both. In the 50 realizations performed all these possibilities were found. When DT appears, there are big fluctuations of the winding number around $\nu = 0$ that produce the wiggling on the averaged value. More than 50 realizations should be performed to smooth out such big fluctuations. Returning to the PT parameter regime (Fig. 3.3) the decay of the initial state is seen to take place during a characteristic time which depends on ν_i. We quantify this time τ as the time for which half of the jump in ν is attained. τ increases as ν_i decreases, and there is a critical value of ν_i, ν_c, such that no decay is observed for $\nu_i < \nu_c$. Then τ diverges (critical slowing down) when ν_i approaches ν_c from

Figure 3.4: a) Temporal evolution of $\bar{\nu}(t)$ for an initial winding numbers of $\nu_i = 4$ in the bichaos regime. $c_1 = 1.6, c_2 = -1.0$. b) Winding number standard deviation σ.

above. This gives a sensible procedure to determine ν_c: Figs. 3.5a and 3.5b show $1/\tau$ as a function of ν_i. In Fig. 3.5a, c_1 is fixed and the different symbols correspond to different values of c_2. In Fig. 3.5b, c_2 is fixed and the symbols correspond to different values of c_1. The values of ν_c have been estimated by extrapolating to $1/\tau = 0$ a linear fit to the points of smallest ν_i in each sequence. Motivated by [83] we have tried to fit the divergence of τ with nontrivial critical exponents, but we have found no significant improvement over the simpler linear fit. The values of ν_c so obtained are plotted in the insets of Figs. 3.5a and 3.5b. The range of conserved winding numbers $[-\nu_c, \nu_c]$ is analogous to the Eckhaus range of stable wavenumbers when working below the BFN line. ν_c can also be obtained by directly determining the value of ν_i below which $\nu(t)$ does not change in any of the realizations. This method can only give integer values of ν_c whereas the method based on τ gives a real number which is preferable when looking for continuous dependences of ν_c on system parameters. The two methods however give consistent results within the discretization indeterminacy.

The insets of Fig. 3.5a and Fig. 3.5b indicate a clear decrease in ν_c as the values of c_1 and c_2 approach the L_1 line. In fact we know that ν_c should be zero to the left of L_1, since no wave maintains its winding number constant there. This lead us to a sensible method for determining the position of line L_1 [125], alternative to the one based in the density of defects used in [165]. It consist in extrapolating the behavior of ν_c to $\nu_c = 0$. In this way the line L_1 is determined as the line at which the range of conserved winding numbers $[-\nu_c, \nu_c]$ shrinks to zero. The analogy with the Eckhaus instability of regular waves is again remarkable: in the same way as the range of Eckhaus-stable wavenumbers shrinks to zero when approaching the BFN line from below, the allowed ν range shrinks to zero when approaching the L_1 line from the right. The difference is that below the BFN line the values of the wavenumber characterizes plane-wave attractors, whereas above that line, ν characterizes phase-turbulent waves. In this picture, the transition line PT–DT appears as the *BFN line* associated to an Eckhaus-like instability for phase turbulent waves.

For the cases of Fig. 3.5a the PT–DT transition is located at $c_1 = 2.1, c_2 = -0.89 \pm 0.02$, and $c_1 = 2.60 \pm 0.02, c_2 = -0.83$ for the case of Fig. 3.5b. The same method to determine

Figure 3.5: a) Inverse of the characteristic time for winding number relaxation as a function of the initial winding number. The value of c_1 is fixed ($c_1 = 2.1$) and c_2 varies from near the B-F line ($c_2 \simeq -0.48$) to the L_1 line ($c_2 \approx -0.9$). Different symbols correspond to $c_2 = -0.6$ (+), $c_2 = -0.7$ (∗), $c_2 = -0.75$ ($\diamond$), $c_2 = -0.8$ ($\triangle$), $c_2 = -0.83$ ($\square$). The inset shows the critical winding number (ν_c) as a function of c_2. b) Idem but the value of c_2 is fixed ($c_2 = -0.75$) and c_1 varies from near the B-F line ($c_1 \simeq -1.33$) to $c_1 = 2.5$. Different symbols correspond to $c_1 = 1.6$ (+), $c_1 = 1.8$ (∗), $c_1 = 1.96$ ($\diamond$), $c_1 = 2.1$ ($\triangle$), $c_1 = 2.3$ ($\square$)$c_1 = 2.5$ ($\times$). The inset shows the critical winding number (ν_c) as a function of c_1

the line $L1$ has been independently introduced in [174, 175]. The coefficients of the linear fit are not universal: they depend of the particular path by which the line L_1 is approached. The agreement with the position of the line as determined by [165, 43], where system sizes similar to ours are used, is good. For example for $c_1 = 2.1$ their value for L_1 is $c_2 = -0.92$. The points marked as + in Fig. 3.1, correspond to runs used to determine the position of the transition line L_1 directly as the line at which defects appear in a long run even with $\nu = 0$. The agreement between all these ways of determining L_1 give consistent results. Below the point P, ν_c goes to zero when the parameters approach the line L_3, not L_1, thus confirming the known behavior that below point P the line separating phase turbulence from defect turbulence when coming from the PT side is actually L_3.

The use of a linear fit to locate the line L_1 is questionable and more complex fits have been tested. However, the simplest linear fit has been found of enough quality for most of the the situations checked, the inset in Fig 3.5b being one of the worst cases. Clearly some theoretical guide is needed to suggest alternative functional forms for $\nu_c(c_1, c_2)$. We notice that the analogous quantity below the BFN line, the Eckhaus wavenumber limit, behaves as $q_E \sim \sqrt{\epsilon}$ for small ϵ, being ϵ the difference between either c_1 or c_2 and its value at the BFN line. From the insets in Figs. 3.5a or 3.5b, this functional form is clearly less adequate than the linear fit used.

Another interesting point to study is the dependence of the final average winding number $\bar{\nu}_f$ on the initial one ν_i. Fig. 3.6 shows an example using $c_1 = 2.1$ and $c_2 = -0.8$. The behavior for other values of the parameters is qualitatively similar. $\bar{\nu}_f$ remains equal

ν_i

18

to the initial value if $\nu_i \leq 5$ during the whole simulation time, so that $\nu_c \approx 5$, a value consistent with the one obtained from the divergence of τ and plotted in in the inset of Fig. 3.5a. For $\nu_i > \nu_c$, the final winding number is always smaller than the initial one. By increasing ν_i a minimum on $\bar{\nu}_f$ is always observed, and then $\bar{\nu}_f$ tends to a constant value.

Figure 3.6: The final averaged winding number $(\bar{\nu}_f)$ as a function of the initial one ν_i. The initial condition is a TW with winding number ν_i for $c_1 = 2.1$ and $c_2 = -0.8$. The dashed line corresponds to the lowest of the two fastest Fourier modes of fastest growth in the linear regime as a function of ν_i.

Figure 3.7: The critical winding number (ν_c) as a function of the length L of the system is shown. Different symbols correspond to $c_1 = 2.1$ and $c_2 = -0.8$ ($\triangle$) and $c_1 = 1.96$ and $c_2 = -0.83$ ($\diamond$). The straight lines are linear fits to the two sets of data.

Figure 3.6 also shows the winding number associated with one of the two Fourier modes of fastest growth obtained from the linear stability analysis of the initial traveling wave. The one shown is the lowest, the other one starts at $\bar{\nu}_f = 28$ and grows further up. Obviously they do not determine the final state in a direct way. This is consistent with

the observation mentioned above that the winding number instability does not develop directly from the linear instability of the traveling wave, but from a later nonlinear competition regime. As stated in the introduction, a powerful way of distinguishing true phase transitions from effective ones is the analysis of finite-size scaling [21]. We have tried to analyze size–effects from the point of view of ν as an order parameter. In the DT state such kind of analysis was performed in [62]. Egolf showed that the distribution of the values taken by the ever-changing winding number is a Gaussian function of width proportional to $\sqrt{L}$. This is exactly the expected behavior for order parameters in disordered phases. In the thermodynamic limit the intensive version of the order parameter, ν/L, would tend to zero so that the disordered DT phase in the thermodynamic limit is characterized by a vanishing intensive order parameter. For the PT states to be true distinct phases, the existence of a nonvanishing ν_c such that ν is constant for $|\nu| < \nu_c$ is not enough. The range of stable winding numbers should also grow at least linearly with L for this range to have any macroscopic significance. The analysis of the growth of ν_c with system size has been performed in points $c_1 = 2.1, c_2 = -0.8$ and $c_1 = 1.96, c_2 = -0.83$ of parameter space. ν_c, determined as explained before, is plotted in Fig. 3.7 for several system sizes for which the statistical sample of 50 runs was collected for each ν_i.

There is a clear increasing, close to linear, of ν_c as a function of L, thus indicating that for this range of system sizes the range of allowed winding numbers is an extensive quantity and then each ν is a good order parameter for classifying well defined PT phases. It should be noted however that for the larger system size for which extensive statistics was collected ($L = 2048$) data seem to show a tendency towards saturation. Thus our study should be considered as not conclusive, and larger systems sizes need to be considered.

3.3   Different asymptotic states in the PT region

Typical configurations of the PT state of zero winding number consist of pulses in the modulus $|A|$, acting as phase sinks, that travel and collide rather irregularly on top of the $k = 0$ unstable background wave (that is, a uniform oscillation)[165, 43]. The phase of these configurations strongly resembles solutions of the Kuramoto-Shivashinsky (KS) equation. Quantitative agreement has been found between the phase of the $\nu = 0$ PT states of the CGLE and solutions of the KS equation near the BFN line[64].

For states with $\nu \neq 0$ a typical state[43] is the one in which an average speed (in a direction determined by the sign of ν) is added to the irregular motion of the pulses. We have found that in addition to these configurations there are other attractors in the PT region of parameters. We have identified [125] three basic types of asymptotic states for $\nu \neq 0$, which we describe bellow. Other states can be described in terms of these basic ones. Except when explicitly stated, all the configurations described in this Section have been obtained by running for long times Eq. (3.1) with the initial condition described before, that is small random Gaussian noise added to a unstable traveling wave. The winding number of these final states is constant and is reached after a transient period in which the winding number might have changed.

Figs. 3.8, 3.9 and 3.11 show examples of the basic states that we call *riding PT* (Fig. 3.8), *quasiperiodic states* (Fig. 3.9) and *frozen turbulence* (Fig. 3.11). For each figure: Panel (a) corresponds to a grey scale space–time plot of $\partial_x \varphi(x, t)$. Panel (b) shows

the value of this quantity and the modulus of the field ($| A |$) as a function of position at the time indicated by an arrow in panels (a) and (d). Panel (c) shows the spatial power spectrum $S(q,t)$ of $A(x,t)$ for the same time. Finally, panel (d) shows the quantity $W = \int | \partial_t S(q,t) | dq$, which is a global measure of the temporal change in the spatial power spectrum.

Riding PT. This state (see Fig. 3.8) is the most familiar one [43]: wiggling pulses in the gradient of the phase with a systematic drift in a direction determined by ν. The modulus of the field consist of a disordered spatial sequence of small pulses and shocks, with $A(x,t)$ always far from zero. The spatial power spectrum $S(q)$ has a peak corresponding to the global wave number (associated in this case with $\nu = -1$) and a broad background associated with the turbulent motion "riding" on the traveling wave. The time evolution of W shows a decay towards a fluctuating non-zero value, indicating that the power spectrum is continuously changing in time as corresponds to the turbulent state reached by the system.

Quasiperiodic states. These states (an example is shown in Fig. 3.9) can be described as the motion of equidistant pulses in the gradient of the phase that travel at constant speed on top of the background wave. The fact that the periodicity of the pulses and that of the supporting wave are not the same justify the name of *quasiperiodic*. We show later that these states correspond to the ones described in Ref. [91]. In Fig. 3.9a, the modulus $| A |$ and the gradient of the phase clearly exhibit uniformly traveling pulses. The spatial power spectrum $S(q)$ (Fig. 3.9c), clearly shows the quasiperiodic nature of this state: A central peak, corresponding to the dominant plane wave, with equally spaced peaks surrounding it, showing the periodicity of the pulses. The peaks are not sharp because this configuration has been obtained from a random perturbation. The decrease of W in Fig. 3.9d, indicates that the peaks are narrowing. Its asymptotic approach to zero indicates that the amplitudes of the main modes will reach a steady value and $S(q)$ becomes time independent. This quasiperiodic configuration is one of the attractors of the dynamics.

More perfect quasiperiodic configurations can be obtained from initial configurations that are already quasiperiodic. Figure 3.10 shows the quantity W for a state generated with $\nu = 18$ for $c_1 = 2.1$ and $c_2 = -0.6$ from an initial traveling wave with a sinusoidal perturbation. The initial traveling wave had $\nu_i = 18$ and the winding number of the sinusoidal perturbation was $\nu = 22$. The spatial power spectrum (shown in the inset at the time indicated by an arrow in the main picture) shows the typical characteristics of a quasiperiodic state.

Frozen turbulence. This state (see Fig. 3.11) was first described in [125]. It consists of pulses in $\partial_x \varphi$ traveling at constant speed on a traveling wave background, as in the quasiperiodic case, but now the pulses are not equidistant from each other (see Fig. 3.11b). The power spectrum at a given time is quite different from the one of a quasiperiodic state. Instead, it is similar to the power spectrum obtained in the *riding PT* state: $S(q)$ is a broad spectrum in the sense that the inverse of the width, which gives a measure of the correlation length, is small compared with the system size. Here however W relaxes to zero, so that the power spectrum finally stops changing (thereby the name *frozen*).

This behavior is an indicator of the fact [125], obvious from Fig. 3.11, that the pattern approaches a state of rigid motion for the modulation in modulus and gradient of the

Figure 3.8: a) Spatiotemporal evolution of $\partial_x \varphi(x, t)$. The lighter grey correspond to the maximum value of $\partial_x \varphi(x, t)$ and darker to the minimum. Last 2000 time units of a run 10^4 time units long for a *riding PT* state at $c_1 = 2.1$, and $c_2 = -0.83$. The initial condition was a TW with $\nu_i = 20$ that decayed to $\nu_f = -1$ after a short time. b) A snapshot of $| A(x, t) |$ and $\partial_x \varphi(x, t)$ as a function of x for $t = 8900$ which is indicated by an arrow in a) and d). c) Spatial power spectrum $S(q)$ as a function of wavenumber at the same time $t = 8900$. d)The time evolution of the quantity W defined in the text. The dashed line indicates the time at which the picture a) starts.

Figure 3.9: Same as in Fig. 3.8 but for last 10^2 time units of a run 10^5 time units long for a quasiperiodic state. The initial condition is random noise with an amplitude of 0.05. $c_1 = 2.0$, and $c_2 = -0.8$. a) and c) correspond to a time $t = 8 \times 10^4$.

Figure 3.10: a)The time evolution of W for a quasiperiodic state. The initial condition is a TW sinusoidally perturbed for $c_1 = 2.1$ and $c_2 = -0.6$. In the inset the spatial power spectrum $S(q)$ as a function of wavenumber at the time $t = 8900$ indicated by an arrow in the main picture.

phase of the unstable background plane wave. That is, the field $A(x, t)$ is of the form:

$$A(x,t) = g(x - vt)e^{i(kx - \omega_k t + \alpha(t))} \tag{3.4}$$

where g is a uniformly translating complex modulation factor. It is easy to see that configurations of the form (3.4) have a time-independent spatial power spectrum. Torcini [174] noticed in addition the function $\alpha(t)$ is linear in t so that the solutions are in fact of the form

$$A(x,t) = f(x - vt)e^{i(kx - \omega t)} \tag{3.5}$$

where again $f(x - vt)$ is a complex valued function and ω can differ from ω_k. The envelopes $g(x - vt)$ or $f(x - vt)$ turn out to be rather irregular functions in the present *frozen turbulence* case, whereas they are periodic in the quasiperiodic configurations discussed above.

After presenting the basic states, we continue addressing some interesting mixed states that can be described in terms of them. Most of the configurations ending up in the frozen turbulence or in the quasiperiodic states have long time transients of the riding turbulence type. Only at long times a decay to rigid propagation occurs. There are cases in which a different type of decay happens. For example Fig. 3.12 shows a case in which the system jumps from a very strong riding turbulence regime to another state, also of the riding turbulence type, but much more regular. The quantity W, shown in Fig. 3.12b, turns out to be a valuable tool in distinguishing the different regimes: a superficial look at Fig. 3.12a could be easily misunderstood as indicating the approach of the system towards a frozen turbulence state, but the lack of decay towards zero of W identifies the final state as a riding turbulence one. The arrows indicate the jump to the second state.

Figure 3.11: Same as in Fig. 3.9 but for last 2500 time units of a run 10^4 time units long for a frozen turbulence state. The initial condition is a TW of $\nu_i = 12$ that decays to $\nu_f = 6$ after a short time. $c_1 = 1.75$, and $c_2 = -0.8$. The time of b) and c) is $t = 8900$, indicated by an arrow as in previous figures.

Figure 3.12: a) Spatiotemporal evolution of $\partial_x \varphi(x,t)$ for a riding turbulence state that decays onto another one. $c_1 = 2.5$, $c_2 = -0.75$. The initial condition is a TW of $\nu_i = 20$ that decays to $\nu_f = -2$ in a short time. b) Time evolution of W. The dashed lines indicate the time interval shown in a) (from $t_1 = 2500$ to $t_2 = 6500$ of a run 10^5 time units long). The arrow indicates the transition from one of the riding turbulence regimes to the other one.

Figure 3.13: a) Spatiotemporal evolution of $\partial_x \varphi(x,t)$ showing intermittency between riding turbulence states. $c_1 = 2.1$, $c_2 = -0.83$. The initial condition is a TW of $\nu_i = 1$ that did not change. b)Time evolution of W. The dashed lines indicate the time interval shown in a) (from $t_1 = 1000$ to $t_2 = 8500$ of a run 10^4 time units long). The arrows indicate the end of a riding turbulence regime and the beginning of another one.

Figure 3.14: a) Spatiotemporal evolution of $\partial_x \varphi(x, t)$. The time interval corresponds to 5500 to 7500 time units of a run 10^4 time units long for a *riding PT* state at $c_1 = 2.1$ and $c_2 = -0.83$. The initial condition was a TW with $\nu_i = 0$ that did not change. b) Snapshots of $\varphi(x, t)$ and $\partial_x \varphi(x, t)$ as a function of x at the time $t = 6980$ indicated by an arrow in a) and d). The dashed lines in the graph of $\varphi(x, t)$ indicate average slopes, that is "local" wavenumbers. c) Spatial power spectrum $S(q)$ as a function of wavenumber at the same time $t = 6980$. d)Time evolution of W. Dashed lines indicate the time interval of picture a).

Fig. 3.13 displays a state characterized by a recurrence between two different riding

turbulence states, showing a kind of temporal intermittency. Fig. 3.14 shows a riding turbulence state with zero winding number. This is not however a typical configuration, since usually for $\nu = 0$ there is no preferred direction for the pulses to drift, whereas the figure shows that in fact there is a local drift at some places of the system. It turns out that this state can be understood as composed by two domains of different local winding number: $\nu = 1$ and $\nu = -1$, so that globally $\nu = 0$. The pulses travel either in one direction or in the other depending of the region of the system in which they are. In Fig. 3.14b a snapshot of the gradient of the phase $\partial_x \varphi(x, t)$ and the phase itself $\varphi(x, t)$ is shown. Lines showing the average trend in the phase are plotted over the phase, clearly identifying the two regions in the system. This coexistence of the different basic states at different places of space, or at different times as in Fig. 3.13, was mentioned in [42] where it was argued to give rise to a kind of spatio-temporal intermittent behavior.

Given the large variety of configurations that are observed, and the very long transients before a jump from one state to another occurs, it would be difficult to conclude from numerical evidence alone that the three kinds of states considered as *basic* above are true asymptotic states. Some analytical insight would be desirable to be sure that these three states are attractors of the dynamics. The next Section is devoted to provide such analytical justification.

3.4   Asymptotic states in terms of the phase dynamics

The question on whether it is possible or not to describe the PT regime of the CGLE from a closed equation for the phase alone has been posed by several authors[158, 77, 64, 45, 119]. A phase equation is obtained by considering a long wavelength perturbation of a plane-wave solution in the CGLE (3.1). It is clear that this phase equation will only describe phase dynamics close to the homogeneous plane-wave (that is the one with $\nu = 0$) if the perturbation is made around the spatially–homogeneous solution. In order to get a description of PT at $\nu \neq 0$ the expansion should be done for a perturbation on a traveling wave solution with wavenumber (k) different from zero,

$$A = (\sqrt{1 - k^2} + a(x, t))e^{i(kx + \varphi(x,t))} , \qquad (3.6)$$

Here k is taken as $k = \frac{2\pi}{L}\nu$. If A satisfies periodic boundary conditions the same conditions apply to ϕ because any global phase winding is included in k (the total phase is $\varphi = kx + \phi$). From general symmetry arguments the general phase equation for $k \neq 0$ should read, up to fourth order in gradients:

$$\begin{aligned}
\partial_t \phi &= \Omega_0 - v_g \partial_x \phi - D_2 \partial_x^2 \phi + D_{11}(\partial_x \phi)^2 + D_3 \partial_x^3 \phi + D_{12}(\partial_x \phi)(\partial_x^2 \phi) \\
&\quad - D_4 \partial_x^4 \phi + D_{13}(\partial_x \phi)(\partial_x^3 \phi) + D_{22}\left(\partial_x^2 \phi\right)^2 + D_{112}(\partial_x \phi)^2(\partial_x^2 \phi) + \dots .
\end{aligned} \qquad (3.7)$$

When $v_g = D_3 = D_{12} = D_{13} = D_{22} = D_{112} = 0$, Eq. (3.7) reduces to the Kuramoto–Sivashinsky (KS) equation [101, 166] that is the lowest order nonlinear phase equation for the case $k = 0$. For $k \neq 0$, Eq. (3.7) was systematically derived up to third order in gradients in [111]. An easy way of obtaining the values of all the coefficients in (3.7) was presented in [103]: First, Ω_0 is related to the frequency of the plane-wave solutions:

$$\Omega_0 = -\omega_k = -c_2 - (c_1 - c_2)k^2 \qquad (3.8)$$

Second, the linear terms can be obtained from the eigenvalue $\lambda(k, q)$ corresponding to the phase-like branch in the linear stability analysis of the wave of wavenumber k with respect to perturbations of wavenumber q[179, 111, 91]:

$$\lambda(k, q) = -iv_g q + D_2 q^2 - iD_3 q^3 - D_4 q^4 + \mathcal{O}(q^5) \tag{3.9}$$

with

$$v_g = 2k(c_1 - c_2) \tag{3.10}$$

$$D_2 = -(1 + c_1 c_2) + \frac{2k^2(1 + c_2^2)}{1 - k^2} \tag{3.11}$$

$$D_3 = \frac{2k(1 + c_2^2)\left[-c_1 + (c_1 + 2c_2)k^2\right]}{(1 - k^2)^2} \tag{3.12}$$

$$D_4 = \frac{1}{2(1 - k^2)^3}\left\{c_1^2(1 + c_2^2) - 2k^2(1 + c_2^2)(c_1^2 + 6c_1 c_2)\right.$$
$$+ \left. k^4\left[4 + (1 + c_2^2)(c_1^2 + 12c_1 c_2) + c_2^2(24 + 20c_2^2)\right]\right\} . \tag{3.13}$$

Third, the nonlinear terms can be obtained from the following consistency relationship: If $(\sqrt{1 - k^2} + a(x, t))e^{i(kx + \phi(x,t))}$ is an exact solution of the CGLE, then $\phi(x, t)$ satisfies the phase equation with coefficients depending on k. In addition if $(\sqrt{1 - k_1^2} + a_1(x, t))e^{i(k_1 x + \phi_1(x,t))}$ is another exact solution of the CGLE, then $\phi_1(x, t)$ satisfies a similar phase equation but with coefficients depending on k_1 instead of k. But this solution can be written as $(\sqrt{1 - k_1^2} + a_1(x, t))e^{i(kx + (k_1 - k)x + \phi_1(x,t))}$ so that $(k_1 - k)x + \phi_1(x, t)$ is also solution of the phase equation with coefficients depending on k (with different boundary conditions). By combining the two equations satisfied by ϕ_1 and expanding the coefficients depending on k_1 as a power series around k (assuming $k_1 - k$ small) the following relationships between linear and nonlinear terms are obtained:

$$D_{11} = -\frac{1}{2}\frac{\partial v_g}{\partial k} , \quad D_{12} = -\frac{\partial D_2}{\partial k} , \quad D_{13} = \frac{\partial D_3}{\partial k} , \quad D_{112} = -\frac{1}{2}\frac{\partial^2 D_2}{\partial k^2} \tag{3.14}$$

So that

$$D_{11} = c_2 - c_1 \tag{3.15}$$

$$D_{12} = -\frac{4k(1 + c_2^2)}{(1 - k^2)^2} \tag{3.16}$$

$$D_{13} = \frac{2(1 + c_2^2)}{(1 - k^2)^3}\left[-c_1 + 6c_2 k^2 + (2c_2 + c_1)k^4\right] \tag{3.17}$$

$$D_{112} = -\frac{2(1 + c_2^2)(3k^2 + 1)}{(1 - k^2)^3} \tag{3.18}$$

The coefficient D_{22} is only obtained following the method to higher order in $(k_1 - k)$. The coefficients up to third order in gradients can be found also in [111] and approximate expressions for them are given in [91].

The traveling wave of wavenumber k becomes unstable when the coefficient D_2 becomes positive. One expects that the first terms in the gradient expansion (3.7) give a good

description of the phase dynamics in the weakly nonlinear regime, that is D_2 positive but small (note that for $k \neq 0$ this includes part of the region below the BFN line in Fig. 3.1). The arguments presented in [103] imply that for D_2 small the relative importance of the different terms in a multiple scale expansion can be established by considering $\phi \sim \partial_x \sim D_2^{1/2}$. Then the dominant terms close to the instability of wave k are the ones containing Ω_0 and v_g. After them, the terms with coefficients D_3 and D_{11} are the most relevant. Up to this order Eq. (3.7) is a Korteweg–de Vries equation (KdV). The terms with D_2, D_4 and D_{12} appear at the next order. The importance of the terms in D_2 and D_4 for a qualitatively correct description of phase dynamics is obvious since they control the stability properties of the wave of wavenumber k. The importance of the term with coefficient D_{12} was stressed in [91, 20]: if it is large enough it can change the character of the bifurcation from supercritical to subcritical.

The detailed comparison of the reduced dynamics (3.7) with the complete CGLE phase dynamics is beyond the scope of the present paper. The aim of this Section is to use Eq.(3.7) just to get some understanding of the asymptotic states presented in Section 3.3. To this end we will use the detailed results available from the work of Chang et al. [40]. These results are obtained for the so-called Kawahara equation [92, 93, 20, 40, 94] which is Eq.(3.7) with $D_{12} = D_{13} = D_{22} = D_{112} = 0$. The term D_{12}, which according to Kuramoto estimations [103] is of the same order for small D_2 as the terms in D_2 and D_4, will thus be neglected. It would be certainly necessary to consider the modifications introduced by the term D_{12} into the results of [40]. This will be briefly discussed at the end of this section. At this point it is interesting to note that, to our knowledge, the only quantitative comparison of the phase dynamics with $k \neq 0$ obtained from a phase equation and from CGLE is [174, 175]. But the phase equation used in these references is the one presented in [158], in which the nonlinear terms considered are only those with coefficients D_{11} and D_{13}. In addition D_{11}, D_{13}, and the coefficients of the linear terms are considered only up to first order in k. Despite the absence of the D_{12} term, the phase equation is found to reproduce well the phase dynamics of the CGLE, an agreement that degrades when the term in D_{13} is suppressed [2]. Clearly further work is needed to establish firmly the relevance of the different terms in (3.7)[3]. Our study will be restricted to the situation of [40] (that is $D_{12} = D_{22} = D_{13} = D_{112} = 0$) since no study of comparable detail for a more complete equation is available in the literature.

The situation of interest here is the one in which the plane waves are unstable, so that D_2, $D_4 > 0$. Making the following changes of variables in (3.7) with $D_{12} = D_{22} = D_{13} = D_{112} = 0$:

$$
\begin{aligned}
\chi &= \sqrt{\frac{D_2}{D_4}}\,(x - v_g t)\ , \\
\tau &= \frac{D_2^2}{D_4}t\ , \\
u(\chi, \tau) &= -\frac{D_{11}D_4^{1/2}}{2D_2^{3/2}}\partial_x\phi(x, t)\ .
\end{aligned}
\tag{3.19}
$$

the Kawahara Equation[92, 93, 20, 40, 94] is obtained

$$
\partial_{tau}u = -\partial_\chi^2 u - 4u\partial_\chi u - \delta\partial_\chi^3 u - \partial_\chi^4 u\ ,
\tag{3.20}
$$

with

$$\delta = -\frac{D_3}{\sqrt{D_2 D_4}} \qquad (3.21)$$

Since ϕ is periodic in x, $u(\chi, t)$ is periodic in χ. In addition $\int_0^L u(\chi, \tau) d\chi = 0$. To have some intuition on the meaning of the parameter δ, its expansion at small k reads

$$\delta \approx 2\sqrt{2}\, k \,\text{sign}\,(c_1)\sqrt{\frac{1 + c_2^2}{|\, 1 + c_1 c_2\,|}} + \mathcal{O}(k^3) \; . \qquad (3.22)$$

It should be noted that δ does not diverge at the BFN line, as the expansion (3.22) seems to suggest, but below it. From Eq. (3.21) it is clear that δ diverges where D_2 vanishes indicating that the corresponding traveling wave of wavenumber k has become Eckhaus unstable.

The Kawahara equation (3.20) has been considered in the context of surface waves on fluid films falling down an inclined or vertical plane [39], and also as a simple generalization of the KS or the KdV equations [92, 93]. It has also been considered in the context of growth shapes [48]. It reduces to KS for $\delta = 0$ (or equivalently for $k = 0$) when written in the original variable φ.

The equation (3.20) has periodic, soliton-like, spatially-irregular, and spatio-temporally chaotic solutions. [92, 93, 94]. In fact, all of these solutions have been analytically shown to exist [40]. All of them except the isolated soliton-like solution [41] are stable in some parameter regimes [40]. These kinds of solutions should manifest themselves (provided the approximate phase description holds) in the time evolution of the phase gradient $\partial_x \varphi$ ($= k + \partial\phi$) of the solutions of the CGLE (3.1) in the PT regime. The analytical results in [40] thus provide a firm basis for true existence of the numerically observed states described in Section 3.3.

The detailed bifurcation analysis in [40] also gives detailed predictions for the wound states of the CGLE, within the range of validity of the phase description. We will reproduce here some of the results in [40] and reinterpret them in terms of the gradient of the phase of CGLE solutions. Our interest is centered in the rigidly moving train of pulses (frozen turbulence and quasiperiodic states) observed in several of the numerical simulations reported in Section 3.3. They are of the form (3.5) and because of (3.19), we have

$$u(\chi, \tau) = H(\xi) \; , \qquad (3.23)$$

with $\xi = \chi - v\tau$, being v the velocity of the train of pulses we want to describe in units of χ and τ. The partial differential equation (3.20) is reduced to an ordinary differential equation (ODE) for $H(\xi)$:

$$H^{iv} + \delta H''' + H'' + 4HH' - vH' = 0 \; . \qquad (3.24)$$

The primes denote differentiation with respect to ξ. After an integration:

$$H''' + \delta H'' + H' - vH + 2H^2 = Q \; . \qquad (3.25)$$

Q is fixed in a nontrivial way by the condition $\int H d\xi = 0$ which follows from our periodic boundary conditions. This third order ODE can be rewritten as a three-dimensional

dynamical system:

$$
\begin{aligned}
u_1' &= u_2 \\
u_2' &= u_3 \\
u_3' &= cu_1 - u_2 - \delta u_3 - 2(u_1)^2
\end{aligned}
\tag{3.26}
$$

with

$$
\begin{aligned}
u_1(\xi) &= H(\chi) - \frac{v}{4} + \sqrt{\frac{c^2}{16} + \frac{Q}{2}} \,, \\
c &= \sqrt{8Q + v^2} \,.
\end{aligned}
\tag{3.27}
$$

Different qualitative behaviors in phase space of the solutions of the dynamical system (3.26) are related to the shape of the solutions of (3.24) [152]. This is illustrated in Fig. 3.15.

We stress that all the solutions of (3.24) represent uniformly translating solutions of (3.20). No information is given on more complicated solutions of (3.20). The left column of Fig. 3.15 shows the possible trajectories of the dynamical system (3.26) while the right column shows the corresponding solution of (3.25), or equivalently $u(\chi, \tau) = H(\xi = \chi - v\tau)$ in equation (3.20). For a fixed point in (3.26) (Fig. 3.15a1) we get a homogeneous solution in (3.20) (Fig. 3.15a2) and (via (3.19)) a traveling wave solution in the CGLE (3.1). For a periodic trajectory in (3.26) (Fig. 3.15b1) we get a train of periodic pulses in the solution of (3.20) (Fig. 3.15b2) and a quasiperiodic solution in CGLE (3.1). An homoclinic trajectory in (3.26) (Fig. 3.15c1) corresponds to a single pulse solution in (3.20) (Fig. 3.15c2). Finally for a chaotic trajectory in (3.26) (Fig. 3.15d1) we have an irregular solution $H(\xi)$ that corresponds to a rigidly traveling spatially irregular solution of (3.20) (Fig. 3.15d2). The chaotic solutions of (3.26) are of the Shil'nikov type [40]. This means that the disordered configurations $H(\xi)$ (and thus u and $\partial_x \varphi$) consist on nearly identical pulses irregularly spaced. This corresponds to the state named *frozen turbulence* for solutions of the CGLE.

The detailed analysis of [40] is done on the one hand by following the sequence of bifurcations of the state in which H is a constant and of the state in which H is close to the KdV soliton (with adequate rescaling Eq. (3.20) reduces to the KdV in the limit $\delta \to \infty$). On the other hand the powerful global theorems of Shil'nikov and their generalizations [186, 129, 107, 4] are used to establish the structure of the solutions of (3.26). The results of [40] relevant to our purposes can be summarized as follows (they can be read-off from figure 3 of Ref. [40]):

1. Periodic solutions of (3.26) exist for all values of δ provided $\mid c \mid > \mid \delta \mid$. They are organized in a variety of branches. Solutions in the same branch differ by their periodicity, and each branch ends in a different kind of solitary-wave solution (infinite spatial period). The shape of the different solitary wave solutions characterizes the different branches.

2. For $\mid \delta \mid \gtrsim 1.1$ only one of the branches of periodic solutions (the *main branch*) remains.

3. Chaotic solutions to (3.26) exist only for $\mid \delta \mid \lesssim 0.84$.

Figure 3.15: Schematic relationship between trajectories of the dynamical system (3.26) in phase space (left column) and solutions $u(\chi, \tau) = H(\xi = \chi - v\tau)$ of equation (3.20) (right column). a1) Fixed point of (3.26), a2) uniform solution of (3.20) (traveling wave in the CGLE (3.1)). b1)Periodic solution (limit cycle) of (3.20), b2) periodic train solution of (3.20) (quasiperiodic solution of the CGLE (3.1)). c1) Homoclinic trajectory of (3.26), c2) single pulse of (3.20). d1) Chaotic trajectory of (3.26), d2) spatially irregular solution of (3.20) (frozen turbulence in the CGLE).

In addition Chang et al. [40] obtained results also for the full equation (3.20), without the restriction to rigidly traveling waves. Their numerical and analytical results can be summarized as

4. Periodic solutions in the main branch with its wavenumber within a given range are linearly stable for all δ. A more precise determination of the range of stable wavenumbers for large δ was performed in [20].

5. In addition to the periodic solutions there are also spatio–temporal chaotic attractors for all δ.

6. If $\mid \delta \mid > 1.1$ only two of these strange attractors remain. For $\mid \delta \mid > 3$ their basin of attraction seems to be much smaller than the one of the periodic solutions.

Expression (3.21) with (3.10)-(3.18) gives the relation between δ and the parameters of the CGLE. $\mid \delta \mid = \infty$ corresponds in Fig. 3.1 to the line at which the wave of wavenumber k becomes Eckhaus unstable. It is approximately parallel and below the BFN line. The other lines of constant δ, for fixed k, are also approximately parallel to the BFN line, and decreasing $\mid \delta \mid$ corresponds to entering into the PT region and going deep into it. All these lines concentrate onto the BFN line as k approaches zero: for $k = 0$, $\delta = 0$ except on the BFN line $1 + c_1 c_2 = 0$ where δ is undefined. We now rephrase the conclusions above in terms of the three basic asymptotic states of the CGLE in the PT regime. They will be valid as long as the phase description (3.20) remains accurate.

1. There are PT solutions of the quasiperiodic type for all values of the parameters (as long as the phase description remains valid). Bounds on their velocity can be in principle obtained, but this is nontrivial since Q is only known in an implicit way.

2. Increasing $\mid \delta \mid$ by approaching the Eckhaus instability for a given k ($D_2 = 0$), or by increasing the winding number reduces the variety of quasiperiodic solutions.

3. Frozen turbulence solutions exist only for $\mid \delta \mid \lesssim 0.84$, that is far enough from the line $D_2 = 0$ or for small enough winding number.

4. There are linearly stable solutions in the main quasiperiodic branch for all values of the parameters.

5. There are also riding turbulence attractors for all values of parameters.

6. For $\mid \delta \mid > 3$, that is at high winding number or close enough to the line $D_2 = 0$ the quasiperiodic solutions have a basin of attraction larger than the riding turbulence ones.

A general feature of these conclusions is that the important quantity is D_2, that is the distance in parameter space from the line at which the k-wave became Eckhaus unstable. This line is *below* the BFN line for $k \neq 0$. Thus not only traveling waves, but also quasiperiodic, frozen turbulence, and riding turbulence attractors should exist below the BFN line for $k \neq 0$. In practice it is relatively easy to find quasiperiodic states below but close the BFN line, but we have been unable so far to find the other two states so far. The difficulty in finding riding turbulence states can be a consequence of the small range of

winding numbers for which they are stable ($|\nu| = L|k|/(2\pi) < \nu_c$) so that the observability condition $\mid \delta \mid < 3$ immediately brings us above the BFN line. Another possibility is that the instability of the $\nu = 0$ plane-wave attractor at the BFN line has consequences of a global character beyond the validity of the phase description.

If the predictions above are true, the more promising zone for obtaining quasiperiodic solutions starting from random perturbations on a traveling wave of given winding number is for parameter values close and above $D_2 = 0$, or for high winding number ($\mid \delta \mid > 3$). In any case no frozen turbulence should be observed in that zone.

Some qualitative aspects of the conclusions above have been shown to be correct. In particular Torcini and collaborators [174, 175] have shown that the average maximal Lyapunov exponent, quantifying the proportion of initial conditions that fall into the spatio–temporal chaotic strange attractors, is a decreasing function of ν.

Our numerical solutions also agree with the prediction that quasiperiodic solutions show up more easily for small D_2. However, their basin of attraction appears to be much smaller than the implied by the conclusions of the phase description since it is reached with very low probability from our initial conditions. This is specially true above the BFN line. The reason for this is probably the effect of the neglected term D_{12}, which is known to reduce the range of stable periodic solutions [20] and even to eliminate it by making the bifurcation subcritical [91]. Above the BFN line the attractor that we observe more frequently at high winding number from our initial conditions is the frozen turbulent state.

A more detailed checking of the predictions above would be desirable. This is however beyond the scope of the present paper since a detailed theoretical analysis of the global properties of the phase space for the equation containing the term D_{12} would be probably needed beforehand. A promising alternative can be the study of the exact equation for $f(x - vt)$ in (3.5) obtained in [175].

3.5 Final Remarks

One-dimensional wound-up phase turbulence has been shown to be much richer than expected. The main results reported here, that is the existence of winding number instability for phase-turbulent waves, the identification of the transition PT-DT with the vanishing of the range of stable winding numbers, and the coexistence of different kinds of PT attractors should in principle be observed in systems for which PT and DT regimes above a Hopf bifurcation are known to exist [114]. To our knowledge, there are so far no observations of the ordered PT states described above. There are however experimental observations of what seems to be an Eckhaus-like instability for non-regular waves in the printer instability system [142]. This suggests that the concept of a turbulent Eckhaus instability can be of interest beyond the range of situations described by the CGLE. A point about which our study is inconclusive is the question on the existence of PT in the thermodynamic limit. The identification of ν as an order parameter identifies the continuation of Fig. 3.7 towards larger system sizes as a way of resolving the question. It should be noted however that although a linear scaling of the order parameter with system size is usual in common phase transitions, broken ergodicity phase transitions, as the present one, generate usually a number of ordered phases growing exponentially with L, not just linearly [141, 122]. We notice however that the results of Section 3.3 show that the states of a given ν are not

pure phases, but different attractors are possible for given ν. An order parameter more refined than ν should be able to distinguish between the different attractors and, since some of them are disordered, the result of an exponentially large number of phases at large L would be probably recovered. The results presented in Section 3.4 give a justification for the existence of the several wound states observed. Further work is needed however to clarify the importance of the different terms in (3.7) and the validity of a phase description.

Chapter 4

Nonlinear Diffusion Control of Spatio-Temporal Chaos

No hearts of gold
No nerves of steel
No blame for what we can
 and cannot feel
No nerves of steel
No hearts of gold
No blame for what we can and
 can't control
Joni Mitchell, *Good friends*

4.1 Introduction

Under nonequilibrium conditions, a spatially extended system often undergoes a transition from a uniform state to a state with spatial variation, usually referred as pattern. Their formation is generally associated with nonlinear effects, which lead to qualitatively new phenomena such as the *Spatiotemporal Chaos*[52] (STC). Loosely, the term spatiotemporal chaos is commonly accepted to refer to a deterministic system that has irregular variation and is unpredictable in detail, both in space and in time. There are known examples of experimental systems, well characterized and precisely controlled[55, 52] that show such a behavior. In most cases STC can be described within the context of weakly nonlinear theories since these states arise in the proximity of threshold. These theories are well developed in the form of so–called complex Ginzburg–Landau equations (CGLE)[51]. The CGLE is a prototypical equation for a complex field A that exhibit STC. It accounts for the slow modulations, in space and time of the oscillatory state in a physical system which undergoes a Hopf bifurcation[179]. The CGLE has different types of STC[43] which have been profusely studied[165, 42, 64, 124, 125].

 The control of the chaotic behavior of dynamical systems with few degrees of freedom has been successively tested in a number of systems[164]. The idea behind the control of

---

[3]This Chapter corresponds to *Nonlinear Diffusion Control of Spatio-Temporal Chaos* by R. Montagne, P. Colet. Submitted for publication (1996).

chaos is to modify the dynamics of the system in such a way that a previously unstable state is now stable. Ideally only the stability is modified, not the state itself (i.e. if that state was a fix point or periodic orbit of the original system is still a fix point or periodic orbit of the modified system). The control of spatiotemporal chaos is a more complicated problem, and so, there is a wide variety of methods intended to control such chaotic behavior. There heve been several attempts to achieve such control in the CGLE. For example, Aranson et. al.[18] stabilize an unstable topological defect, whose analytical expression is known, by adding an extra term in the CGLE. The defect acts as a source of traveling waves which sweep all the other fluctuations to the system boundary. Stabilization of a plane wave extended through all the system has been achieved by adding time-delayed feedback terms to the CGLE. The feedback can be either local[29] (at each spatial point, the field at the same point at previous times is feeded back) or global[121, 24] (at each spatial point a term proportional to the integral of the field over the spatial variable is feeded back). In both cases, the added terms vanish for the stabilized plane wave solution, so it is possible to stabilize precisely the same plane waves which are unstable in the original CGLE. However, the added global feedback terms do not preserve the phase invariance of the original CGLE.

Feedback is the most used approach for chaos control in spatially extended systems. It has been applied to a nonlinear drift-wave equation driven by a sinusoidal wave [67] and, in conjunction with a spatial filter it has also been applied to stabilize rolls and hexagonal structures in a model for a transversally extended three level laser[118] and to control filamentation in a model for wide aperture semiconductor lasers based on the Swift-Hohenberg equation[85]

In this work we explore a different way to stabilize unstable periodic solution based not in feedback terms but in nonlinear diffusion effects. Specifically, we show that stabilization of unstable plane wave solutions of the CGLE in the region of STC can be achieved adding a nonlinear diffusion (or diffraction) term. The added term preserves the intrinsic phase invariance of the CGLE equation and it vanishes when the stabilizing effect is achieved so the modified equation has as solution the same plane wave as the original one. Nonlinear diffraction effects are present in optical systems where the Fresnel number is intensity dependent. It appears naturally, for instance as a higher order term in the Kerr effect.

In section 4.2 we briefly describe the parameter regions for which different chaotic behaviors have been found for the CGLE and we introduce the modified equation. Section 4.3 is devoted to the linear stability analysis of the plane wave solutions. We calculate for which parameters the added term is able to stabilize plane waves in the STC regions of the CGLE. In section 4.4 the analytical prediction of the linear stability analysis is verified by numerical simulations of the equations. Finally we give some concluding remarks in section 4.5.

4.2   Model

The one dimensional CGLE[51, 179, 178, 134] for a complex field $A(x, t)$, describes the slow dynamics of spatially extended systems close to a Hopf bifurcation,

$$\partial_t A = A + (1 + ic_1)\partial_x^2 A - (1 + ic_2)|A|^2 A . \tag{4.1}$$

We will assume periodic boundary conditions through all the work. This equation admits plane wave solutions of the form

$$A_{pw}(x,t) = Qe^{i(kx-\omega t)} , \tag{4.2}$$

with amplitude $Q = \sqrt{1-k^2}$, $|k| < 1$ and frequency $\omega = c_2 + (c_1 - c_2)k^2$.

For $1 + c_1 c_2 > 0$ plane wave solution are linearly stable for wave numbers smaller than a limit value $|k| \leq k_E$. For $|k| > k_E$, plane waves are unstable to phase perturbations (Eckhaus instability [61]). The limit value k_E is given by

$$k_E^2 = \frac{1 + c_1 c_2}{3 + c_1 c_2 + 2c_2^2} . \tag{4.3}$$

The stability range vanishes at $1 + c_1 c_2 = 0$ (the Benjamin–Feir–Newell (BFN) line), and no stable plane wave solution exist for $1 + c_1 c_2 < 0$.

Numerical work for L (length of the system) large [43, 165, 42, 64, 124, 125, 174] has identified regions of the parameter space displaying different kinds of regular and spatio-temporal chaotic behavior, leading to a "phase diagram" for the CGLE in the plane c_1–c_2. The five different regions, each leading to a different asymptotic phase, are shown in Fig. 4.1 as a function of the parameters c_1 and c_2.

Two of these regions are in the BFN stable zone and the other three in the BFN unstable one. The NO CHAOS region, in the BFN stable zone, is a large region where the evolution ends in a plane wave with a wave number $|q| \leq q_E$ for almost all the initial conditions. Also in the BFN stable zone there is the Spatio–Temporal Intermittency (STI) region[42]. Despite the fact that there exist stable plane waves, the evolution from random initial conditions is not attracted to them but to a chaotic attractor in which typical configurations of the field A consist of patches of plane waves interrupted by turbulent bursts. The modulus of A in such bursts typically touches zero quite often. On the other hand, above BFN line, the evolution ends in a spatiotemporal chaos for almost every initial condition. The Defect Turbulence (DF) region is a strongly disordered region in which the modulus of A has a finite density of space-time zeros [165, 42]. The Phase Turbulence (PT)[165, 43, 46, 45, 119, 64] region is a weakly disordered one in which $|A(x,t)|$ remains away from zero. Nevertheless, under a particular type of initial condition it is possible to end in a ordered state[125, 174]. Finally, the Bi-Chaos region is such that, depending on the particular initial condition, the system ends on attractors similar to the ones in regions of PT DT, or in a new attractor in which the configurations of A consists of patches of phase and defect turbulence. A detailed description could be found in [43].

We consider a modification of CGLE in such a way that the plane wave stability region is increased. We will show that this can be achieved be replacing the coefficient c_1 by $c_1 + \gamma(|A|^2/|A_{pw}|^2 - 1)$ where γ is a constant and $|A_{pw}|$ is the modulus of the plane wave to be stabilized. Notice that as the added term $\epsilon(|A|^2/|A_{pw}|^2 - 1)$ vanishes identically for $A = A_{pw}$, any plane wave A_{pw} that is a solution of (4.1) is also a solution of the modified equation. We are not changing the solution but we will change its stability. The modified CGLE is explicitly given by,

$$\partial_t A = A + [1 + ic_1 + i\gamma(|A|^2/|A_{pw}|^2 - 1)]\partial_x^2 A - (1 + ic_2)|A|^2 A . \tag{4.4}$$

It is also important to note that this modification introduced above, preserves the phase invariance $A \rightarrow Ae^{i\psi}$, with ψ being an arbitrary phase.
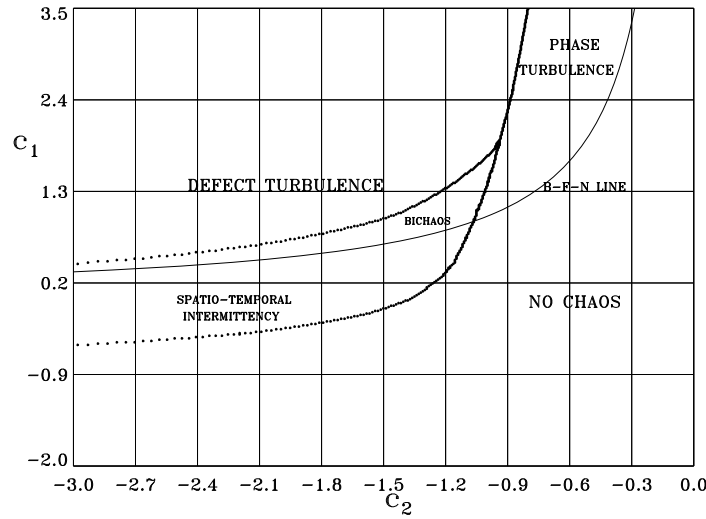
Figure 4.1: Regions of the parameter space $c_1 - c_2$ for which the $d = 1$ CGLE display-ing different kinds of regular and chaotic behavior. The analytically obtained line, the Benjamin-Feir–Newell line (BFN line) is also shown.

From another point of view, eq. (4.4) can be rewritten as

$$\partial_t A = A + [1 + i\tilde{c}_1 + ic_{NL}|A|^2]\partial_x^2 A - (1 + ic_2)|A|^2 A\,, \tag{4.5}$$

with $\tilde{c}_1 = c_1 - \gamma$ and $c_{NL} = \gamma/|A_{pw}|^2$. In this way, the stabilizing added term can be seen as a nonlinear diffusive term in the CGLE.

4.3 Stability analysis

We study the stability of the plane wave solutions (4.2) of eq. (4.4) by a standard lin-earization procedure. Consider the time evolution of small perturbations in the amplitude and phase,

$$A(x,t) = (Q + \epsilon r(x,t))e^{i(kx-\omega t+\epsilon\phi(x,t))}\,, \tag{4.6}$$

where $r(x,t)$ and $\phi(x,t)$ are real perturbations in the amplitude and phase respectively and ϵ is a formal parameter to keep track of small numbers.

Substituting (4.6) in (4.4) yields to a polynomial in ϵ up to order ϵ^5. The terms of order ϵ^0 vanish identically. The first order terms yield the linearized equations for the perturbations

$$\partial_t r = 2Q^2 r - 2Qk\partial_x\phi - 2c_1k\partial_x r - c_1 Q\partial_x^2\phi + \partial_x^2 r\,, \tag{4.7}$$

$$\partial_t \phi = -2c_2 Q r + 2\gamma\frac{k^2}{Q}r - 2c_1 k\partial_x\phi + 2\frac{k}{Q}\partial_x r + \partial_x^2\phi + \frac{c_1}{Q}\partial_x^2 r\,. \tag{4.8}$$

We consider solutions of (4.7) and (4.8) proportional to $e^{\eta t+iqx}$, where for periodic bound-ary conditions q is real whereas η is in general a complex quantity. By substituting in

(4.7) and (4.8) we obtain the dispersion relation

$$\begin{vmatrix} \eta + 2Q^2 + q^2 + 2ic_1qk & 2iqk - c_1q^2 \\ c_1q^2 + 2c_2Q^2 - 2iqk + 2\gamma k^2 & \eta + q^2 + 2ic_1qk \end{vmatrix} = 0 \,. \tag{4.9}$$

The solutions of (4.9) are

$$\eta = -(Q^2 + q^2 + 2ic_1qk) \pm \sqrt{u + iv} \,, \tag{4.10}$$

where u and v are polynomials

$$\begin{aligned} u &= Q^4 + 4q^2k^2 - 2c_1c_2Q^2q^2 - c_1^2q^4 - 2\gamma c_1q^2k^2 \,, & (4.11) \\ v &= 4qk(c_1q^2 + c_2Q^2 + \gamma k^2) \,. & (4.12) \end{aligned}$$

The real part of η indicates the growth rate,

$$Re(\eta) = -Q^2 - q^2 \pm \sqrt{\frac{u + \sqrt{u^2 + v^2}}{2}} \,. \tag{4.13}$$

We have two different branches [111, 91, 179] which are usually called "amplitude" and "phase modes" due to the fact that for a real Ginzburg-Landau equation, the eigenvalues are related specifically to amplitude and phase perturbations. Although this is not the case for the CGLE, the names are still used.

The "amplitude modes" correspond to the negative sign of the square root in (4.13). For any value of c_1, c_2 and k, $Re(\eta)$ as function of the perturbation wavelength q is always negative and takes the value $Re(\eta) = -2Q^2$ at $q = 0$. The added γ term modifies only slightly the position of the branch but it never changes the negative character of $Re(\eta)$.

The "phase modes" are associated with the positive sign square root in (4.13). This branch vanishes identically at $q = 0$ for any value of the parameters c_1, c_2 or plane wave wavelength k, so all the plane wave solutions are marginally stable. The origin of this neutral stability is the phase invariance $A \to Ae^{i\psi}$ of the solutions of eq. (4.1) and (4.4). For q very large, this branch is negative and behaves as $-q^2$, so short wavelength perturbations are always damped. However, in general, long wavelength perturbations can be unstable, to see this we expand (4.13) for small q.

$$Re(\eta) = Dq^2 + O(q^4) \,, \tag{4.14}$$

where

$$D = -1 - c_1c_2 + 2(1 + c_2^2)\frac{k^2}{Q^2} + \gamma\left(-\frac{c_1k^2}{Q^2} + 4\frac{c_2k^4}{Q^4}\right) + 2\gamma^2\frac{k^6}{Q^6} \,. \tag{4.15}$$

If this coefficient is positive, there is a range of unstable perturbation wavelengths. For the unperturbed CGLE, $\gamma = 0$, the requirement $D < 0$ leads to the standard Eckhaus instability limit: $|k| < k_E$ with k_E given by (4.3).

For $\gamma \neq 0$ the coefficient D depends on even powers of k up to the 6th power, so one has to solve a cubic equation to find explicitly the limits of the range of values of k for which plane waves are stable. In Figs. 4.2 - 4.4 we plotted this range as a function of the parameter c_1 for several values of γ and c_2. Fig. 4.2 shows the stability region for $c_2 = -0.3$ and different values of γ as indicated in the figure caption. The first thing to

notice is that the added term does not affect to the stability of the homogeneous solution $k = 0$, this is in fact the general case for any value of parameters c_1 and c_2 as can be seen from equations (4.10), (4.11) and (4.12) where γ only appears in terms with powers of k. For plane waves with $k \neq 0$ the stability range clearly changes with the value of γ as displayed in Fig 4.2 b)-d). For small γ (Fig. 4.2 b) the stability range is increased for large values of c_1 and slightly reduced for $c_1 \lesssim 0.5$, therefore, the added stabilizing term has the opposite effect for small c_1. For the values of c_1 displayed on the figure, the last plane wave in losing stability is still the homogeneous solution as it was in the case $\gamma = 0$.
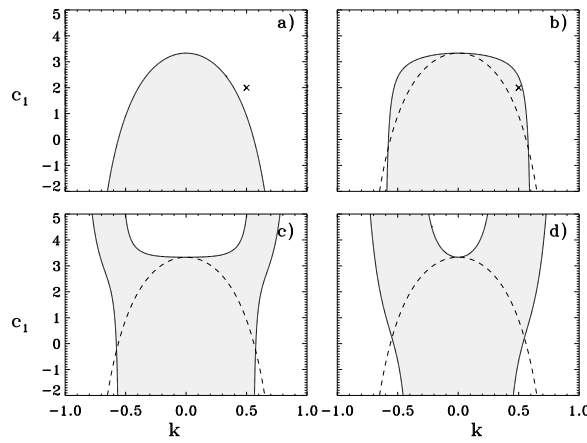

Figure 4.2: Stability region for the plane wave (4.2) for $c_2 = -0.3$ for a) $\gamma = 0$, b) $\gamma = 0.5$, c) $\gamma = 0.7$, d) $\gamma = 2$. For comparison, the boundary of the stability region for $\gamma = 0$ is shown in figs. b)-d) as a dashed line.

For $\gamma > 0.6$ the shape of the stability range is strongly changed as can be seen in Fig. 4.2c-d for $\gamma = 0.7$ and $\gamma = 2$. Now there are plane waves with $k \neq 0$ which are stable for values of c_1 well above the stability limit of the homogeneus solution, in the region of phase turbulence of the original CGLE (see Fig. 4.1).

Figs. 4.3 and 4.4 show the stability region for $c_2 = -0.9$ and $c_2 = -2.1$ and several values of γ. As γ is increased the stability region changes its shape in a similar way as before but at larger values of γ. For $c_2 = -0.9$ it is possible to stabilize plane waves in the region of phase turbulence taking $\gamma \geq 2$, and for $c_2 = -2.1$ stabilization in the region of defect turbulence is possible for $\gamma \geq 4$.
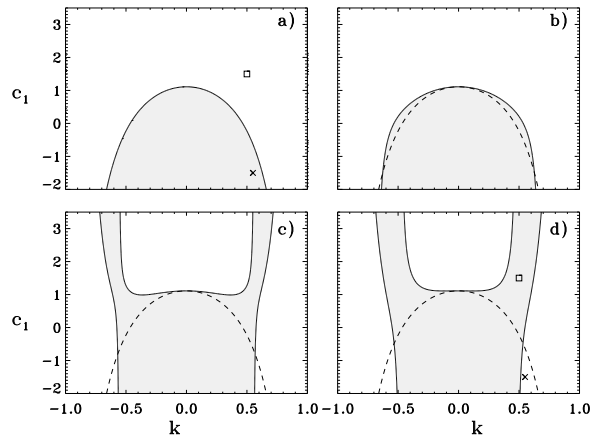
Figure 4.3: Stability region for the plane wave (4.2) for $c_2 = -0.9$ for a) $\gamma = 0$, b) $\gamma = 1$, c) $\gamma = 2$, d) $\gamma = 3$. For comparison, the boundary of the stability region for $\gamma = 0$ is shown in figs. b)-d) as a dashed line.

Fig. 4.4c) for $c_2 = -2.1$ and $\gamma = 4$ shows an interesting intermediate shape. There are three stability regions so plane waves can exist below the BFN line and well above it, in defect turbulence, but not for values of c_1 just above the BFN line. Also there is no wavevector q for which plane waves are both stable below and above the BFN line. As γ is increased the three regions coalesce and become a single one, as seen for $\gamma = 6$. This general behavior is observed also for other values of c_2 for intermediate values of γ which are not shown in Figs. 4.2 and 4.3.
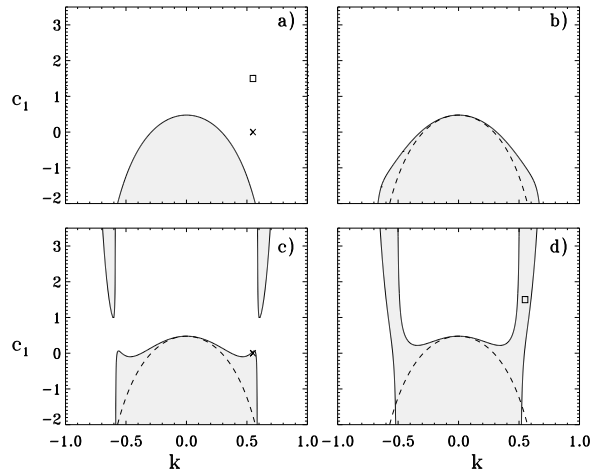

Figure 4.4: Stability region for the plane wave (4.2) for $c_2 = -2.1$ for a) $\gamma = 0$, b) $\gamma = 2$, c) $\gamma = 4$, d) $\gamma = 6$. For comparison, the boundary of the stability region for $\gamma = 0$ is shown in figs. b)-d) as a dashed line.

The overall picture is as follows (see Fig. 4.5, which is, in fact, a view of an extended

area in the k–c_1 plane of the results plotted in Fig. 4.3b)). For $\gamma = 0$ and a fixed c_2 the stability region in the k–c_1 plane is limited by a branch of eq. (4.3) (dashed line) whose vertex corresponds to the BFN point. Keeping c_2 fixed and decreasing the value of c_1 the width of the stability region $|k| < k_E$ increases and for $c_1 \to -\infty$, $k_E \to 1$. For any small $\gamma > 0$ there are three stability regions in the k–c_1 plane. From eq. (4.15) one can show that for $c_1 \to -\infty$ the limits of the first region (labeled R1 on fig. 4.5) approach the two vertical asymptotes $k_{A\pm} = \pm\sqrt{c_2/(c_2 - \delta)}$ (dotted lines).

On the other hand two new stability regions ($D < 0$) appear symmetrically at very large values of c_1 and for values of $|k|$ between the vertical asymptotes and 1 (regions R2 and R3). The existence of these new regions, which for $c_1 \to \infty$ broaden and cover the intervals $k \in [-1, k_{A-}]$ and $k \in [k_{A+}, 1]$, implies that for any nonvanishing γ there will be always stable plane waves for any value of c_2 well above the BF line. However, if γ is very small these regions are located at very large, and quite unrealistic, values of c_1. As δ is increased the regions R2 and R3 extend to lower values of c_1 until they coalesce with the region R1.
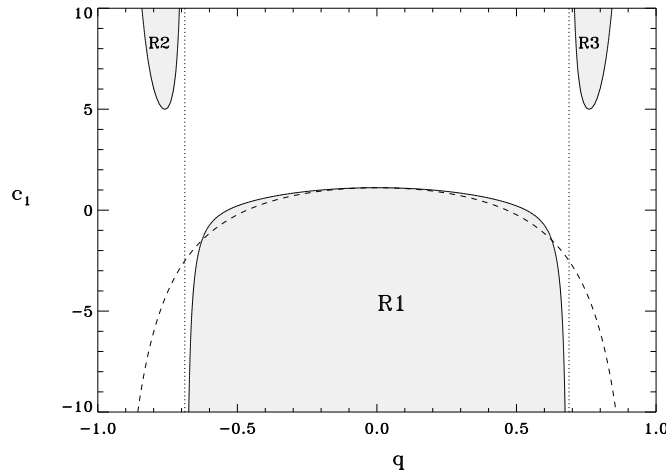
Figure 4.5: Stability region for the plane wave (4.2) for $c_2 = -0.9$ for $\gamma = 1$. The dashed line shows the Eckhaus stability limit for the unmodified CGLE. The vertical dotted lines show the asymptotic lines $k = k_A\pm$ (see text).

4.4   Numerical simulations

We have performed numerical simulations of eq. (4.1) and (4.4) using a pseudospectral code with periodic boundary conditions and second-order accuracy in time. Spatial resolution was typically 1024 modes. Time step was typically $\Delta t = .001$ except when differently stated in the figure captions. Since very small effects have been explored, care has been taken of confirming the invariance of the results with decreasing time step and increasing number of modes. System size was always taken as $L = 512$. The details of the numerical method can be seen elsewhere[123]. We start for an initial condition which corresponds

to a plane wave plus a small perturbation

$$A(x, t = 0) = \sqrt{1 - k^2}e^{ikx} + \sigma\xi(x) \tag{4.16}$$

where $\xi(x)$ is a complex gaussian random perturbation of zero mean and variance $\langle\xi(x)\xi^*(x')\rangle = 2\delta(x - x')$.

We have performed numerical simulations in different regions of the phase diagram (4.1) to verify the results obtained from the linear stability analysis when finite size perturbations are applied. We have found a very good agreement between the prediction of the linear stability analysis and the numerical simulations. As characteristic examples we show the following results.

Fig. 4.6 shows the results of numerical simulations for $c_1 = 2$, $c_2 = -0.3$. We start with an Eckhaus unstable plane wave with $k_i = 0.5 > k_E$ which is perturbed adding noise as it was explained above ($\times$ point in Fig. 4.2a)). For $\gamma = 0$ the system evolves from the initial plane wave to a stable wave with $k \approx 0.3 < k_E$, although the transients can be very long. Fig. 4.6c) shows the amplitudes and phase gradient of the final plane wave at $t = 19000$. For $\gamma = 0.5$, as predicted by the linear stability analysis ($\times$ point in Fig. 4.2b)), the initial plane wave is stable, so the random perturbation dyes out and the system settles down to a pure plane wave with the initial wavelength k_i (Fig. 4.6d)).

Fig. 4.7 shows a case where the added term unstabilizes a plane wave. For $c_1 = -1.5$, $c_2 = -0.9$ a plane wave with $k = 0.55$ is stable in the unmodified ($\gamma = 0$) CGLE ($\times$ point in Fig. 4.3a)) but the same plane wave becomes unstable in the modified CGLE for $\gamma = 3$ ($\times$ point in Fig. 4.3d)). For this case, it can be seen how the system evolves to another plane wave with wave number $k \approx 0.32$ within the stability range. As in the previous case, the transients can last for quite a long time.

Fig. 4.8 shows stabilization of plane waves at the parameter values $c_1 = 1.5$ and $c_2 = -0.9$. This point corresponds to the phase turbulence regime (see fig. phasediagram), where no plane waves are stable for the unmodified CGLE. As predicted by the linear stability analysis (square points in Fig. 4.3a) and d)) a perturbed plane wave with $k = 0.5$ can easily be stabilized with $\gamma = 3$, while for $\gamma = 0$ the same initial condition decays in time $t = 80$ (approx.) to phase turbulence.

Fig. 4.9 shows a case of stabilization of plane waves for $c_1 = 0$ and $c_2 = -2.1$, in the region of spatio-temporal intermittency. In this region there are stable plane waves with $|k|$ small enough, but if $|k| > k_E$ the initial perturbed plane wave evolves to an spatio temporal intermittent behavior[42]. However, the modification introduced allows to completely suppress the typical defects and other localized objects of STI regime, leading the system to a well behaved plane wave. The initial condition in this case was a plane wave with $k = 0.55$ ($\times$ points in Fig. 4.4a) and c)).

Finally Fig. 4.10 obtained for parameter values $c_1 = 1.5$ and $c_2 = -2.1$ shows stabilization of plane waves in the region of defect turbulence, where in the unperturbed case there are no stable plane waves and the field A shows the presence of defects. Again as predicted by the linear stability analysis a perturbed plane wave with $k = 0.55$ (square point in Fig. 4.4a) and d)) can be stabilized with $\gamma = 6$ washing out all the defects.

Figure 4.6: Spatiotemporal evolution of the CGLE (4.4) for $c_1 = 2$, $c_2 = -0.3$ starting from a perturbed plane wave (4.16) with $k = 0.5$ and $\sigma = 0.01$. Figs. a) and b) show $|A|$ with time running upwards from $t = 0$ to $t = 20000$, and x in the horizontal direction for $\gamma = 0$ and $\gamma = 0.5$ respectively. The value of the modulus $|A(x,t)|$ and phase gradient $\partial_x \phi(x,t)$ at $t = 19000$ are displayed in c) and d) for $\gamma = 0$ and $\gamma = 0.5$ respectively. Integration performed with a time step $\Delta t = 0.01$.

Figure 4.7: Spatiotemporal evolution of the CGLE (4.4) for $c_1 = -1.5$, $c_2 = -0.9$ starting from a perturbed plane wave (4.16) with $k = 0.55$ and $\sigma = 0.01$. Figs. a) and b) show $|A|$ with time running upwards from $t = 0$ to $t = 20000$, and x in the horizontal direction for $\gamma = 0$ and $\gamma = 3$ respectively. The value of the modulus $|A(x,t)|$ and phase gradient $\partial_x \phi(x,t)$ at $t = 19200$ are displayed in c) and d) for $\gamma = 0$ and $\gamma = 3$ respectively. Integration performed with a time step $\Delta t = 0.01$.
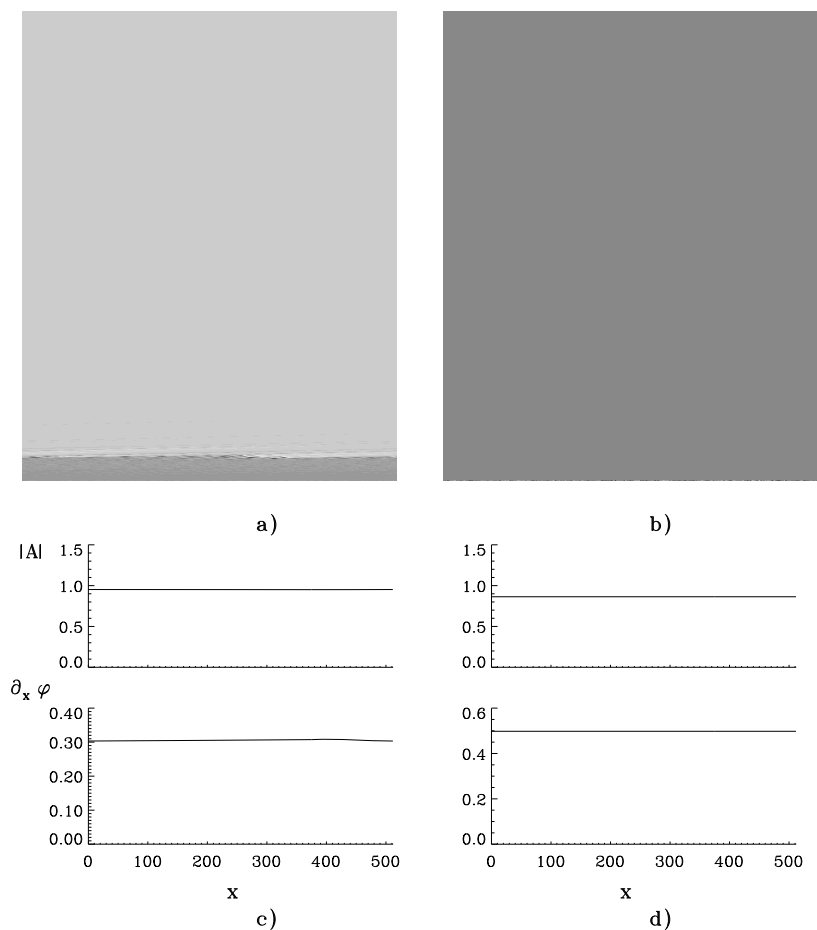
Figure 4.8: Spatiotemporal evolution of the CGLE (4.4) for $c_1 = 1.5$, $c_2 = -0.9$ starting from a perturbed plane wave (4.16) with $k = 0.5$ and $\sigma = 0.01$. Figs. a) and b) show $|A|$ with time running upwards from t_0 to $t = 1000$ and x in the horizontal direction for $\gamma = 0$ and $\gamma = 3$ respectively. The value of the modulus $|A(x,t)|$ and phase gradient $\partial_x \phi(x,t)$ at $t = 950$ are displayed in c) and d) for $\gamma = 0$ and $\gamma = 3$ respectively.
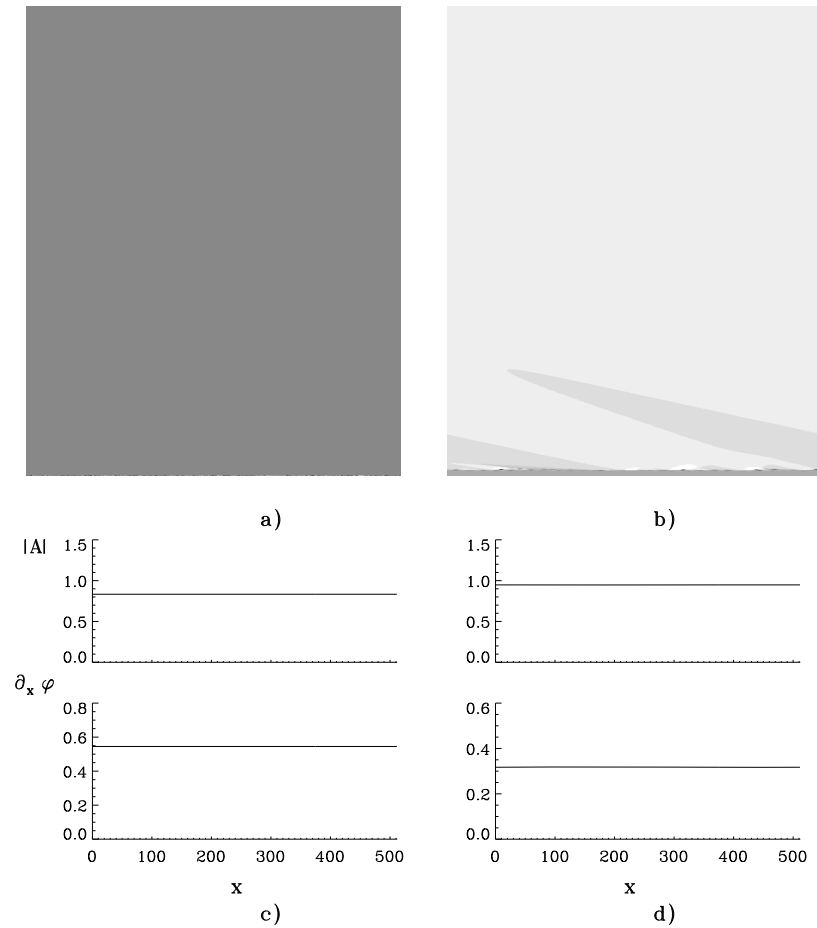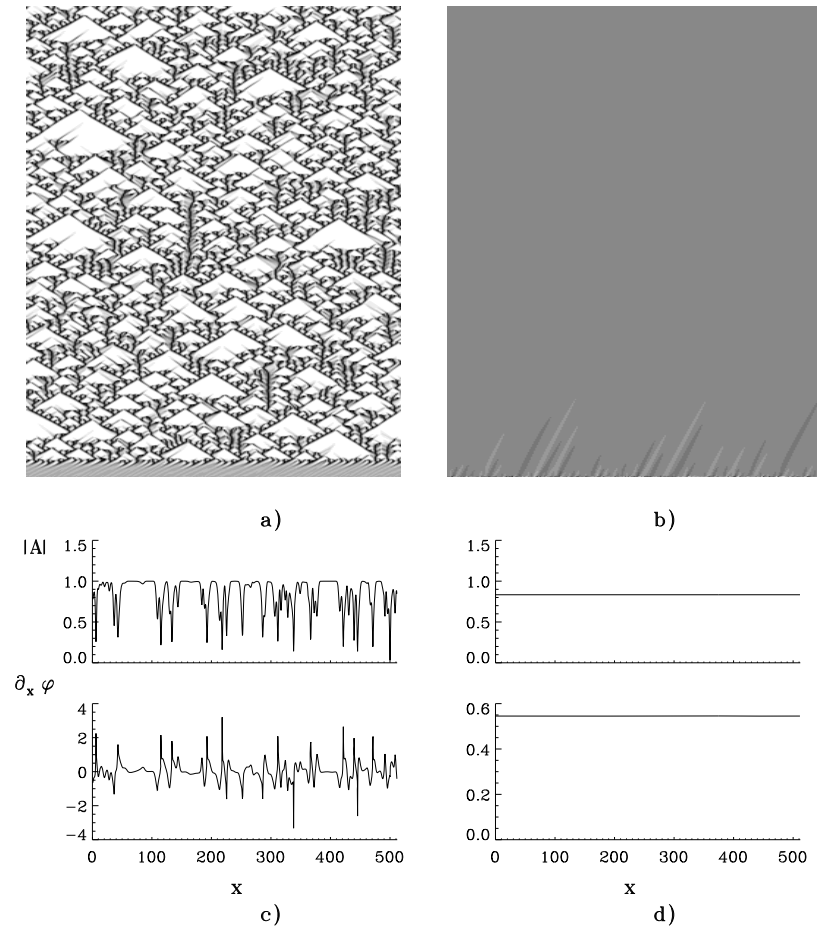
Figure 4.9: Spatiotemporal evolution of the CGLE (4.4) for $c_1 = 0$, $c_2 = -2.1$ starting from a perturbed plane wave (4.16) with $k = 0.55$ and $\sigma = 0.01$. Figs. a) and b) show $|A|$ with time running upwards from t_0 to $t = 1000$ and x in the horizontal direction for $\gamma = 0$ and $\gamma = 4$ respectively. The value of the modulus $|A(x, t)|$ and phase gradient $\partial_x \phi(x, t)$ at $t = 950$ are displayed in c) and d) for $\gamma = 0$ and $\gamma = 4$ respectively.
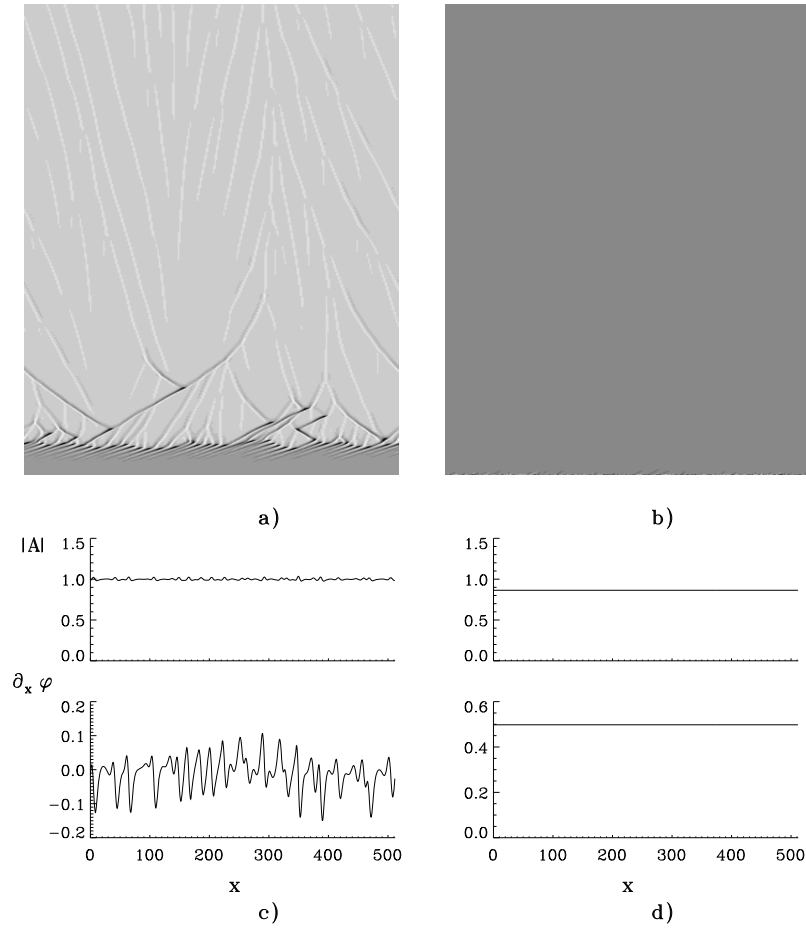
Figure 4.10: Spatiotemporal evolution of the CGLE (4.4) for $c_1 = 1.5$, $c_2 = -2.1$ starting from a perturbed plane wave (4.16) with $k = 0.5$ and $\sigma = 0.01$. Figs. a) and b) show $|A|$ with time running upwards from t_0 to $t = 1000$ and x in the horizontal direction for $\gamma = 0$ and $\gamma = 6$ respectively. The value of the modulus $|A(x,t)|$ and phase gradient $\partial_x \phi(x,t)$ at $t = 950$ are displayed in c) and d) for $\gamma = 0$ and $\gamma = 6$ respectively.
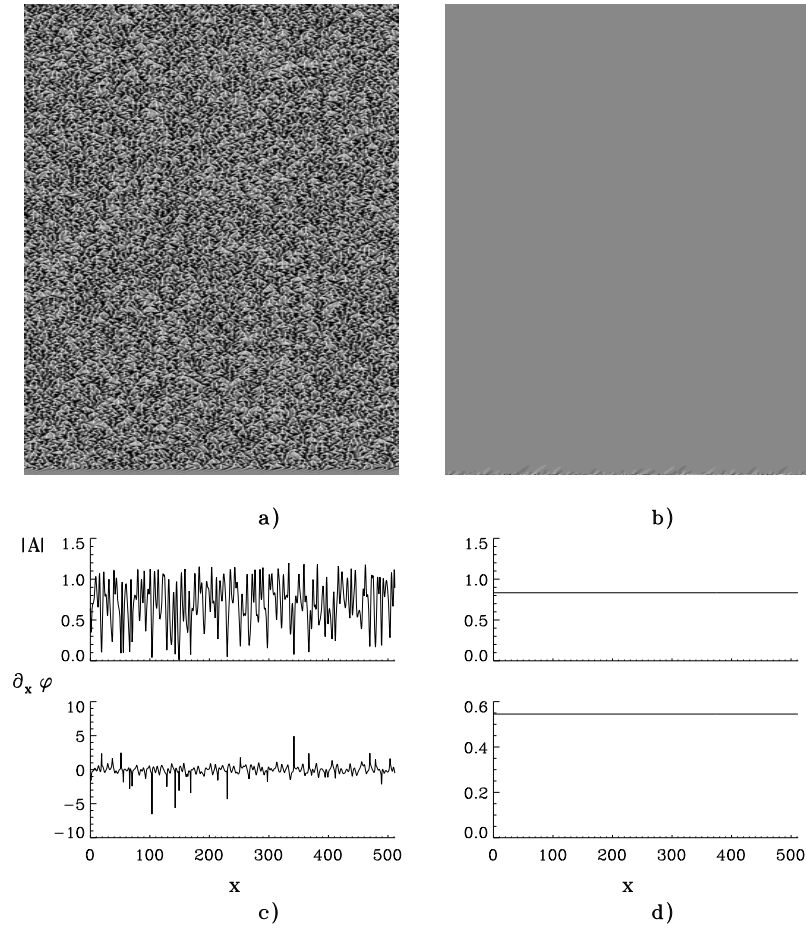
4.5 Concluding Remarks

We have stabilized unstable plane wave solutions in different parameter regions of the CGLE where spatiotemporal chaos exist. This have been done by adding a term to the CGLE which vanish for the stabilized plane wave, so that the stabilized plane waves are exacly the same unstable solutions of the original CGLE. The added term can be seen as a nonlinear diffusive term and preserves the intrinsic phase invariance of the original equation. Although our method does not change the stability of the homogeneous solution $k = 0$, it is quite effective in stabilizing plane waves with non zero wavevector. We have calculated analytically the parameter regions where plane waves can be stabilized including regions of phase turbulence, spatiotemporal intermittency, bichaos and defect turbulence. We have shown that the numerical integration of the modified CGLE is in excellent agreement with the linear stability analysis predictions. Our analysis also shows that in general, in systems where nonlinear contributions to the diffusion or diffraction are not negligible, these terms can change significantly the regions in parameter space for which plane waves are stable.

Chapter 5

Synchronization of Spatiotemporal Chaos

There is chaos to the order
Random things you can't prevent
There could be trouble around the corner
There could be beauty down the street
Synchronized –like magic
Good friends you and me.

Joni Mitchell, *Good friends*

5.1 Introduction

Two issues of high current interest in the general field of nonlinear dynamics are the quantitative characterization of different regimes of spatiotemporal complex dynamics in extended systems [52, 55] and the synchronization of chaotic oscillators [143, 47]. The characterization of low dimensional chaos is now a mature subject with well established techniques, including techniques of chaos control. In this context, the demonstration that the familiar phenomenon of synchronization of two regular oscillators [89, 185] by a weak coupling can also be displayed by chaotic oscillators is an important new idea. This conceptual development has opened a new avenue of research with interesting practical implications. Chaos in extended systems is a much less mature subject and many investigations are still at the level of classifying different types of behavior. Concepts and methods of Statistical Mechanics are commonly invoked in terms of "phase diagrams" and transitions among different "phases" of behavior[165, 42, 36]. Still, the possibility of a synchronized behavior of spatially extended systems in a spatiotemporal disordered phase is an appealing idea that we address in this Letter. More specifically we will consider an extended one-dimensional system in a chaotic regime known as Spatiotemporal Intermittency (STI)[42] and we will characterize a coupled STI regime.

---

[4]This Chapter corresponds to *Synchronization of Spatiotemporal Chaos: The regime of coupled Spatiotemporal Intermittency* by A. Amengual, E. Hernández-García, R. Montagne and M. San Miguel, submitted for publication (1996).

By synchronization of two chaotic oscillators O_1 and O_2 it is meant in a strict sense that plotting the time series $O_1(t_i)$ *vs* $O_2(t_i)$ one obtains a straight line of unit slope. For many practical applications, synchronization of chaotic oscillations calls for an expanded framework and the concept of "generalized synchronization" has been introduced [156, 97] as the appearance of a functional dependence between the two time series. In this context we understand here by synchronization the situation in which $O_1(t_i)$ becomes a given known function of $O_2(t_i)$, while for independent chaotic oscillators $O_1(t_i)$ and $O_2(t_i)$ are independent variables. Transferring these concepts to spatially extended systems, we search for correlations between the space(x_i)-time(t_j) series of two variables $O_1(x_i, t_j)$ and $O_2(x_i, t_j)$. The synchronization of O_1 and O_2 occurs when these two space-time series become functionally dependent. This idea is different from the one much studied in the context of coupled map models in which the coupling and emerging correlations are among the local oscillators of which the spatially extended system is composed. Here we search for correlations of two variables at the same space-time point.

5.2   STI in the Coupled CGLE

Our study has been carried out in the context of Complex Ginzburg Landau Equations (CGLE) which give a prototype example of chaotic behavior in extended systems[51, 179]. Our results show that the coupling between two complex amplitudes A_1 and A_2 ($O_1 = |A_1|$ and $O_2 = |A_2|$) in a STI regime described below, establishes spatiotemporal correlations which preserve spatiotemporal chaos but lead to a synchronized behavior: Starting from the independent STI dynamics of A_1 and A_2, coupling between them leads to a STI regime dominated by the synchronized chaotic motion of localized structures in space and time for A_1 and A_2. An additional effect observed in our model is that the coupled STI regime is destroyed for coupling larger than a given threshold, so that the two variables remain strongly correlated but each of them shows regular dynamics. At this threshold maximal mutual information and anticorrelation of $|A_1|$ and $|A_2|$ are approached.

The CGLE is the amplitude equation for a Hopf bifurcation for which the system starts to oscillate with frequency ω_c in a spatially homogenous mode. When, in addition, the Hopf bifurcation breaks the spatial translation symmetry it identifies a preferred wavenumber K_c. In one-dimensional systems the amplitudes A_1 and A_2 of the two counter-propagating traveling waves with frequency ω_c and wavenumbers $\pm K_c$ becoming unstable satisfy coupled CGLE of the form

$$\begin{aligned}
\partial_t A_{1,2} &= \mu A_{1,2} + (1 + i\alpha)\partial_x^2 A_{1,2} \\
&\quad - (1 + i\beta)\left(|A_{1,2}|^2 + \gamma|A_{2,1}|^2\right) A_{1,2} \,.
\end{aligned} \tag{5.1}$$

Eq. (5.1) is written here in the limit of negligible group velocity. In particular, this limit is of interest to describe the coupled motion of the two complex components of a Vector CGLE. In this context, (5.1) is used to describe vectorial transverse pattern formation in nonlinear optical systems. In this case, $A_{1,2}$ stand for the two independent circularly polarized components of a vectorial electric field amplitude [159, 17]. The parameter μ measures the distance to threshold and γ is the coupling parameter, taken to be a real number. Homogeneous solutions of Eq. (5.1) are of the form

$$A_{1,2}(x, t) = Q_{1,2}e^{i\omega_{1,2}t} \,. \tag{5.2}$$
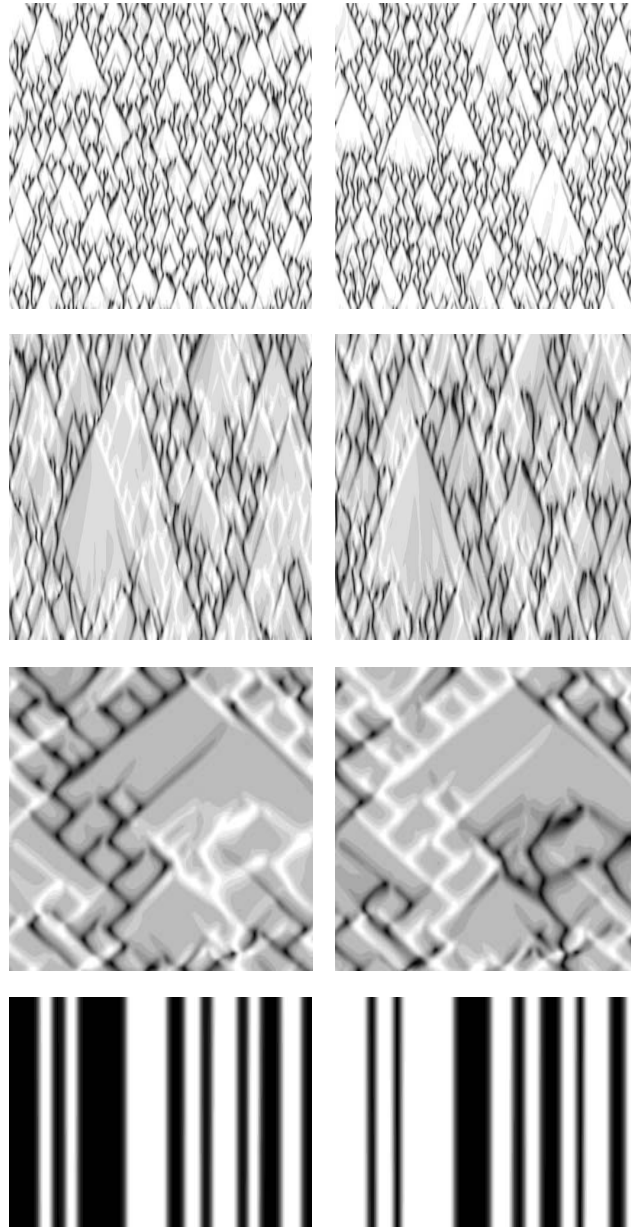
Figure 5.1: Space-time plot ot the modulus $|A_1|$ (left) and $|A_2|$ (right) for four values of the coupling parameter γ: From top to bottom, $\gamma = 0.1, 0.5, 0.95$ and 1.05. The horizontal axis represents space and the vertical axis time (2000 time units for $\gamma = 0.95$, 100 for $\gamma = 1.05$ and 200 in the other two plots). The gray levels change linearly from the minimum (black) to the maximum (white) of the modulus. The parameters are $\mu = 1$, $\alpha = 0.2$ and $\beta = -2.0$. For $\gamma = 0.1$, the structures appearing in $|A_1|$ and $|A_2|$ are almost independent. However, for $\gamma = 0.5$, the defects in $|A_1|$ (black and white structures) becomes slightly synchronized with the defects in $|A_2|$ and, for $\gamma = 0.9$, the synchronization is almost complete.

where: $\omega_{1,2} = -\beta(Q_{1,2}^2 + \gamma Q_{2,1}^2)$. For $\gamma = 0$, $Q_{1,2}^2 = \mu$, and the two amplitudes satisfy independent CGLE whose phase diagram has been studied in much detail in terms of the parameters α and β [43, 125]. For $\gamma = 0$, solutions of the type (5.2), and other plane waves of different periodicities, are known to be linearly stable below the Benjamin-Feir (BF) line $(1 + \alpha\beta > 0)$. Above this line regimes of phase and defect chaos occur. However, for a range of parameters below the BF line there is an additional attractor coexisting with the one of plane waves in which the system displays a form of spatiotemporal chaos known as STI. In this attractor the solution is intermittent in space and time. Space–time plots of $|A_1|$ or $|A_2|$ in the STI regime for $\gamma = 0$ are qualitatively similar to the ones shown in Fig. 5.1a.

The question we address here is how the STI regimes of A_1 and A_2 change when the coupling γ is introduced. We first recall that for a weak coupling situation ($\gamma < 1$) the solution (5.2) with $Q_{1,2}^2 = \mu/(1 + \gamma)$ is linearly stable below the same BF-line $1 + \alpha\beta > 0$ [159] whereas the additional solutions with $Q_1 = 0$ or $Q_2 = 0$ are unstable. For large coupling $\gamma > 1$ the competition between the two amplitudes is such that only one of them survives. Linearly stable solutions are either $Q_1 = \sqrt{\mu}$, $Q_2 = 0$, or $Q_2 = \sqrt{\mu}$, $Q_1 = 0$. For the marginal coupling $\gamma = 1$, $Q_1^2 + Q_2^2 = \mu$ and the phase $\chi = \arctan(Q_1/Q_2)$ is arbitrary. In addition to these ordered states we also find a STI attractor for coupled CGLE and values of α and β which are in the STI region of a single CGLE. Changes of such STI behavior with varying γ are shown in Fig. 5.1 [5].

For small coupling ($\gamma << 1$) we observe that $|A_1|$ and $|A_2|$ follow nearly independent dynamics with the flat grey regions in the space-time plot being laminar regions separated by localized structures that appear, travel and annihilate. In the laminar regions configurations close to (5.2) with $Q_1 = Q_2$ occur. Disorder occurs via the contamination by localized structures. These structures have a rather irregular behavior and, in a first approach they can be classified of either of two types, hole–like or pulse–like[179]. In Fig. 5.1 these hole–like and pulse–like structures are associated to black and white localized structures respectively. It is argued that the domain of parameters in which STI exists in the limit $\gamma \to 0$ is determined by the condition of stability for those localized structures [149]. As γ increases we observe two facts: First, both $|A_1|$ and $|A_2|$ continue to display STI dynamics although in larger and slower space-time scales. Second, and more interesting, is that the dynamics of $|A_1|$ and $|A_2|$ become increasingly correlated. This is easily recognized by focusing in the localized structures: A black traveling structure in the space-time plot of $|A_1|$ has its corresponding white traveling structure in the space-time plot of $|A_2|$ and vice versa. In the vicinity of the localized structures, and emerging from them, there appear travelling wave solutions of (5.1) but with different wavenumber for $|A_1|$ and $|A_2|$ so that $|A_1| \neq |A_2|$. This results in laminar states occurring in the same region of space-time for $|A_1|$ and $|A_2|$. The coupled STI dynamical regime is dominated by localized structures in which maxima of $|A_1|$ occur allways togheter with minima of $|A_2|$ and vice versa. Eventually (going beyond the marginal coupling $\gamma = 1$) the STI dynamics is destroyed and $|A_1|$ and $|A_2|$ display only laminar regions in which either $|A_1|$ or $|A_2|$ vanish separated by domain walls. In the optical interpretation of (5.1) the laminar gray regions in Fig. 5.1 ($|A_1| = |A_2|$) corresponds to transverse domains of linearly polarized light, although with a random direction of linear polarization. The localized structures are essentially circularly polarized objects since one of the two amplitudes dominates over the other. Around these structures the plane wave solutions with $|A_1| \neq |A_2|$ have different

frequencies, so that they correspond to depolarized solutions of (5.1) [159]. As $\gamma > 1$, localized traveling structures dissapear and one is left with circularly polarized domains separated by polarization walls. It is usually argued that for $\gamma > 1$ the dynamics of the coupled CGLE (5.1) is well represented by a single CGLE since only one of the two waves survives. This is certainly not true in the STI domain of parameters considered here since a single CGLE would give rise to STI dynamics whereas the coupled set (5.1) does not for $\gamma > 1$. In general a description in terms of a single CGLE would not be reliable for parameter values at which the single amplitude dynamics produces amplitude values close to zero.

5.3 Characterization of the STI

We next show that the correlations observed for increasing γ in Fig. 5.1 are in fact a kind of spatiotemporal synchronization, in the generalized sense defined in [156, 97]. To this end a characterization of the synchronizing process can be given by analyzing the joint distribution of the two variables. This distribution and values of $|A_1|$ versus $|A_2|$ are plotted in Fig.5.2. The cloud of points correspond to the different space–time points of Fig. 5.1.
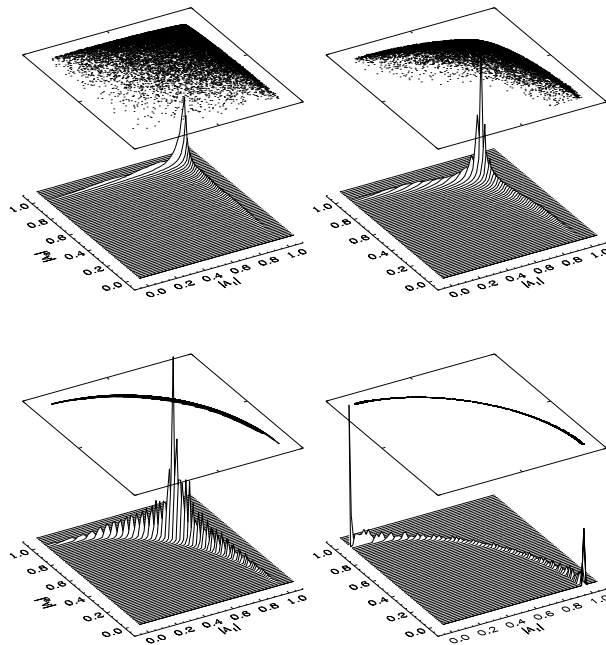
Figure 5.2: Comparison of the states reached at long times starting from noise for (from left to right, and from top to bottom) $\gamma = 0.1, 0.5, 0.95$ and 1.05. The joint probability distribution $p(|A_2|, |A_1|)$ is shown as a 3D surface. The vertical scale is arbitrary, the same in the first three plots and three times larger for $\gamma = 1.05$. On top of each surface, $|A_1(x, t)|$ vs $|A_2(x, t)|$ are shown in the form of a dotted plot obtained from the values of $|A_1|$ and $|A_2|$ at space-time points during a time interval of 50 units.

For $\gamma \ll 1$ we obtain a diffuse cloud of points indicating essentially independent dynamics. The concentration of points around $|A_1|^2 = |A_2|^2 = \mu/(1 + \gamma)$ corresponds to the laminar regions, but excursions away from that solution are independent. As the coupling is increased with $\gamma < 1$ the cloud of points approaches the curve given by $|A_1|^2 + |A_2|^2 = \mu$. This indicates synchronization of the dynamics of structures departing from the laminar regions. The points with larger values of $|A_1|$ and smaller values of $|A_2|$ (and vice versa) correspond to the localized traveling structures. Intermediate points among these ones and those around $|A_1| = |A_2|$ correspond to the regular solutions of non-zero wavenumber that surround the localized structures. The special case of marginal coupling is discussed below, but as we enter into the strong coupling situation ($\gamma > 1$) the cloud of points concentrates in the regions $|A_1|^2 = \mu$, $|A_2| = 0$ and $|A_2|^2 = \mu$, $|A_1| = 0$, while intermediate points correspond to the domain walls separating these ordered regions. It should be pointed out that we are considering just the modulus of the complex fields $A_{1,2}$. The coupled phase dynamics does not show synchronization, at least not in an obvious manner, so that we are in a case of partial synchronization as considered in [155].

A quantitative measure of the synchronizing process can be given in terms of information measures [120]. The entropy $H(X) = -\sum_x p(x) \ln p(x)$, where $p(x)$ is the probability that X takes the value x, measures the *randomness* of a discrete random variable X. For two random discrete variables, X and Y, with a joint probability distribution $p(x, y)$, the mutual information $I(X, Y) = -\sum_{x,y} p(x, y) \ln[p(x)p(y)/p(x, y)]$ gives a measure of the statistical dependence between both variables, the mutual information being 0 if and only if X and Y are independent. Considering the discretized values of $|A_1|$ and $|A_2|$ at space time points as random variables $X = |A_1|$, $Y = |A_2|$, their mutual information is a measure of their synchronization. In Fig. 5.3(left) we have plotted the mutual information and the entropy of $|A_1|$ and $|A_2|$ as a function of γ [6]. This graph shows that the entropy of $|A_1|$ and $|A_2|$ remains constant for increasing values of γ, so that increasing γ does not reduce the uncertainty associated with the single-point distributions of $A_{1,2}$. This indicates that synchronization is not here the result of reduced randomness due to the increase of time and length scales observed in Fig. 5.1. However, the larger is γ the larger becomes the mutual information, approaching its maximum possible value ($I = H(|A_1|) = H(|A_2|)$) as $\gamma \to 1$. An additional quantitative measurement of synchronization is given by the linear correlation coefficient $\rho = (\langle |A_1||A_2|\rangle - \langle |A_1|\rangle\langle |A_2|\rangle)(var(|A_1|)var(|A_2|))^{-1/2}$, with $var(x)$ the variance of x. This coefficient, plotted as a function of γ in Fig. 5.3 (right), is negative indicating that when $|A_1|$ increases, $|A_2|$ decreases, and vice versa. Our quantitative indicators of synchronization, I and ρ, approach their maximum absolute values as $\gamma \to 1$. We also observe that the regime of coupled STI disappears for $\gamma > 1$. In fact, the generalized synchronization observed, manifested by the tendency of the space-time signals towards the functional relation $|A_1|^2 + |A_2|^2 = \mu$, is probably related to the fact that for $\gamma = 1$ this is an attracting manifold for homogeneous states: Writing (5.1) in terms of $R^2 \equiv |A_1|^2 + |A_2|^2$ and $\chi = \arctan(|A_1|/|A_2|)$, it is immediate to see that homogeneous solutions for $\gamma = 1$ are $R^2 = \mu$ and χ arbitrary. To understand the preferences for these solutions it is instructive to look at the transient dynamics starting from random initial conditions (see Fig. 5.4). $R(x, t)$ has a very fast evolution towards $R = \sqrt{\mu}$ with no regime of STI existing at any time. During this fast evolution, the phase $\chi(x, t)$ covers almost completely the range of its possible values. The late stages of the dynamics are characterized by a spatial diffusion of the phase $\chi(x, t)$ until it reaches a space-independent

arbitrary value $\chi(x, t) = \chi_0$. In a $|A_1|$ vs $|A_2|$ dotted plot as the ones in Fig. 5.2 this is visualized by a cloud of points quickly approaching $R^2 = \mu$ and then collapsing into a single point. Runs with different random initial conditions lead to different χ_o. An underlying reason for the special dynamical behavior at $\gamma = 1$ is the separation of time scales for R and χ. For $\gamma \neq 1$, the zero wavenumber components of R and χ have a nonzero driving force and they compete dynamically but, at $\gamma = 1$, $\chi(k = 0)$ is a marginal variable, while $R(k = 0)$ is strongly driven. As a consequence, R relaxes quickly towards $R^2 = \mu$. Once R becomes space-homogeneous, the different wavenumber components of $A_{1,2}$ are decoupled and the zero wavenumber solution wins by diffusion of χ (see Fig. 5.5).
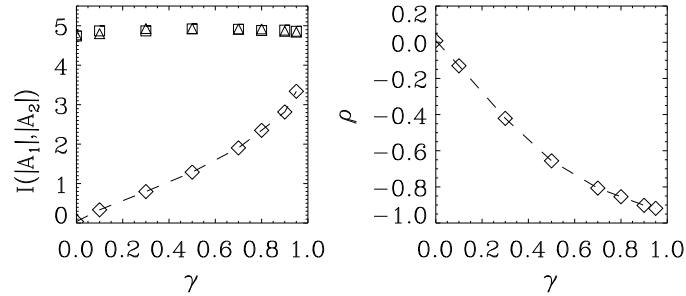
Figure 5.3: Left: Entropy of $|A_1|$ ($\square$) and $|A_2|$ ($\triangle$) and their mutual information I ($\diamond$) as a function of γ. Right: Correlation coefficient ρ of $|A_1|$ vs $|A_2|$ as a function of γ.
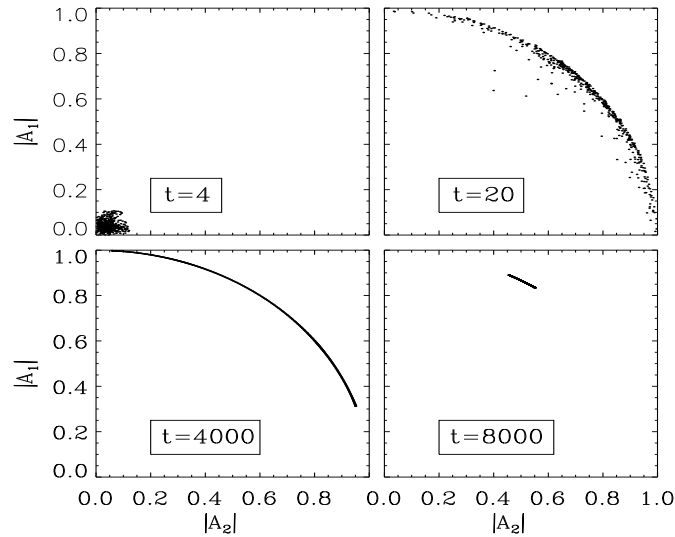
Figure 5.4: Temporal sequence of $|A_1|$ vs $|A_2|$ for $\gamma = 1.0$. The other model parameters are: $\mu = 1$, $\alpha = 0.2$ and $\beta = -2.0$. The system quickly evolves into a state with $|A_1|^2 + |A_2|^2 = \mu$, later on it will eventually finish in an homogeneous state.

In some of our simulations the STI has been observed to disappear for a coupling smaller than $\gamma = 1$, but this seems to be a consequence of finite-size effects: The size of the laminar portions of Fig.(5.1) increases with the coupling γ. When this size becomes similar to system size, one of the stable plane waves can occupy the whole system, thus preventing any further appearance of defects and STI. For a given initial condition, with parameters $\alpha = 0.2$ and $\beta = -1.4$, and a system size $L = 512$ the STI regime was seen to disappear at $\gamma = 0.85$. As soon as the system size was doubled the STI regime reappeared again. By reducing system size to $L = 256$ the STI regime disappeared for smaller γ. The conclusion from this an other numerical experiments is that STI exists for all $\gamma < 1$ in the same range of parameters as it exists in the single CGLE, with time and length scales diverging as γ approaches 1, where STI disappears.
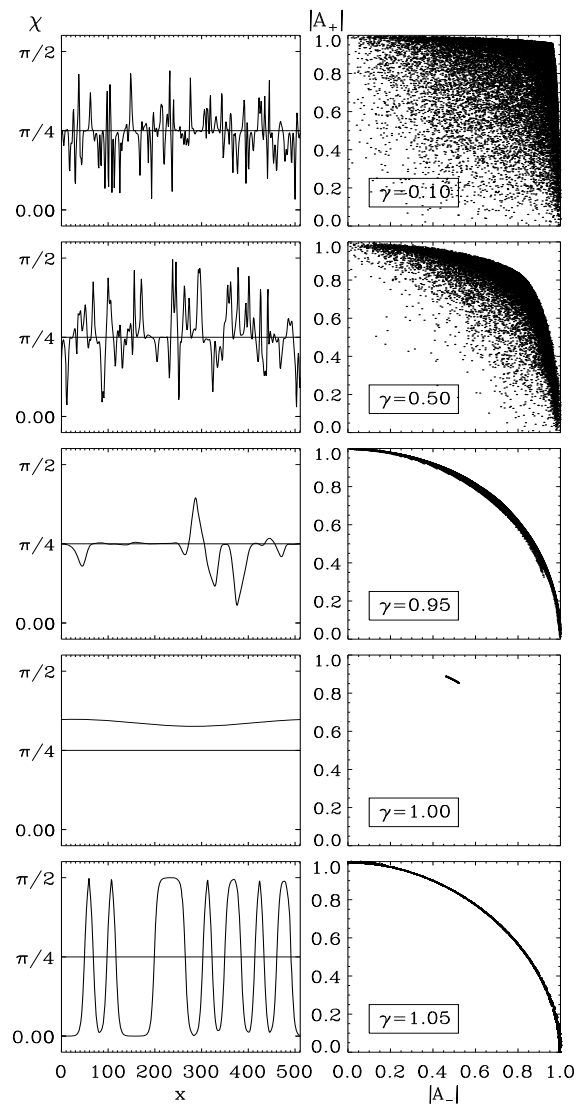
Figure 5.5: Comparison of the states reached by the system at large time starting from noise for $\gamma = 0.95, 1.00$ and 1.05. (Model parameters: $\mu = 1$, $\alpha = 0.2$ and $\beta = -2.0$.)

5.4 Conclusions

In summary we have described a regime of synchronized STI dominated by the space-time synchronization of localized structures. Synchronization is measured by a mutual information and a correlation parameter that take their absolute maximum value at the boundary between weak and strong coupling $\gamma = 1$. Beyond this boundary ($\gamma > 1$) STI disappears but the strong, coupled system dynamics cannot be described in terms of a single dominant amplitude.

Chapter 6

Conclusions

When I look at the granite markers
Those tribute to finality - to eternity
And then I looked at myself here
Chicken scratching for my immortality.
Joni Mitchell, *Hejira*

In this thesis we have addressed different questions in the general context of the analysis of Spatio–temporal complex dynamics. The example chosen to study, the *Complex Ginzburg–Landau Equation* (CGLE) is a paradigm of complex behaviour. Questions addressed include the feasibility of a description in terms of a nonequilibrium potential, characterization of a phase transition between different states of Spatio–Temporal Chaos (STC), control and stabilization of ordered states within a STC phase and synchronization of STC in an extended system.

The first thing settled down in this thesis is that the complex dynamics present by this equation is not due to the lack of a Lyapunov potential. After an extensive discussion on the different types of dynamics the term, generally loosely used, *non–potential dynamics* has been discussed. The approximate Lyapunov functional introduced by Graham and co–workers for the CGLE has been numerically tested. Our results provide evidence that the existence of complex spatiotemporal dynamics is not necessarily associated with the nonexistence of a Lyapunov functional. Complex dynamics can occur within the attractors defined by the functional. This opens the possibility to use methods of Statistical Mechanics based on free energy functionals. However, so far, the knowledge of the Lyapunov potential has been of little help in characterizing phases of STC in the CGLE.

A different approach has been followed to give a description of the Phase Turbulence regime of the CGLE. The description of the PT regime had been previously restricted in most cases to configurations of zero winding number. We have found a much richer behaviour considering states with non–zero winding number (*wound states*). This study has allowed us to give a novel statistical characterization of the transition between Phase Turbulence and Defect Turbulence. We have identified the PT-DT transition with the vanishing of the range of stable winding numbers ν of turbulent states. The PT–DT transition can then be interpreted as an ergodicity–breaking transition. Our results also suggest that the concept of a turbulent Eckhaus instability can be of interest beyond the range of situations described by the CGLE. However, a point about which our study

is inconclusive is the question on the existence of PT in the thermodynamic limit. The identification of ν as an order parameter leads to future investigation towards larger system sizes as a way of resolving the question. In addition of characterizing the PT–DT transition our numerical results reveal the coexistence of different PT attractors that, in principle should be observed in systems for which PT and DT regimes above a Hopf bifurcation are known to exist. These attractors have been explained in term of three basic states: riding turbulence, frozen turbulence and quasiperiodic states. These basic states have been justified through an analytical study on the phase equation associated to the CGLE. Still, further work is needed to clarify the importance of the different terms in the phase equation and the validity of a phase description.

We have also analyzed the issue of control of STC in the CGLE. The usual way to stabilize unstable solutions in extended systems is adding feedback terms to the original equation. Here, we show how the addition of a nonlinear complex diffusion is an appropriate means to obtain stabilization. This has been demonstrated analytically and checked numerically. In particular we have shown how traveling waves of finite wave number can be stabilized deep in the regions of DT, PT and Spatio Temporal Intermittency (STI).

Finally we have addressed the question of synchronization of STC. For this purpose, we have studied two coupled CGLE. We show that this model exhibits a regime of coupled STI which disappears when crossing from weak to strong coupling regime. Synchronized STC is observed within the weak coupling regime. This dynamical regime is dominated by coupled localized structures with a chaotic evolution in space–time. The degree of synchronization as a function of coupling has been characterized by mutual information measures and correlation coefficients.

As a final remark it should be said that still a full statistical characterization of the different regimes of the CGLE and the transition among them is lacking. In particular the role of the localized coherent structures in the dynamics of the disordered regimes is still an open field that deserves further study. .

Appendix A

Numerical Integration of the CGLE

The time evolution of the complex field $A(x, t)$ subjected to periodic boundary conditions is obtained numerically from the integration of the CGLE in Fourier space. The method is pseudospectral and second order accurate in time. Each Fourier mode A_q evolves according to:

$$\partial_t A_q(t) = -\alpha_q A_q(t) + \Phi_q(t) , \tag{A.1}$$

where α_q is $(1 + ic_1)q^2 - 1$, and Φ_q is the amplitude of mode q of the non-linear term in the CGLE. At any time, the amplitudes Φ_q are calculated by taking the inverse Fourier transform $A(x, t)$ of A_q, computing the non-linear term in real space and then calculating the direct Fourier transform of this term. A standard FFT subroutine is used for this purpose [151].

Eq. (A.1) is integrated numerically in time by using a method similar to the so called two-step method [150]. For convenience in the notation, the time step is defined here so as the time is increased by $2\delta t$ at each iteration.

When a large number of modes k is used, the linear time scales α_q can take a wide range of values. A way of circumvent this stiffness problem is to treat exactly the linear terms by using the formal solution:

$$A_q(t) = e^{-\alpha_q t} \left(A_q(t_0)e^{-\alpha_q t_0} + \int_{t_0}^{t} \Phi_q(s)e^{\alpha_q s}ds \right) . \tag{A.2}$$

From here the following relationship is found:

$$\frac{A_q(t + \delta t)}{e^{-\alpha_q \delta t}} - \frac{A_q(t - \delta t)}{e^{\alpha_q \delta t}} = e^{-\alpha_q t} \int_{t-\delta t}^{t+\delta t} \Phi_q(s)e^{\alpha_q s}ds . \tag{A.3}$$

The Taylor expansion of of $\Phi_q(s)$ around $s = t$ for small δt gives an expression for the r.h.s. of Eq. (A.3):

$$\Phi_q(t)\frac{e^{\alpha_q \delta t} - e^{-\alpha_q \delta t}}{\alpha_q} + \mathcal{O}(\delta t^3) . \tag{A.4}$$

Substituting this result in (A.3) we get:

$$A_q(n + 1) = e^{-2\alpha_q \delta t} A_q(n - 1) + \frac{1 - e^{-2\alpha_q \delta t}}{\alpha_q}\Phi_q(n) + \mathcal{O}(\delta t^3) . \tag{A.5}$$

where expressions of the form $f(n)$ are shortcuts for $f(t = n\delta t)$. Expression (A.5) is the so called "slaved leap frog" of Frisch et al.[66]. To use this scheme the values of the field at the first two time steps are required. Nevertheless, this scheme alone is unstable for the CGLE. This is not explicitly stated in the literature and probably a corrective algorithm is also applied. To obtain such correction it is straightforward, by following steps similar to the ones before, to derive the auxiliary expression

$$A_q(n) = e^{-\alpha_q \delta t} A_q(n-1) + \frac{1 - e^{-\alpha_q \delta t}}{\alpha_q} \Phi_q(n-1) + \mathcal{O}(\delta t^2)\,, \qquad (A.6)$$

The numerical method we use, which we will refer to as the two–step method, provides the time evolution of the field from a given initial condition by using Eqs. (A.5) and (A.6) as follows:

1. $\Phi_q(n-1)$ is calculated from $A_q(n-1)$ by going to real space.

2. Eq. (A.6) is used to obtain an approximation to $A_q(n)$.

3. The non-linear term $\Phi_q(n)$ is now calculated from this $A_q(n)$ by going to real space.

4. The field at step $n+1$ is calculated A.5 by using $A_q(n-1)$ and $\Phi_q(n)$.

At each iteration, we get $A_q(n+1)$ from $A_q(n-1)$, and the time advances by $2\delta t$. Note that the total error is $\mathcal{O}(\delta t^3)$, despite the error in intermediate value obtained with Eq. (A.6) is $\mathcal{O}(\delta t^2)$. The method can be easily made exact for plane waves (3.2) of wavenumber k (and then more precise for solutions close to this plane wave) simply by replacing the nonlinear term Φ_q in (A.1) by $\Phi_q + (1 + ic_2)(1 - k^2)A_q$, and taking away the corresponding term from α_q. We have not implemented this improvement because we were mostly interested in solutions changing its winding number, so that they are not close to the same plane wave all the time.

The number of Fourier modes depends on the space discretization. We have used $dx = 1$ and usually $N = 512$. The numerical method has been checked by integrating plane-wave solutions. The amplitude and frequency of the field obtained numerically will differ slightly from the exact amplitude and frequency, not only due to round-off errors, but also due to the fact that the method is approximate. The method has been tested by using a stationary unstable plane wave of wave number k as initial condition. The numerical round-off errors will eventually move the solution away from the plane–wave unstable state. To be precise, in a typical run with $c_1 = -1.0$ and $c_2 = 2.4$, with $dt = 0.01$ and $k_0 = 0.123$, the amplitude was kept constant to the fifth decimal digit during ~ 8000 iterations. In comparison, when a gaussian noise with an amplitude as small as 10^{-7} is added to the plane wave, the modulus is maintained equal to its steady value (up to the fifth decimal) during 1500 iterations. The frequency ω_q determined numerically by using $dt = 0.01$ fits the exact value up to the fourth decimal digit.

The integration method introduced here has also been used in the case of the Vectorial CGLE[17, 16].

Appendix B

Analytical solutions of the CCGLE

A systematic derivation of solutions of the CGLE has not been achieved yet. Only a partial success was obtained (see section 1.3.3) deriving a particular set of solutions as the Bekki–Nozaki family solutions with the Painlevé method[49]. This method (or the Hirota's method used by Bekki and Nozaki themselves) proves to be of little help when applied to a simple generalization of the CGLE such as two coupled CGLE (CCGLE).

In this appendix I will show how it is possible to construct localized solutions for the CCGLE using as a starting point the solutions of the CGLE. The algebra is very simple and I will show only the main steps for the derivation of the results.

The starting point is the CCGLE presented in chater 5,

$$\partial_t A_{1,2} = A_{1,2} + \alpha_0 \partial_x^2 A_{1,2} - \alpha_1 \left(\mid A_{1,2} \mid^2 + \gamma \mid A_{2,1} \mid^2 \right) A_{1,2} \,, \tag{B.1}$$

where $\alpha_0 = (1 + i\alpha)$ and $\alpha_1 = (1 + i\beta)$. We look for solutions of the form:

$$A_1(x, t) = e^{i\varphi(x,t)} A_2(x, t) \tag{B.2}$$

Substituting (B.2) in equation (B.1) I reduce the two original coupled p.d.e. to another set of equation for φ and A_2. This set of p.d.e. corresponds to the conditions that φ and A_2 have to fulfill in order to have a solution of the form (B.2). The condition is

$$\left\{ \partial_t \, \varphi \quad - \quad \alpha_0 \left[i \partial_x^2 \varphi - (\partial_x \varphi)^2 \right] \right\} A_2 = 2i\alpha_0 \partial_x \varphi \partial_x A_2 \tag{B.3}$$

$$\partial_t A_2 \quad = \quad A_2 + \alpha_0 \partial_x^2 A_2 - \alpha_1 \left(1 + \gamma \right) \mid A_2 \mid^2 A_2 \,, \tag{B.4}$$

It should be noted that the condition for A_2 (B.4) is the usual CGLE,

$$\partial_t A_2 = A_2 + b \, \partial_x^2 A_2 - c \mid A_2 \mid^2 A_2 \,, \tag{B.5}$$

where $b = 1 + i\alpha$ and $c = (1 + \gamma) + i(1 + \gamma)\beta$.

This means that the solutions of this CGLE (B.5) are solutions of the original equation (B.1) with A_1 of the form given by (B.2) and φ any *real* solution of (B.3).

Now we search for simple particular cases of the equation (B.3). The first simple case is assuming that φ only depends on time $\varphi(x, t) = \varphi(t)$. For this simple case, it is straightforward to demonstrated that the only possible solution of this form is $\varphi(t) = \varphi = constant$.

Although being a simple case, it is an important case. The result is that *any* solution A_2 of the CGLE (B.5) is also solution of the CCGLE (B.1) with $A_1 = e^{i\varphi} A_2$ and φ a real constant. Thus all the localized solution,moving fronts, pulses, B–N solutions, found for the CGLE (displayed in 1.3.3) are also solution of the CCGLE.

More complicated cases could be analized. Preliminary work indicates that there are no other simple cases that fulfill all the conditions[7].

Bibliography

Bibliography

[1] Rayleigh considered a fluid contained between two infinite, plane, parallel, horizontal plates where the temperatures are maintained constant. His boundary conditions were that the vertical velocity component w and the temperature disturbance θ had to vanish at the top and bottom plates. In modern terminology that means that both boundaries were considered free surfaces and perfect thermal conductors. However, by choosing a free boundary condition Rayleigh had, unknowingly, lost connection with Bénard's experiment because they were affected, in a crucial way, by surface tractions originating from surface tension gradients. Also Rayleigh's work resulted in the long-lasting misconception that the hexagonal Bénard cells are an example, and the most characteristic example, of buoyancy-driven convection, not a surface-tension-driven example.

[2] A. Torcini, private communication.

[3] A related question that also needs further study is the appearance of singularities at finite time in the solutions of (3.7) [45, 91].

[4] Simply stated Shil'nikov theory establishes that in a three dimensional dynamical system with a fixed point being a saddle-focus (i.e. unstable in one direction and oscillatory stable in the other) and provided there exists, for a value of the parameters, a trajectory homoclinic to the fixed point, the eigenvalues obtained through a linearization around the fixed point determine the global behaviour for this value of the parameters and a neighbourhood of it. If these eigenvalues are $\lambda_{1,2} = -\rho \pm i\omega$ and $\lambda_3 = \lambda$ $(\rho,\lambda > 0)$, then if $\rho < \lambda$ there is a countable infinity of chaotic trajectories near the homoclinic one. Proximity to the homoclinic trajectory implies that the shape of the chaotic trajectory is, as commented in the text, a sequence of irregularly spaced pulses. On the contrary, if $\rho > \lambda$ there are no chaotic trajectories. For a more precise statement of the theorems see [186, 129, 107].

[5] Our numerical integration is performed by a second order pseudospectral method described elsewhere [123]. All the numerical results presented in this paper have been obtained for $L = 512$, and we take $\mu = 1$ without loss of generality. The initial condition is white Gaussian noise with a mean squared amplitude of 0.002 . In Fig. 5.1, the same initial condition is taken for all values of γ.

[6] To calculate H and I we have discretized the range of possible values $0 <| A_i |< 1.1$ in $N = 200$ bins. Therefore, the maximum possible entropy is $\ln 200 = 5.3$.

[7] V. Caselles, private communication.

[8] *New Trends in Nonlinear Dynamics: Nonvariational Aspects* (Estella, Spain, 1991), North-Holland. Appeared in Physica D, **61**.

[9] AHLERS, G. *Bull. Am. Phys. Soc. 17* (1972), 59.

[10] AHLERS, G. Low temperature studies of the Rayleigh-Bénard instability and turbulence. *Phys. Rev. Lett. 33* (1974), 1185.

[11] AHLERS, G., AND BEHRINGER, R. P. Evolution of turbulence from the Rayleigh-Bénard instability. *Phys. Rev. Lett. 40* (1978), 712.

[12] AKHMANOV, S. A., VORONTSOV, M. A., YU, V., LARICHEV, A. V., AND ZHELEZNYKH, N. I. Controlling transverse-wave interaction in nonlinear optics: generation and interaction of spatiotemporal structures. *J. Opt. Soc. Am. B 9* (1992), 78.

[13] AKHMEDIEV, N., AND AFANASJEV, V. Novel arbitrary–amplitude soliton solutions of the cubic–quintic complex Ginzburg–Landau equation. *Phys. Rev. Lett. 75* (1995), 2320.

[14] AKHMEDIEV, N., AFANASJEV, V., AND SOTO–CRESPO, J. Singularities and special soliton solutions of the cubic–quinitc complex Ginzburg–Landau equation. *Phys. Rev. E 53* (1996), 1191.

[15] ALBARÈDE, P., AND PROVANSAL, M. Quasiperiodic cylinder wakes and the Ginzburg–Landau model. *J. Fluid Mech. 291* (1995), 191.

[16] AMENGUAL, A., HERNÁNDEZ-GARCÍA, E., MONTAGNE, R., AND SAN MIGUEL, M. Syncronization of spatiotemporal chaos: The regime of coupled spatio temporal intermittency. *Phys. Rev. Lett. 78* (1997), 4379.

[17] AMENGUAL, A., WALGRAEF, D., SAN MIGUEL, M., AND HERNÁNDEZ-GARCÍA, E. Wave–unlocking transition in resonantly coupled Complex Ginzburg–Landau Equation. *Phys. Rev. Lett. 76* (1996), 1956.

[18] ARANSON, I., LEVINE, H., AND TSIMRING, L. Controlling spatiotemporal chaos. *Phys. Rev. Lett. 72* (1994), 2561.

[19] ARECCHI, F. T. *Transient statistical dynamics of lasers.* Cambridge University, New York, 1990, p. 261.

[20] BAR, D. E., AND NEPOMNYASHCHY, A. A. Stability of periodic waves governed by the modified Kawahara equation. *Physica D 86* (1995), 586.

[21] BARBER, M. N. The dynamics of first order phase transitions. In *Phase Transitions and Critical Phenomena*, C. Domb and J. L. Lebowitz, Eds., vol. 8. Academic, London, 1983, p. 146.

[22] BARTUCCELLI, M., CONSTANTIN, P., DOERING, C. R., GIBBON, J. D., AND GISSELFÄLT, M. On the possibility of soft and hard turbulence in the complex Ginzburg-Landau equation. *Physica D 44* (1990), 421.

[23] BATCHELOR, G. *An introduction to fluid dynamics*. Cambridge University, New York, 1967.

[24] BATTOGTOKH, D., AND MIKHAILOV, A. Controlling turbulence in the complex Ginzburg–Landau equation. *Physica D 90* (1996), 84.

[25] BEKKI, N., AND NOZAKI, K. Formation of spatial patterns and holes in the generalized Ginzburg-Landau equation. *Phys. Lett. A 110* (1985), 133.

[26] BÉNARD, H. Les tourbillons cellulaires dans une nappe liquide. *Re. Gén. Sciences Pure Appl. 11* (1900), 1261.

[27] BÉNARD, H. Les tourbillons cellulaires dans une nappe liquide transportant de la chaleur par convection en reégime permanent. *Ann. Chim. Phys. 23* (1901), 62.

[28] BERGÉ, P., POMEAU, Y., AND VIDAL, C. *Order within Chaos*. Wiley, New York, 1986.

[29] BLEICH, M., AND SOCOLAR, J. E. S. Stability of periodic orbits controlled by time–delay feedback. *Phys. Lett. A 210* (1996), 87.

[30] BODENSCHATZ, E., DE BRUYN, J., AHHLERS, G., AND CANNELL, D. S. Transitions between patterns in thermal convection. *Phys. Rev. Lett. 67* (1991), 3078.

[31] BODENSCHATZ, E., MORRIS, S. W., DE BRUYN, J. R., CANNELL, D. S., AND AHLERS, G. Convection in gasses at elevated pressures. In *Pattern formation in complex dissipative systems*, S. Kai, Ed. World Scientific, Singapore, 1992, p. 227.

[32] BOHR, T., BOSCH, E., AND VAN DER WATER, W. Spatiotemporal chaos. *Nature 372* (1994), 48.

[33] BOHR, T., JENSEN, M. H., PALADIN, G., AND VULPIANI, A. *Dynamical systems approach to Turbulence*. Cambridge University, Cambridge, 1998.

[34] BUSSE, F. H. Nonlinear properties of thermal convection. *Rep. Prog. Phys. 41* (1978), 1929.

[35] CAPONERI, M., AND CILIBERTO, S. Thermodynamics of spatiotemporal chaos: An experimental approach. *Phys. Rev. Lett. 64* (1990), 2775.

[36] CAPONERI, M., AND CILIBERTO, S. Thermodynamic aspects of the transition to spatiotemporal chaos. *Physica D 58* (1992), 365.

[37] CHAN, S. Steady state kinetics of diffusionless first order phase transformations. *J. Chem. Phys. 67* (1977), 5755.

[38] CHANDRASEKHAR, S. *Hydrodynamic and Hydromagnetic Stability*. Oxford, Clarendon Press., 1961.

[39] CHANG, H.-C. Wave evolution on a falling film. *Annu. Rev. Fluid Mech. 26* (1994), 103.

[40] CHANG, H.-C., DEMEKHIN, E., AND KOPELEVICH, D. Laminarizing effects of dispersion in an active–disipative medium. *Physica D 63* (1993), 299.

[41] CHANG, I. H.-C., DEMEKHIN, E., AND KOPELEVICH, D. Stability of a solitary pulse against wave packet disturbance in an active medium. *Phys. Rev. Lett. 75* (1995), 1747. The instability of the isolated pulse has been shown to be not absolute but just of the convective type.

[42] CHATÉ, H. Spatiotemporal intermittency regimes of the one-dimensional complex Ginzburg-Landau equation. *Nonlinearity 7*, 1 (1994), 185.

[43] CHATÉ, H. Disordered regimes of the one-dimensional complex ginzburg-landau equation. In *Spatiotemporal Patterns in Nonequilibrium Complex Systems*, P. Cladis and P. Palffy-Muhoray, Eds., vol. XXI of *Santa Fe Institute in the Sciences of Complexity*. Addison-Wesley, New York, 1995, pp. 5–49.

[44] CHATÉ, H., AND MANNEVILLE, P. Stability of the Bekki-Nozaki hole solutions to the one-dimensional complex Ginzburg-Landau equation. *Phys. Lett. A 171* (1992), 183.

[45] CHATÉ, H., AND MANNEVILLE, P. Phase turbulence. In *A Tentative Dictionary of Turbulence*, P. Tabeling and O. Cardoso, Eds. Plenum, New York, 1995.

[46] CHATÉ, H., AND MANNEVILLE, P. Phase diagram of the two-dimensional complex Ginzburg-Landau equation. *Physica A 224* (1996), 348.

[47] COLET, P., AND ROY, R. Digital communication with syncronized chaotic lasers. *Opts. Lett. 19* (1994), 2056.

[48] CONRADO, C. V., AND BOHR, T. Singular growth shapes in turbulent field theories. *Phys. Rev. Lett. 72* (1994), 3522.

[49] CONTE, R., AND MUSETTE, M. Linearity inside nonlinearity: exact solutions to the complex Ginzburg–Landau equation. *Physica D 69* (1993), 1.

[50] COULLET, P., GIL, L., AND ROCA, F. Optical vortices. *Opt. Comm. 73* (1989), 403.

[51] CROSS, M., AND HOHENBERG, P. Pattern formation outside of equilibrium. *Rev. Mod. Phys. 65* (1993), 851. and references therein.

[52] CROSS, M., AND HOHENBERG, P. Spatiotemporal chaos. *Science 263* (1994), 1569.

[53] D'ARCY WENTWORTH THOMPSON. *On growth and form.* Dover Publications, New York, 1992. first edition in 1942.

[54] DECKER, W., PESCH, W., AND WEBER, A. Spiral defect chaos in Rayleigh–Bénard convection. *Phys. Rev. Lett. 73* (1994), 648.

[55] DENNIN, M., AHLERS, G., AND CANNELL, D. S. Spatiotemporal chaos in electro-convection. *Science 272* (1996), 388.

[56] DESCALZI, O. *Gradient Expansion of the Nonequilibrium Potential for the Super-critical Ginzburg-Landau Equation*. PhD thesis, Univ. Essen, 1993.

[57] DESCALZI, O., AND GRAHAM, R. Gradient expansion of the nonequilibrium potential for the supercritical Ginzburg-Landau equation. *Phys. Lett. A 170* (1992), 84.

[58] DESCALZI, O., AND GRAHAM, R. Nonequilibrium potential for the Ginzburg-Landau equation in the phase-turbulence regime. *Z. Phys. B 93* (1994), 509.

[59] DOERING, C. R., GIBBON, J. D., HOLM, D. D., AND NICOLAENKO, B. Low-dimensional behaviour in the complex Ginzburg-Landau equation. *Nonlinearity 1* (1988), 279.

[60] DONNELLY, R. J., AND FULTZ, D. *Proc. Nat. Acad. Sci. 46* (1960), 1150.

[61] ECKHAUS, W. *Studies in nonlinear stability theory*. Springer, Berlin, 1965.

[62] EGOLF, D. *Characterization of extensively chaotic states and transitions*. PhD thesis, Duke University, 1994.

[63] EGOLF, D., AND GREENSIDE, H. Relation between fractal dimension and spatial correlation length for extensive chaos. *Nature 369* (1994), 129.

[64] EGOLF, D., AND GREENSIDE, H. Characterization of the transition from defect to phase turbulence. *Phys. Rev. Lett. 74* (1995), 1751.

[65] FAUVE, S. Woods Hole Oceanographic Institution Technical Report, 1991. Tech. rep., GFD Summer School Program, Woods Hole, 1992.

[66] FRISCH, U., SHE, Z. S., AND THUAL, O. Viscoelastic behavior of cellular solutions to theKuramoto–Sivashinsky model. *J. Fluid Mech. 168* (1986), 221.

[67] GANG, H. Controlling chaos in systems described by partial differential equations. *Phys. Rev. Lett. 71* (1993), 3794.

[68] GINZBURG, V., AND LANDAU, L. *JEPT 20* (1950), 1064.

[69] GLUCKMAN, B. J., MARCQ, P., BRIDGER, J., AND GOLLUB, J. P. Time averaging of chaotic spariotemporal wave patterns. *Phys. Rev. Lett. 71* (1993), 2034.

[70] GOLLUB, J. Spirals and chaos. *Nature 367* (1994), 318.

[71] GRAHAM, R. In *Fluctuations, Instabilities and Phase Transitions*, T. Riste, Ed. Plenum, New York, 1975, p. 270.

[72] GRAHAM, R. Macroscopic potentials, bifurcations and noise in dissipative systems. In *Theory of continuous Fokker-Plank systems*, F. Moss and P. V. E. M. Clintock, Eds., vol. 1 of *Noise in nonlinear dynamical systems*. Cambridge University, Cambridge, 1989, p. 225.

[73] GRAHAM, R. Fluctuations in the steady states. In *XXV Years of Nonequilibrium Statistical Mechanics*, L. Brey, J. Marro, M. Rubí, and M. San Miguel, Eds., vol. 446 of *Lecture Notes in Physics*. Springer, Berlin, 1995, p. 125.

[74] GRAHAM, R., AND TÉL, T. Potential fot the complex Ginzburg–Landau equation. *Europhys. Lett. 13* (1990), 1715.

[75] GRAHAM, R., AND TÉL, T. Steady-state ensemble for the complex Ginzburg-Landau equation with weak noise. *Phys. Rev. A 42* (1990), 4661.

[76] GRAHAM, R., AND TÉL, T. Nonequilibrium potentials in spatially extended pattern forming systems. In *Instabilities and Nonequilibrium Structures III*, E. Tirapegui and W. Zeller, Eds. Reidel, Dordrecht, 1991, p. 125.

[77] GRINSTEIN, G., JAYAPRAKASH, C., AND PANDIT, R. Conjetures about phase turbulence in the complex Ginzburg-Landau equation. *Physica D 90* (1996), 96.

[78] GUNTON, J. D., SAN MIGUEL, M., AND SAHNI, P. The dynamics of first order phase transitions. In *Phase Transitions and Critical Phenomena*, C. Domb and J. L. Lebowitz, Eds., vol. 8. Academic, London, 1983.

[79] H. CALISTO, E. C., AND TIRAPEGUI, E. *J. of Stat. Phys. 69* (1992), 1115.

[80] HAKEN, H. Cooperative phenomena in systems far from thermal equilibrium and in nonphysical systems. *Rev. Mod. Phys. 47* (1975), 67.

[81] HAKEN, H. *Synergetics*. Springer, Berlin, 1983.

[82] HERNÁNDEZ-GARCÍA, E., SAN MIGUEL, M., TORAL, R., AND VIÑALS, J. Noise and pattern selection in the one-dimensional Swift-Hohenberg equation. *Physica D 61* (1992), 159.

[83] HERNÁNDEZ-GARCÍA, E., VIÑALS, J., TORAL, R., AND SAN MIGUEL, M. Fluctuations and pattern selection near an Eckhaus instability. *Phys. Rev. Lett. 70* (1993), 3576.

[84] HIROTA. *Phys. Rev. Lett. 27* (1971), 1192.

[85] HOCHHEISER, D., MOLONEY, J. V., AND LEGA, J. Controlling optical turbulence. *Phys. Rev. A 55* (1997), R4011.

[86] HOHENBERG, P. C., AND HALPERIN, B. I. Theory of dynamical critical phenomena. *Rev. Mod. Phys. 49* (1978), 535.

[87] HOHENBERG, P. C., AND SHRAIMAN, B. I. Chaotic behavior of an extended system. *Physica D 37* (1989), 109.

[88] HU, Y., ECKE, R., AND AHLERS, G. Time and length scales in rotating Rayleigh–Bénard convection. *Phys. Rev. Lett. 74* (1995), 5040.

[89] Huygens, C. *J. des Scavans*, no.11, mar 16; no.12, mar 23 (1665). Huygens' notebook is reprinted in C. Huygens, in *Œuvres Complètes de Christiaan Huygens* (Societé Hollandaise des Sciences, Amsterdam, 1888–1950), Vol. 17, p. 185.

[90] Jackson, E. A. *Perspectives of nonlinear dynamics*, vol. 1. Cambridge University, New York, 1989.

[91] Janiaud, B., Pumir, A., Bensimon, D., Croquette, V., Richter, H., and Kramer, L. The eckhaus instability for traveling waves. *Physica D 55* (1992), 269.

[92] Kawahara, T. Formation of saturated solitons in a nonlinear dispersive system with instability and dissipation. *Phys. Rev. Lett. 51* (1983), 381.

[93] Kawahara, T., and Toh, S. Nonlinear dispersive periodic waves in the presence of instability and damping. *Phys. Fluids 28* (1985), 1636.

[94] Kawahara, T., and Toh, S. Pulse interaction in an unstable disipative–dispersive nonlinear system. *Phys. Fluids 31* (1988), 2103.

[95] Kishiba, S., Toh, S., and Kawahara, T. An estimation of energy spectra of the Ginzburg–Landau chaos. *Physica D 54* (1991), 43.

[96] Kivshar, Y. Dark solitons in nonlinear optics. *IEEE J. Quantum Electron. 29* (1993), 250.

[97] Kocarev, L., and Parlitz, U. Generalized syncronization, predictability, and equivalence of unidirectionally coupled dynamical systems. *Phys. Rev. Lett. 76* (1996), 1816.

[98] Kolodner, P. Stable, unstable, and defected confined states of traveling-wave convection. *Phys. Rev. E 50* (1994), 2731.

[99] Kolodner, P., Slimani, S., Aubry, N., and Lima, R. Characterization of dispersive chaos and related states of binary-fluid convection. *Physica D 85* (1995), 165.

[100] Koschmieder, E. L. *Bénard cells and Taylor vortices*. Cambridge University, Cambridge, 1993.

[101] Kuramoto, Y. Diffusion–induced chaos in reaction system. *Progr. Theor. Phys. Suppl. 64* (1978), 346.

[102] Kuramoto, Y. *Chemical Oscillations, Waves, and Turbulence*. Springer, Berlin, 1984.

[103] Kuramoto, Y. Phase dynamics of weakly unstable periodic structures. *Progr. Theor. Phys. 71* (1984), 1182.

[104] Kuramoto, Y., and Koga, S. *Progr. Theor. Phys. Suppl. 66* (1981), 1081.

[105] Kuramoto, Y., and Tsuzuki, T. Reductive perturbation approach to chemical instabilities. *Progr. Theor. Phys. 52* (1974), 356.

[106] KURAMOTO, Y., AND TSUZUKI, T. Persistant propagation of concentration waves in dissipative media from thermal equilibrium. *Progr. Theor. Phys. 55* (1976), 356.

[107] KUZNETSOV, Y. A. *Elements of Applied Bifurcation Theory*. Springer, New York, 1995.

[108] LANDAU, L. *JEPT 11* (1937), 545.

[109] LEFEVER, R. Dissipative structures in chemical systems. *J. Chem. Phys. 49* (1968), 4977.

[110] LEFEVER, R., AND NICOLIS, G. Dissipative structures in chemical systems. *J. Theor. Biol. 30* (1971), 267.

[111] LEGA, J. *Topological defects associated with the breaking of time-translation invariance*. PhD thesis, Univ. Nice, 1989.

[112] LEGA, J., JANIAUD, B., JUCQUOIS, S., AND CROQUETTE, V. Localized phase jumps in the wave trains. *Phys. Rev A 45* (1992), 5596.

[113] LEWEKE, T., AND PROVANSAL, M. Determination of the parameters of the Ginzburg–Landau wake model form experiments on a bluff ring. *Europhys. Lett. 27* (1994), 655.

[114] LEWEKE, T., AND PROVANSAL, M. Model for the transition in bluff body wakes. *Phys. Rev. Lett. 72* (1994), 3174.

[115] LEWEKE, T., PROVANSAL, M., AND BOYER, L. Stability of vortex shedding modes in the wake of a ring at low Reynolds numbers. *Phys. Rev. Lett. 71* (1993), 3469.

[116] LIBCHABER, A., AND MAURER, J. Local probe in a Rayleigh–Bénard experiment in liquid helium. *J. Phys. Lett. 39* (1978), 369.

[117] LORENZ, E. N. Deterministic nonperiodic flow. *J. Atmos. Sci. 20* (1963), 131.

[118] LU, W., YU, D., AND HARRISON, R. Control of patterns in spatiotemporal chaos in optics. *Phys. Rev. Lett. 76* (1996), 3316.

[119] MANNEVILLE, P., AND CHATÉ, H. Phase turbulence in the two–dimensional complex Ginzburg–Landau equation. *Physica D 96* (1996), 30.

[120] MCELIECE, R. J. *The theory of information and coding : a mathematical framework for communication*, vol. 3 of *Encyclopedia of Mathematics and its Applications*. Addison-Wesley, New York, 1977.

[121] MERTENS, F., IMBIHL, R., AND MIKHAILOV, A. Turbulence and standing waves in oscillatory chemical reactions with global coupling. *J. Chem. Phys. 101* (1994), 9903.

[122] MEZARD, M., PARISI, G., AND VIRASORO, M. A. *Spin glass theory and beyond*. World Scientific, Singapore, 1987.

[123] MONTAGNE, R., HERNÁNDEZ-GARCÍA, E., AMENGUAL, A., AND SAN MIGUEL, M. Wound–up phase turbulence in the Complex Ginzburg-Landau equation. *Phys. Rev. E 56* (1997), 151.

[124] MONTAGNE, R., HERNÁNDEZ-GARCÍA, E., AND SAN MIGUEL, M. Numerical study of a Lyapunov functional for the Complex Ginzburg-Landau equation. *Physica D 96* (1996), 47.

[125] MONTAGNE, R., HERNÁNDEZ-GARCÍA, E., AND SAN MIGUEL, M. Winding number instability in the phase–turbulence regime of the Complex Ginzburg-Landau equation. *Phys. Rev. Lett. 77* (1996), 267.

[126] MORRIS, S. W., BODENSCHATZ, E., CANNELL, D. S., AND AHLERS, G. Spiral defect chaos in large aspect ratio Rayleigh–Bénard convection. *Phys. Rev. Lett. 71* (1993), 2026.

[127] NAGY-UNGVARAI, Z., AND MÜLLER, S. C. Wave propagation in chemical nonequilibrium systems: new experimental results. In *Propagation in systems far from equilibrium*, J. E. Wesfreid, H. R. Brand, P. Manneville, G. Albinet, and N. Boccara, Eds. Springer, Berlin, 1988, p. 100.

[128] NASUNO, S., SASAKI, O., KAI, S., AND ZIMMERMANN, W. Stability diagram in electohydrodynamic convection of nematics. In *Pattern formation in complex dissipative systems*, S. Kai, Ed. World Scientific, Singapore, 1992, p. 275.

[129] NAYFEH, A. H., AND BALACHANDRAN, B. *Applied nonlinear dynamics*. Wiley, New York, 1995.

[130] NEUFELD, M., AND FRIEDRICH, R. Statistical properties of the heat transport in a model of rotating Bénard convetion. *Phys. Rev. E 51* (1995), 2033.

[131] NEWELL, A. Envelope equations. *Lect. Appl. Math. 15* (1974), 157.

[132] NEWELL, A. C. *Solitons in mathematics and physics*. CBMS-NSF regional conference series in applied mathematics. SIAM, Philadelphia, 1983.

[133] NEWELL, A. C. Patterns in nonlinear optics: A paradigm. In *Spatiotemporal Patterns in Nonequilibrium Complex Systems*, P. Cladis and P. Palffy-Muhoray, Eds., vol. XXI of *Santa Fe Institute in the Sciences of Complexity*. Addison-Wesley, New York, 1995, p. 3.

[134] NEWELL, A. C., PASSOT, T., AND LEGA, J. Order parameter equations for patterns. *Annu. Rev. Fluid Mech. 25* (1993), 399.

[135] NEWELL, A. C., AND WHITEHEAD, J. A. Finite bandwith, finite amplitude convection. *J. Fluid Mech. 38* (1969), 279.

[136] NICOLIS, G. *Introduction to Nonlinear Science*. Cambridge University, Cambridge, 1995.

[137] NICOLIS, G., AND PRIGOGINE, I. *Self-organization in Nonequilibrium Systems, from Dissipative Structures to Order through Fluctuations*. Wiley, New York, 1977.

[138] NIEMELA, J. J., AHLERS, G., AND CANNELL, D. S. Localized traveling–wave states in binary–fluid convection. *Phys. Rev. Lett. 64* (1990), 1365.

[139] NING, L., HU, Y., ECKE, R., AND AHLERS, G. Spiral and temporal averages in chaotic patterns. *Phys. Rev. Lett. 71* (1993), 2216.

[140] NOZAKI, K., AND BEKKI, N. Exact solutions of the generalized Ginzburg-Landau equation. *J. Phys. Soc. Japan 53* (1984), 1581.

[141] PALMER, R. Broken ergodicity. In *Lectures in the Sciences of Complexity*, D. Stein, Ed., vol. I of *Santa Fe Institute in the Sciences of Complexity*. Addison-Wesley, New York, 1989.

[142] PAN, L., AND DE BRUYN, J. Nonuniform broken-parity waves and the Eckhaus instability. *Phys. Rev. E 49* (1994), 2119.

[143] PECORA, L. M., AND CARROL, T. L. Synchronization in chaotic systems. *Phys. Rev. Lett. 64* (1990), 821.

[144] PEREIRA, N. R., AND STENFLO, L. Nonlinear Schrödinger equation incluidng growth and damping. *Phys. Fluids 20* (1977), 1733.

[145] PÉREZ-GARCÍA, C., CERISIER, P., AND OCCELLI, R. Pattern selection in the Bénard-Marangoni instability. In *Propagation in systems far from equilibrium*, J. E. Wesfreid, H. R. Brand, P. Manneville, G. Albinet, and N. Boccara, Eds. Springer, Berlin, 1988, p. 232.

[146] PETROSSIAN, A., PINARD, M., MAÎTRE, A., COURTOIS, J. Y., AND GRYNBERG, G. Transverse-pattern formation for counterpropagating laser beams in rubidium vapour. *Europhys. Lett. 18* (1992), 689.

[147] POMEAU, Y., AND MANNEVILLE, P. Stability and fluctuations of a spatially periodic convective flow. *J. Phys. Lett 40* (1979), L609.

[148] POPP, S., STILLER, O., ARANSON, I., AND KRAMER, L. Hole solutions in the 1d complex Ginzburg–Landau equation. *Physica D 84* (1995), 398.

[149] POPP, S., STILLER, O., ARANSON, I., WEBER, A., AND KRAMER, L. Localized hole solutions and spatiotemporal chaos in the 1d complex Ginzburg–Landau equation. *Phys. Rev. Lett. 70* (1993), 3880.

[150] POTTER, D. *Computational Physics*. John Wiley & sons, New York, 1973.

[151] PRESS, W. H. *Numerical Recipes*. Cambridge University, Cambridge, 1989.

[152] PUMIR, A., MANNEVILLE, P., AND POMEAU, Y. *J. Fluid Mech. 135* (1983), 27.

[153] RAYLEIGH, L. On convection currents in a horizontal layer of fluid when the higher temperature is in the under side. *Phil. Mag. 32* (1916), 157.

[154] RICA, S., AND TIRAPEGUI, E. Interaction of defects in two dimensional systems. *Phys. Rev. Lett. 64* (1990), 878.

[155] ROSENBLUM, M. G., PIKOVSKY, A. S., AND KURTHS, J. Phase syncronization of chaotic oscillators. *Phys. Rev. Lett. 76* (1996), 1804.

[156] RULKOV, N. F., SUSHCHIK, M. M., TSIMRING, L. S., AND ABARBANEL, H. D. I. Generalizd syncronization of chaos in directionally coupled chaotic systems. *Phys. Rev. E 51* (1995), 980.

[157] SAKAGUCHI, H. Breakdown of phase dynamics. *Prog. Theor. Phys. 84* (1990), 792.

[158] SAKAGUCHI, H. Phase turbulence and mutual entrainment in a coupled oscillator system. *Prog. Theor. Phys. 83* (1990), 169.

[159] SAN MIGUEL, M. Phase instabilities in the laser vector Complex Ginzburg–Landau Equation. *Phys. Rev. Lett. 75* (1995), 425.

[160] SAN MIGUEL, M., AND SAGUÉS, F. Dynamics of transient pattern formation in nematic liquid crystals. *Phys. Rev. A 36* (1987), 1883.

[161] SASA, S., AND IWAMOTO, T. Stability of phase–singular solutions to the complex Ginzburg–Landau equation. *Phys. Lett. A 175* (1993), 289.

[162] SCHIELEN, R., DOELMAN, A., AND DE SWART, H. On the nonlinear dynamics of free bars in straight channels. *J. Fluid Mech. 252* (1993), 325.

[163] SEGEL, L. A. Distant sidewalls cause slow amplitude modulation of scellular convection. *J. Fluid Mech. 38* (1969), 203.

[164] SHINBROT, T., GREBOGI, C., OTT, E., AND YORKE, J. Using small perturbations to control chaos. *Nature 363* (1993), 411.

[165] SHRAIMAN, B., PUMIR, A., VAN SAARLOOS, W., HOHENBERG, P., CHATÉ, H., AND HOLEN, M. Spatiotemporal chaos in the one-dimensional complex Ginzburg-Landau equation. *Physica D 57* (1992), 241.

[166] SIVASHINSKY, G. Nonlinear analysis of hydrodynamic instability in laminar flames–I. derivation of basic equations. *Acta Astronautica 4* (1977), 1177.

[167] STEWARTSON, K., AND STUART, J. T. A nonlinear instability theory for a wave system in plane Poiseuille flow. *J. Fluid Mech. 48* (1971), 529.

[168] STILLER, O., POPP, S., ARANSON, I., AND KRAMER, L. All we know about hole solutions in the CGLE. *Physica D 87* (1995), 361.

[169] STILLER, O., POPP, S., AND KRAMER, L. From dark solitons in the defocusing nonlinear Schrödinger to holes in the complex Ginzburg–Landau equation. *Physica D 84* (1995), 424.

[170] SWINNEY, H., AND GOLLUB, J., Eds. *Hydrodynamic instabilities and the transition to turbulence.* Springer, Berlin, 1985.

[171] SZÉPFALUSY, P., AND TÉL, T. *Phys. Rev. A 112* (1982), 146.

[172] TAYLOR, G. I. Stability of a viscous liquid contained between two rotating cylinders. *Phil. Trans. Roy. Soc. London A 223* (1923), 289.

[173] T.B.BENJAMIN, AND FEIR, J. The disintegration of wave trains on deep water. *J. Fluid Mech. 27* (1967), 417.

[174] TORCINI, A. An order parameter for the transition from phase to amplitude turbulence. *Phys. Rev. Lett. 77* (1996), 1047.

[175] TORCINI, A., FRAUENKRON, H., AND GRASSBERGER, P. Studies of the phase turbulence in the one dimensional Complex Ginzburg-Landau equation. *Phys. Rev. E 55* (1997), 5073.

[176] VAN HECKE, M. *The amplitude description of nonequilibrium patterns*. PhD thesis, Leiden University, 1996.

[177] VAN HECKE, M., AND VAN SAARLOOS, W. Convection in rotating annuli: Ginzburg–Landau equations with tunable coefficients. *Phys. Rev. E 55* (1997), R1259.

[178] VAN SAARLOOS, W. The complex Ginzburg-Landau equation for beginners. In *Spatiotemporal Patterns in Nonequilibrium Complex Systems*, P. Cladis and P. Palffy-Muhoray, Eds., vol. XXI of *Santa Fe Institute in the Sciences of Complexity*. Addison-Wesley, New York, 1995, p. 19.

[179] VAN SAARLOOS, W., AND HOHENBERG, P. Fronts,pulses,sources and sinks in generalized complex Ginzburg-Landau equations. *Physica D 56* (1992), 303. and (Errata) Physica D **69**, 209 (1993).

[180] VIÑALS, J., HERNÁNDEZ-GARCÍA, E., TORAL, R., AND SAN MIGUEL, M. Numerical study of the dynamical aspects of pattern selection in the stochastic Swift-Hohenberg equation in one dimension. *Phys. Rev. A 44* (1991), 1123.

[181] WALGRAEF, D. *Spatio-temporal pattern formation : with examples from physics, chemistry, and materials science*. Springer, New York, 1997.

[182] WALGRAEF, D., DEWEL, G., AND BORKMANS, P. Nonequilibrium phase transition and chemical instabilities. *Adv. Chem. Phys 49* (1982), 311.

[183] WALGRAEF, D., DEWEL, G., AND BORKMANS, P. Chemical waves in a two–dimensional oscillating system. *J. Chem. Phys 78* (1983), 3043.

[184] WEISS, J., TABOR, M., AND CARNEVALE, G. *J. Math. Phys. 24* (1983), 522.

[185] WIESENFELD, K., COLET, P., AND STROGATZ, S. H. Syncronization transitions in a disordered Josephson series array. *Phys. Rev. Lett. 76* (1996), 404.

[186] WIGGINS, S. *Introduction to applied nonlinear dynamical systems and chaos*. Springer, New York, 1990.

[187] XI, H., GUNTON, J. D., AND VIÑALS, J. Spiral defect chaos in a model of Rayleigh–Bénard convection. *Phys. Rev. Lett. 71* (1993), 2030.

[188] ZAKHAROV, V., Ed. *What is integrability?* Springer, Berlin, 1991.

Curriculum Vitae

Héctor Raúl Montagne Dugrós

Date of birth	April 28, 1957
Place of birth	Montevideo, Uruguay

EDUCATION

1989	"Licenciado en Física". Facultad de Ciencias, Universidad de la República, Montevideo, Uruguay.
1991	"Magister en Física" (*M.Sc.*) Facultad de Ciencias, Universidad de la República, Montevideo, Uruguay, thesis "Bifurcaciones en un Modelo de Tres Modos de Ondas de Rossby y de Deriva" . Advisor A. Sicardi Schifino.

LIST OF PUBLICATIONS

- *Nonlinear Three–Wave Interaction Description for a Global Drift Wave Turbulence* by A. C. Sicardi Schifino and R. Montagne. Physica Scripta, **47**, 2, pag. 244 (1993).

- *Three Modes Nonlinear Statistical Description for a Global Drift Wave Turbulence* by R. Montagne, A. C. Sicardi Schifino. In "Instabilities and Nonequilibrium Structures IV", Eds. E. Tirapegui and W. Zeller, Kluwer Academic Publishers, Dordrecht, 289, (1993).

- *Cascading Process in the Flute–Mode Turbulence of a Plasma* by R. González, D. Gómez C. Ferro Fontán A. C. Sicardi Schifino, R. Montagne. Phys. Fluids B, **5** (6), 1790 (1993).

- *Multiple front propagation into unstable states* by R. Montagne, A. Amengual, E. Hernández-García and M. San Miguel, Phys. Rev. E, **50**, 377 (1994).

- *Computational studies of the complex Ginzburg-Landau equation and its non equilibrium potential* by R. Montagne, E. Hernández-García and M. San Miguel. In "3rd Granada Lectures in Computational Physics", Eds. P.L. Garrido and J. Marro, Springer-Verlag, Heildelberg,317,(1995)

- *Multiple front propagation in a potential non-gradient system* by M. San Miguel, R. Montagne, A. Amengual, E. Hernández-García. In "Instabilities and Nonequilibrium Structures V", Eds. E. Tirapegui and W. Zeller, Kluwer Academic Publishers, Dordrecht, 85,(1996).

- *Winding number instability in the phase-turbulence regime of the Complex Ginzburg-Landau Equation* by R. Montagne, E. Hernández-García and M. San Miguel, Phys. Rev. Lett., **77**, 267 (1996).

- *Numerical Study of a Lyapunov functional for the Complex Ginzburg-Landau Equation.* by R. Montagne, E. Hernández-García and M. San Miguel, Physica D, **96**, 47 (1996).

- *Wound-up phase turbulence in the Complex Ginzburg–Landau Equation* by A. Amengual, R. Montagne, E. Hernández-García and M. San Miguel, submitted for publication (1996).

- *Synchronization of Spatiotemporal Chaos: The regime of coupled Spatiotemporal Intermittency* by A. Amengual, R. Montagne, E. Hernández-García and M. San Miguel, submitted for publication (1996).

- *Nonlinear Diffusion Control of Spatio-Temporal Chaos* by R. Montagne, P. Colet. submitted for publication (1996).